

Molecular and Cell Biological Studies on Novel ALG-2-Interacting Proteins

(新規 ALG-2 相互作用タンパク質に関する
分子細胞生物学的研究)

SASAKI (OSUGI) Kanae

Department of Applied Molecular Biosciences

Graduate School of Bioagricultural Sciences

Nagoya University

March 2014

Contents	Page
Abbreviations	1
Introduction	2
Chapter I	8
Chapter II	36
References	74
Acknowledgements	84

Abbreviations

a.a.: amino acids

ABM: ALG-2-binding motif

CBB: Coomassie Brilliant Blue R-250

ER: endoplasmic reticulum

FW: Far-Western

GFP: green fluorescent protein

GST: glutathione-S-transferase

IgG: immunoglobulin G

IP₃R1: inositol 1,4,5-trisphosphate receptor type 1

mAb: monoclonal antibody

NP-40: Nonidet P-40

pAb: polyclonal antibody

PAGE: polyacrylamide gel electrophoresis

PEF: penta-EF-hand

PMSF: phenylmethylsulfonyl fluoride

PRR: proline-rich region

PVDF: polyvinylidene difluoride

qPCR: quantitative PCR

RRM: RNA recognition motif

TG: thapsigargin

WB: Western blotting

Introduction

The intracellular Ca^{2+} signaling pathway is important for the control of broad cellular processes from fertilization, contraction, cell differentiation and proliferation to apoptosis. Resting cells constantly sustain the cytoplasmic concentration of Ca^{2+} at the extremely low level compared with the extracellular concentration. Stimuli such as membrane depolarization, extracellular signaling molecules or intracellular messengers trigger an exponential elevation of the cytoplasmic concentration of Ca^{2+} from 10^{-7} M to 10^{-5} M by the influx of extracellular Ca^{2+} and the release of Ca^{2+} from endoplasmic reticulum/sarcoplasmic reticulum (SR). Intracellular various Ca^{2+} -binding proteins translate the chemical signal of Ca^{2+} mobilization into diverse biochemical responses and modulate the Ca^{2+} signal spatially and temporally.

The EF-hand, one of Ca^{2+} -binding motifs, is defined by its helix–loop–helix secondary structure, and Ca^{2+} binds to the loop (Gifford *et al.*, 2007). EF-hands tend to occur in pairs, which form a discrete domain so that most EF-hand proteins have multiple EF-hands (Figure 1A). A group of proteins containing five serially repetitive EF-hand motifs was named the penta-EF-hand (PEF) family and includes the calpain small subunit, sorcin, grancalcin, peflin and ALG-2 (apoptosis-linked gene 2) (Figure 1B) (Maki *et al.*, 1997, Maki *et al.*, 2002). ALG-2 contains eight alpha helices that fold into five EF-hands in the structure and forms a homodimer or a heterodimer with peflin through EF5 (fifth EF-hand) (Jia *et al.*, 2001; Kitaura *et al.*, 2001; Suzuki *et al.*, 2008). Ca^{2+} binds to EF1 and EF3 strongly, and to EF5 weakly (Figure 2).

ALG-2 (also named PDCD6, programmed cell death 6), a prototypical member of the PEF protein family, was identified as a pro-apoptotic factor in T-cell hybridoma (Vito *et al.*, 1996). Although no abnormal phenotypes appeared in ALG-2 knockout mice (Jang *et al.*, 2002), Rao *et al.* reported that ALG-2 functions as a pro-apoptotic factor in the ER stress-induced cell death (Rao *et al.*, 2004). Other accumulating data suggest involvement of ALG-2 in apoptosis (Draeby *et al.*, 2007, Mahul-Mellier *et al.*, 2008), cell cycle (Hoj *et al.*, 2009) and signal transduction (Hwang *et al.*, 2002, Chen *et al.*, 2005, Park *et al.*, 2012, Rho *et al.*, 2012). Correlation between gene expression level of ALG-2 and malignant progression in pulmonary adenocarcinoma and gastric cancer was also reported (Yamada *et al.*, 2008; Aviel-Ronen *et al.*, 2008), indicating that ALG-2 may be useful as a prognostic biomarker. However, details of its physiological functions

have remained unclear. For contribution to development of novel cancer therapy, functional analyses of ALG-2 at a molecular level are needed.

Binding to Ca^{2+} induces the conformational change of ALG-2 and enables ALG-2 to interact with various proteins. ALIX (ALG-2-interacting protein X, also named AIP1 and PDCD6IP) is the first protein reported as an ALG-2-interacting factor (Missotten *et al.*, 1999; Vito *et al.*, 1999). Suzuki *et al.* elucidated the structure of the complex between ALG-2 and an ALIX oligopeptide (799-QGPPYPTYPGYGYSQ-814) by X-ray crystallography (Suzuki *et al.*, 2008). The Ca^{2+} -dependent interaction between them is explained as follows: (1) Binding of Ca^{2+} to EF3 causes change in the side chain configuration of Arg¹²⁵, present in the loop connecting EF3 and EF4; (2) The conformational change makes a primary hydrophobic pocket (Pocket 1) accessible to the ALIX peptide; (3) Entry of the peptide induces half closure of Pocket 1 by moving the Arg¹²⁵ side chain to complete the peptide trapping.

Several research groups have identified Ca^{2+} -dependent ALG-2-interacting proteins such as annexin A11 (Sato *et al.*, 2002a), annexin A7 (Sato *et al.*, 2002b), Sec31A (Yamasaki *et al.*, 2006; Shibata *et al.*, 2007), TSG101 (Katoh *et al.*, 2005), PLSCR3 (Shibata *et al.*, 2008) and Scotin (Draeby *et al.*, 2007). Most of them tend to contain Pro-rich region (PRR), which is structurally flexible and an important region to interact with ALG-2 (Figure 3). Shibata *et al.* previously identified the ALG-2-binding sites (ABS) of ALIX, PLSCR3 and Sec31A (Shibata *et al.*, 2004; Shibata *et al.*, 2008; Shibata *et al.*, 2010). Some ALG-2-interacting proteins were classified into Alix-type and non-Alix-type according to the homology to ABS of ALIX and the ability of binding to ALG-2^{ΔGF122} which is an alternatively spliced isoform lacking G¹²¹F¹²² (Missotten *et al.*, 1999; Vito *et al.*, 1999; Shibata *et al.*, 2008; Shibata *et al.*, 2010). PLSCR3 contains two sequences to interact with ALG-2. One is highly homologous to ALIX ABS and can bind to ALG-2^{WT} [a longer isoform is designated wild type (WT) for convenience] but not ALG-2^{ΔGF122}. The other is similar to Sec31A ABS and has the ability of binding to both ALG-2 isoforms as well as Sec31A. Comparison of these binding sequences and X-ray crystal structure analyses of ALG-2/ALIX peptide complex revealed two ALG-2-binding motifs: ABM-1, PPYP(x)_nYP (x, variable; n=4 in ALIX and PLSCR3-ABS1); ABM-2, PxPGF (x, variable; Sec31A and PLSCR3-ABS2) (Suzuki *et al.*, 2008; Maki *et al.*, 2011).

In this study, first, to gain important clues about new functions of ALG-2, I searched

for new ALG-2-interacting proteins by *in silico* screening of PRR proteins based on two types of ABMs. Among the positive proteins, I focused on two RNA processing-related proteins, PATL1 (Pat1-like protein, also named Pat1b) and CHERP (Ca²⁺ Homeostasis Endoplasmic Reticulum Protein) for further investigation. PATL1, a well-known component of the P-body that is a cytoplasmic non-membranous granule composed of translation-inactive mRNAs and proteins involved in mRNA decay (Scheller *et al.*, 2007; Ozgur *et al.*, 2010). In Chapter I, I described results of the interaction analysis between ALG-2 and PATL1 and their subcellular localizations, which indicated that PATL1 is a novel ALG-2-interacting protein.

CHERP was previously reported to localize to ER and to function in intracellular Ca²⁺ mobilization in T-cells (LaPlante *et al.*, 2000; O'Rourke *et al.*, 2003). However, it has regions that are presumed to be involved in RNA processing. Especially, the region rich in Arg and Ser is homologous to RS (Arg/Ser) domains found in Ser/Arg-rich splicing factors (SR proteins) that function as constitutive and alternative splicing regulators. In Chapter II, I described that CHERP is a novel Ca²⁺-dependent ALG-2-interactive target in the nucleus. I also showed new findings that CHERP and ALG-2 participate in regulation of alternative splicing.

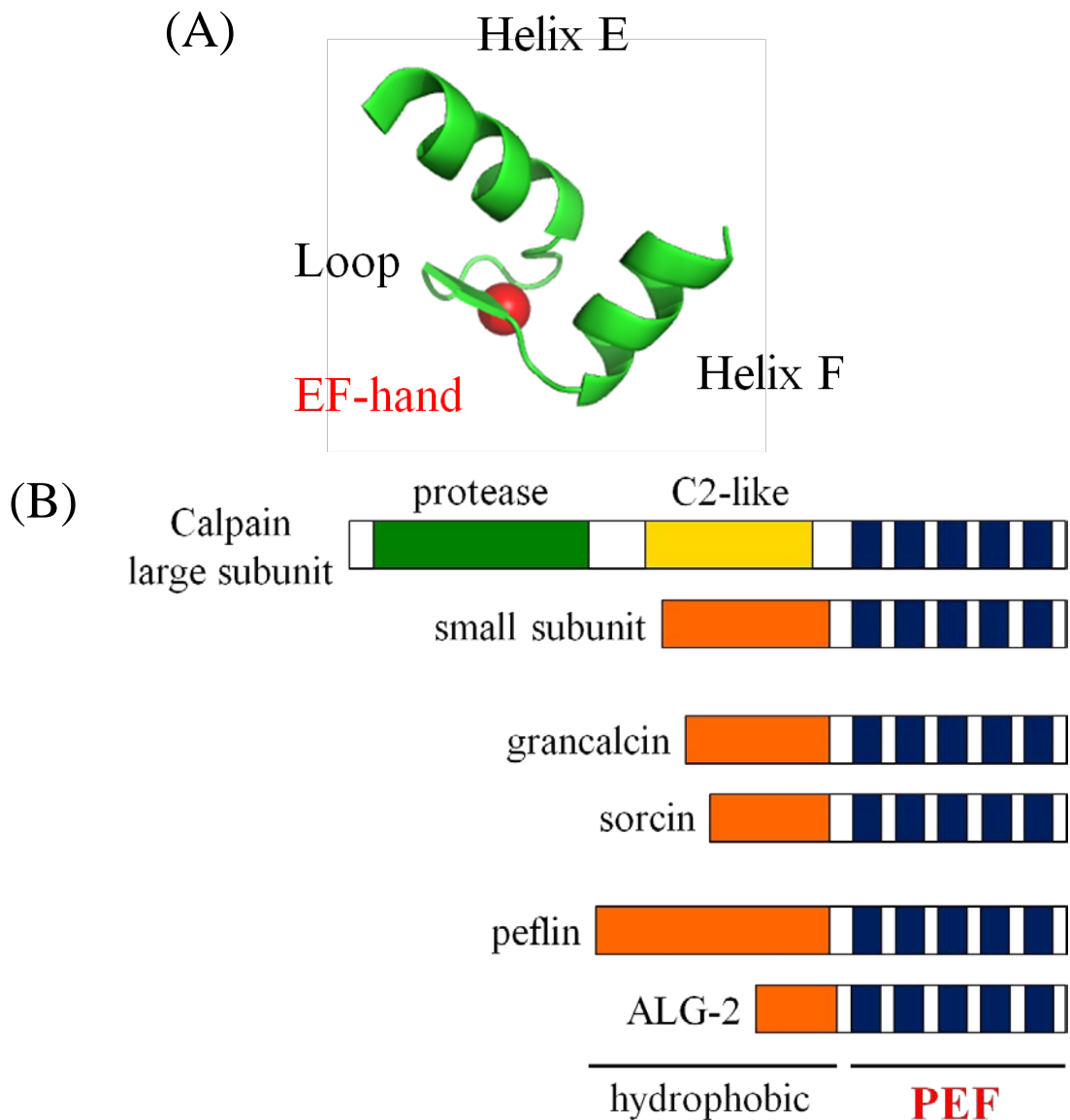


Figure 1. The structure of EF-hand in parvalbumin and schematic diagrams of the penta-EF-hand protein family.

(A) The EF-hand is composed of a helix-loop-helix structural module. This Ca^{2+} -binding motif, formed by helices E and F, was first observed in the crystal structure of parvalbumin. The second Ca^{2+} -binding site in the refined crystal structure of carp parvalbumin (PDB ID: 5CPV) is shown in cartoon representation with PyMol. A calcium atom is shown by a red sphere.

(B) The penta-EF-hand family possess five serially repetitive EF-hand motifs (PEF). EF-hands are shown as blue boxes. Regions rich in hydrophobic residues (aromatic and aliphatic residues) and small side chains (Gly, Pro, Ala) are shown as orange boxes.

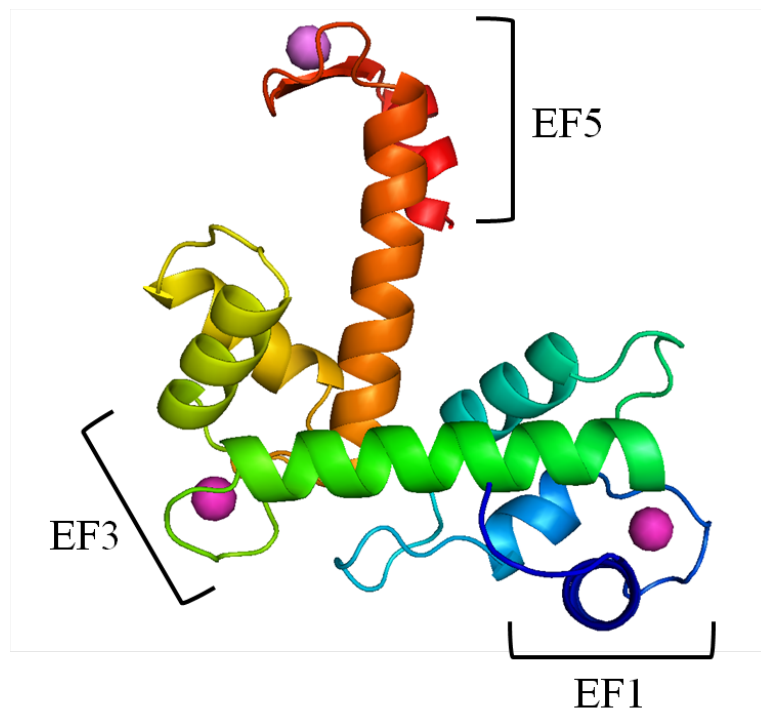
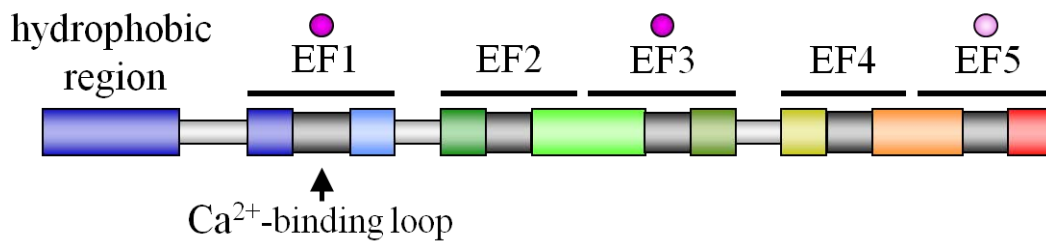


Figure 2. The schematic diagram and 3-D structure of ALG-2.

The structure of Ca^{2+} -bound form of human ALG-2. Calcium atoms are shown as purple spheres. 3-D structure of ALG-2 (PDB ID: 2ZN9) is shown in cartoon representation with PyMol and colored similar to the above scheme.

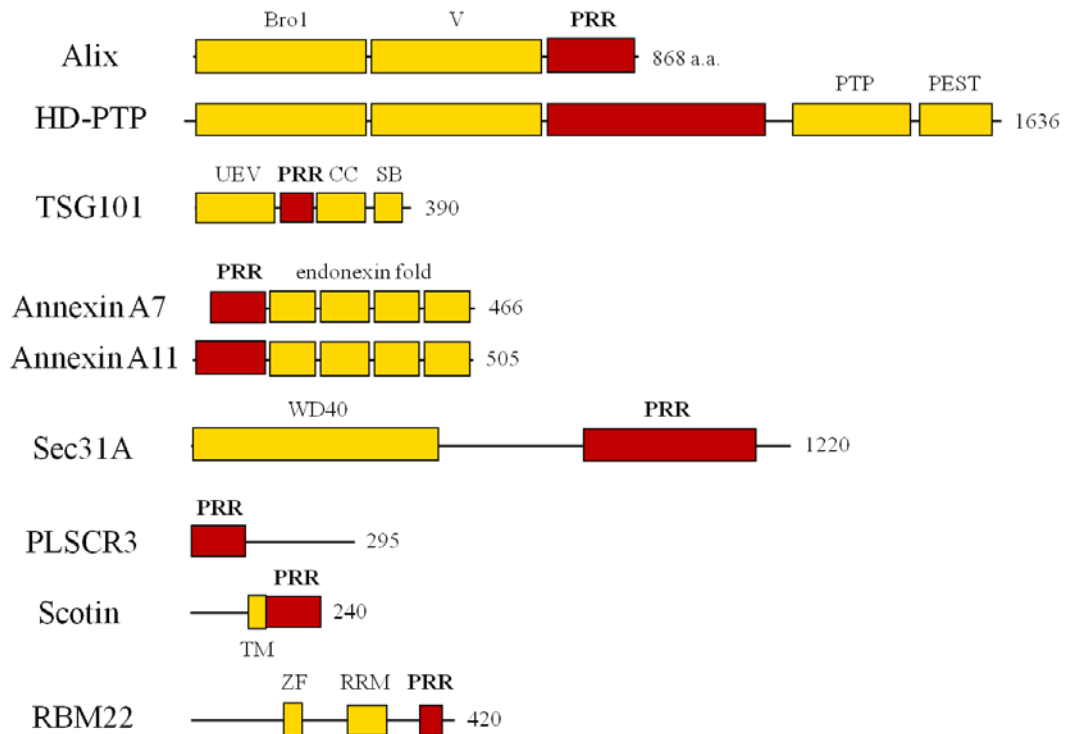


Figure 3. The schematic diagram of ALG-2-interacting proteins.

ALG-2 interacts with various proteins in a Ca^{2+} -dependent manner. Most of them contain PRR (Pro-Rich Region), which is structurally flexible and an important region to interact with ALG-2.

Chapter I

Identification of the P-body component PATL1
as a novel ALG-2-interacting protein by in silico
and Far-Western screening of proline-rich proteins

Abstract

ALG-2 (also named PDCD6) is a 22-kDa Ca^{2+} -binding protein that contains five serially repetitive EF-hand motifs and belongs to the penta-EF-hand (PEF) family including the calpain small subunit. Upon binding to Ca^{2+} , ALG-2 changes its conformation and interacts with various proteins such as ALIX and Sec31A at their specific sites containing an ALG-2-binding motif (ABM) present in their respective Pro-rich region (PRR). In this study, to search for novel ALG-2-interacting proteins, I first performed *in silico* screening of ABM-containing PRRs in a human protein database. I selected 17 sequences and expressed the PRR or full-length proteins fused with green fluorescent protein (GFP) in HEK293T cells and analyzed their abilities to bind to ALG-2 by Far-Western blotting using biotinylated ALG-2 as a probe. As a result, I found 10 positive new ALG-2-binding candidates with different degrees of binding ability. For further investigation, I selected PATL1 (alternatively designated Pat1b), a component of the P-body, which is a cytoplasmic granule composed of translation-inactive mRNAs and proteins involved in mRNA decay. Interactions between GFP-PATL1 and ALG-2 as well as its alternatively spliced shorter isoform ALG-2 ^{Δ GF122} were confirmed by pulldown assays using glutathione-S-transferase (GST)-fused ALG-2 proteins. Furthermore, Ca^{2+} -dependent interactions between endogenous PATL1 and ALG-2 proteins were demonstrated by a co-immunoprecipitation assay using their specific antibodies. In immunofluorescence microscopic analyses, PATL1 as well as DCP1A, a well-known P-body marker, co-localized with a subset of ALG-2, whereas most of ALG-2 co-localized with Sec31A, a coat component of the COPII transport vesicle. This is the first report showing punctate localization of ALG-2 to P-bodies, which are defined non-membranous granular structures in the cytoplasm.

Introduction

ALG-2 (also named PDCD6, programmed cell death 6) was identified as a pro-apoptotic factor in T-cell hybridoma and named after apoptosis-linked gene 2 (Vito *et al.*, 1996). Although no abnormal phenotypes appeared in ALG-2 knockout mice (Jang *et al.*, 2002), accumulating data suggest involvement of ALG-2 in apoptosis in cultured mammalian cells (Rao *et al.*, 2004; Draeby *et al.*, 2007; Mahul-Mellier *et al.*, 2008), cell cycle (Hoj *et al.*, 2009), signal transduction (Hwang *et al.*, 2002; Chen *et al.*, 2005; Park *et al.*, 2012; Rho *et al.*, 2012) and cancer (Yamada *et al.*, 2008; Aviel-Ronen *et al.*, 2008). However, details of its physiological functions have remained unclear. ALG-2 is a 22-kDa Ca^{2+} -binding protein containing five serially repetitive EF-hand motifs (penta-EF-hand, a PEF domain) (Maki *et al.*, 1997; Maki *et al.*, 2002). Upon binding to Ca^{2+} , ALG-2 changes its conformation (Maki *et al.*, 1998) and interacts with various proteins such as ALIX (Missotten *et al.*, 1999; Vito *et al.*, 1999), annexin A11 (Satoh *et al.*, 2002a), annexin A7 (Satoh *et al.*, 2002b), Sec31A (Yamasaki *et al.*, 2006; Shibata *et al.*, 2007), TSG101 (Katoh *et al.*, 2005), PLSCR3 (Shibata *et al.*, 2008) and Scotin (Draeby *et al.*, 2007). These proteins each contain a proline-rich region (PRR) that is essential for interaction with ALG-2. Generally, PRRs in proteins are flexible and accommodate binding sites for various interacting proteins (Williamson *et al.*, 1994; Kay *et al.*, 2000; Ren *et al.*, 2011). Indeed, our research group previously identified ALG-2-binding sites (ABS) in ALIX (Shibata *et al.*, 2004), Sec31A (Shibata *et al.*, 2010) and PLSCR3 (Shibata *et al.*, 2008), in which there are two binding sites (PLSCR3-ABS1 and -ABS2). Comparison of these binding sequences and X-ray crystal structure analyses of ALG-2/ALIX peptide complex as well as apo-ALG-2 revealed two ALG-2-binding motifs: ABM-1, PPYP(x)_nYP (x, variable; n=4 in ALIX and PLSCR3-ABS1); ABM-2, PxPGF (x, variable; Sec31A and PLSCR3-ABS2) (Suzuki *et al.*, 2008; Maki *et al.*, 2011). While ALG-2^{ΔGF122} (an alternatively spliced shorter isoform lacking Gly¹²¹Phe¹²², see Ref Maki *et al.*, 2011) does not bind to ALIX, it binds to Sec31A and PLSCR3 (Shibata *et al.*, 2007; Shibata *et al.*, 2008), supporting the presence of two different modes of interactions between ALG-2 and its binding partners. In this study, to search for new ALG-2-interacting proteins, I performed *in silico* screening based on these previous findings: two types of ABMs in PRRs.

After selecting promising candidates for novel ALG-2-interacting proteins, I performed binding assays by expressing each PRR or full-length protein fused with

green fluorescent protein (GFP) in HEK293T cells followed by immunoprecipitation and Far-Western (FW) blotting with biotinylated ALG-2 as a probe. Among the positive proteins, I focused on PATL1 (also named Pat1b), a well-known component of the P-body that is a cytoplasmic non-membranous granule composed of translation-inactive mRNAs and proteins involved in mRNA decay (Scheller *et al.*, 2007; Ozgur *et al.*, 2010). PATL1 has ABM-2 and I confirmed interaction between GFP-PATL1 and both isoforms of ALG-2 fused with glutathione-S-transferase (GST) by pulldown assays. Furthermore, I showed co-immunoprecipitation of endogenous PATL1 and ALG-2 in a Ca^{2+} -dependent manner and partial co-localization of ALG-2 and PATL1 at P-bodies by indirect immunofluorescence microscopic analyses using specific antibodies, indicating that PATL1 is a novel ALG-2-interacting protein.

Materials and Methods

Antibodies and reagents

The following antibodies were purchased: rabbit anti-GFP serum suitable for immunoprecipitation (Catalog No. A-6455, Invitrogen/Molecular Probes, Carlsbad, CA, USA), mouse anti-GFP monoclonal antibody (mAb) (clone B-2, Santa Cruz Biotechnology, Santa Cruz, CA, USA) and mouse anti-DCP1A mAb (clone 3G4, Abnova, Taipei, Taiwan). Affinity-purification of rabbit anti-human ALG-2 polyclonal antibody (pAb) using the recombinant ALG-2 protein immobilized on an N-Hydroxysuccinimide (NHS) column was described previously (Shibata *et al.*, 2007). Anti-human ALG-2 antiserum was also raised in a goat using recombinant ALG-2 protein as an antigen, and antibody was similarly affinity-purified. Anti-human PATL1 antisera were raised in rabbits using a PATL1 C-terminal region (450-770 a.a.) protein (PATL1Ct) that was fused with glutathione-S-transferase (GST) as an antigen, and specific antibodies were affinity-purified using PATL1Ct fused with maltose-binding protein (MBP).

In silico screening

A database search for ABM-containing protein sequences was performed by using 'XaaRR-Scan', a custom-made program (Maze Inc., Tokyo, Japan) that was designed to find a segment containing motifs of interest in a region rich in specified amino acid residues. Protein sequences containing PRR and ABM-1 or ABM-2 were searched for under the following conditions: Query Amino Acid (s), P; Window Size, 20; Slide Size, 1; Content Threshold (%), 25; Minimum Segment Size, 30; Sequence (s) in Segment for ABM-1 (PPYP, PxYP, PYP, YP_(x)₃₋₅YP, YPYP) and for ABM-2 (PxPGF, PxPGW); database, UniProt/SwissProt (<http://www.uniprot.org/>). Each scoring value of an ABM-1 type motif was defined as follows: PPYP [5], PxYP [3], PYP [3], YP_{xxxx}YP [5], YP_{xxx}YP [3], YP_{xxxxx}YP [3]. The total score of each protein selected by XaaRR-Scan was calculated by summation of individual motif scores.

Plasmid construction

Human cDNAs of proteins with high XaaRR-Scan scores were purchased from Open Biosystems (Lafayette, CO, USA) or obtained by PCR-cloning from human cDNA libraries with a KOD-Plus-Ver.2 DNA polymerase (Toyobo, Osaka, Japan) using specific primers (see Table I-1), and the cDNAs of full-lengths or fragments encoding

PRRs were inserted between the *EcoRI* site and the *SalI* site of pEGFP-C3 using an In-Fusion Advantage PCR Cloning Kit (Clontech). Construction of pGFP-Alix and that of pEGFP-C1/hPLSCR3N (1-78 a.a.) were described previously (Shibata *et al.*, 2008; Katoh *et al.*, 2003). pmEGFP-C3/HsSec31A.L1 was derived from pFLAG-Sec31A (Shibata *et al.*, 2007). Construction of pmEGFP-C2/annexin VII and that of pAnx11Nt-EGFP will be described elsewhere. A human cDNA of PATL1Nt (1-123 a.a.) was obtained from a human embryonic kidney (HEK) 293 cell cDNA library by the PCR method using specific primers (5'-atactcgagccccaagaatgttcgctacga-3' and 5'-gaacttcagatccatcccag-3') designed on the basis of the registered cDNA sequence (NCBI accession number NM_152716.2) and inserted into the *XhoI/EcoRI* site of pEGFP-C1 (pEGFPC1/PATL1Nt). To construct pEGFP-C1/PATL1 PRR, a cDNA fragment encoding a PRR of PATL1 (122-363 a.a.) was amplified by PCR using the cDNA clone MHS1010-99621899 (Open Biosystems) that corresponds to isoform 2, lacking 1-143 a.a. of isoform 1, and the fragment was inserted into the *EcoRI/SalI* sites of pEGFP-C1. To construct pEGFP-C2/PATL1Ct and pEGFP-C1/PATL1ΔNt, a 1.2-kb *SalI* fragment encoding 363-770 a.a. of PATL1 was inserted into the *SalI* site of pEGFP-C1 and into the *SalI* site of pEGFP-C1/PATL1PRR, respectively. To construct pEGFP-C1/PATL1FL, an *XhoI/EcoRI* fragment from pEGFP-C1/PATL1Nt was inserted into the *XhoI/EcoRI* site of pEGFP-C1/PATL1ΔNt.

Cell culture and DNA transfection

HEK293T and HeLa SS4 cells (subcloned HeLa cells, see Ref Shibata *et al.*, 2007) were cultured in DMEM supplemented with 10% fetal bovine serum (FBS), 100 units/ml penicillin and 100 μg/ml streptomycin at 37 °C under humidified air containing 5% CO₂. One day after the cells had been seeded, the cells were transfected with the expression plasmid DNAs by the conventional calcium phosphate precipitation method for HEK293T cells or by using FuGENE 6 (Roche Applied Science) for HeLa cells.

Immunoprecipitation

HEK293T cells transfected with expression plasmids for GFP and GFP-fused proteins were harvested and washed in PBS (137 mM NaCl, 2.7 mM KCl, 8 mM Na₂HPO₄ and 1.5 mM KH₂PO₄, pH 7.4) and then lysed in buffer T (50 mM Tris-HCl, pH 7.5, 150 mM NaCl, 1.5 mM MgCl₂, 0.2% Triton X-100, 0.1 mM pefabloc, 3 μg/ml leupeptin, 1 μM E-64, 1 μM pepstatin, 0.2 mM PMSF). Supernatants obtained by centrifugation at 10,000g were incubated with rabbit anti-GFP antiserum at 4 °C for 1 h. Then the supernatants were incubated with Protein G Sepharose (GE Healthcare Japan, Tokyo) at

4 °C for 1 h. After the beads had been recovered by low-speed centrifugation (700g) for 1 min and washed in lysis buffer T, the immunoprecipitation products were subjected to SDS-PAGE followed by Western blot analysis (WB) and Far Western blot analysis (FW).

In the case of immunoprecipitating endogenous PATL1 with rabbit anti-PATL1 pAb, cells were lysed with buffer H (20 mM HEPES-NaOH, pH 7.4, 142.5 mM KCl, 1.5 mM MgCl₂, 0.2% NP-40, 0.1 mM pefabloc, 3 µg/ml leupeptin, 1 µM E-64, 1 µM pepstatin, 0.2 mM PMSF), and either CaCl₂ (final concentration, 100 µM) or EGTA (final concentration, 5 mM) was added to the cleared lysate to examine Ca²⁺-dependency for interaction with ALG-2. RNase A (final concentration, 125 µg/ml) was also added to exclude potential RNA-binding protein-dependent indirect interactions with ALG-2. Since Protein G Sepharose beads gave higher background signals of ALG-2, Dyna beads Protein G (Invitrogen/Life Technologies Japan, Tokyo) were used, and the beads were collected using a magnetic stand and washed with lysis buffer H containing 100 µM CaCl₂ or 5 mM EGTA.

Western blot and Far-Western blot analyses

Proteins were resolved by SDS-PAGE, transferred to polyvinylidene difluoride (PVDF) membranes (Immobilon-P, Millipore, Bedford, MA, USA), and probed with either specific antibodies for WB or biotinylated ALG-2 (bio-ALG-2) for FW (previously designated bio-ALG-2 overlay assay) essentially as described previously (Sato *et al.*, 2002; Shibata *et al.*, 2008). Chemiluminescent signals were detected by a LAS-3000mini lumino-image analyzer (Fujifilm, Tokyo, Japan) using Super Signal West Pico Chemiluminescent Substrate (Thermo Fisher Scientific Inc., IL, USA).

GST-pulldown

Pulldown assays using GST-fused ALG-2 were carried out essentially as described previously (Shibata *et al.*, 2007; Katoh *et al.*, 2005). Briefly, HEK293T cells were transfected with the expression plasmids for GFP-fused proteins, and the cleared lysates prepared using lysis buffer H were incubated with glutathione Sepharose beads carrying GST-ALG-2 for 2 h on ice in the presence of 10 µM CaCl₂ and RNase A (final concentration, 125 µg/ml). Then the beads were pelleted by low-speed centrifugation and washed three times with lysis buffer H containing 10 µM CaCl₂. The proteins bound to the beads were subjected to SDS-PAGE followed by WB.

Immunofluorescence microscopic analysis

Immunostaining was performed essentially as described previously (Ichioka *et al.*, 2008). Briefly, HeLa cells (2×10^4) were seeded on 18×18 ^{mm}/_{mm} coverslips in dishes of 3 cm in diameter, washed in PBS, fixed in 4% (w/v) paraformaldehyde in PBS at 4 °C for 1 h, and then permeabilized in 0.1% Triton X-100 in PBS at room temperature for 5 min. After blocking with 0.1% (w/v) gelatin in PBS at room temperature for 1 h, the cells on the coverslips were incubated with primary antibodies ($\times 50$ dilution of goat anti-ALG-2 pAb, $\times 500$ dilution of rabbit anti-PATL1 pAb and $\times 200$ dilution of mouse anti-DCP1A mAb) at 4 °C overnight and then with secondary antibodies (each $\times 1000$ dilution of Alexa Fluor 488-labeled donkey anti-goat IgG, Alexa Fluor 555-labeled donkey anti-rabbit IgG and Alexa Fluor 647-labeled donkey anti-mouse IgG) at room temperature for 1 h. Finally, they were mounted with antifading solution [25 mM Tris-HCl, pH 8.7, 10% polyvinyl alcohol, 5% glycerol, 2.5% 1, 4-diazobicyclo (2,2,2)-octane] and analyzed under a confocal laser-scanning microscope FV1000-D equipped with a 60x, 1.35 numerical aperture (NA) oil-immersion objective (UPLSAPO60XO, Olympus, Tokyo). Fluorescence intensities were quantitatively analyzed with ImageJ, a Java-based image processing program developed at the National Institutes of Health and freely available online (<http://rsb.info.nih.gov/ij/>). For analysis of transiently expressed GFP-PAL1 in HeLa cells, $\times 50$ dilution of goat anti-ALG-2 pAb and $\times 1,000$ dilution of Alexa Fluor 555-labeled donkey anti-goat IgG were used as primary and secondary antibodies, respectively, and fluorescence was analyzed with LSM5 PASCAL equipped with a 63x, 1.40 NA oil-immersion objective (Plan-APOCHROMAT 63x/1.40 Oil, Carl Zeiss, Oberkochen, Germany).

Results

In silico screening of new ALG-2-interacting proteins

For searching a database, I used modified motifs of ABM-1 (PPYP, PxYP, PYP, YP(x)₃₋₅YP) based on the variability in the identified or predicted ALG-2-binding sites in ALIX, PLSCR3, annexin A7 (ANXA7) and annexin A11 (ANXA11). Furthermore, since substitution of Phe⁴⁹ with Trp in PLSCR3 increased the binding ability (data not shown), PxPGF/W was assigned as ABM-2. I searched a human protein database in UniProt/SwissProt with the custom-made XaaRR-Scan program under the following conditions: presence of ABM-1 or ABM-2 in a segment of PRR longer than 30 a.a. and containing 25% or more of Pro. A total of 246 ABM-1-type proteins (258 segments) and 36 ABM-2-type proteins (37 segments) were extracted from 20332 entries. After scoring the extracted sequences, I arbitrarily selected 8 proteins with high scores from the ABM-1 type and 10 proteins with potential physiological functions of interest from the ABM-2 type. Since SHISA4 has both motifs of ABM-1 and ABM-2, I selected a total of 17 candidates for *in vitro* binding assays (see Table I-2 for their annotations).

Far-Western analyses

To investigate direct interactions between ALG-2 and the selected candidates, I expressed GFP-fused proteins encoding only a PRR fragment or the full-length in HEK293T cells, immunoprecipitated them with anti-GFP antiserum, and performed Far-Western blot (FW) analyses using biotinylated ALG-2 (bio-ALG-2) as a probe. As shown in each lower panel of Fig. I-1, A-D, signals of GFP-fused proteins (PRR fragment, -p; full-length, -f) were detected in similar intensities by Western blot (WB) analyses of the immunoprecipitates in each series of experiments. In contrast, signal intensities of FW were variable (upper panels). While no signal was observed for GFP used as a negative control (ctrl), positive signals with different intensities were observed for four ABM-1-type proteins (CHERP-p, GRINA-p, MISS-f, VPS37C-p), five ABM-2-type proteins (BCL9-p, LITFL-p, PATL1-p, RBBP6-p, SYVN1-p, TFG-p) and one ABM-1 plus ABM-2-type protein (SHISA4-p) in addition to the previously known ALG-2-interacting proteins (ALIX, ANXA7, ANXA11, Scotin, PLSCR3, Sec31A, RBM22) (Fig. I-1, A-D). Signals stronger than or similar to those for ALIX and Sec31A, which were used as positive controls, were detected for CHERP-p, VPS37C-p and PATL1-p (Fig. I-1, A-D, see Table I-2 for semi-quantitative evaluation). Since the signal of GFP-PATL1-p overlapped with the non-specific signal of IgG heavy chain (Fig. I-1D,

upper panel, single asterisk), I re-examined the ability of PATL1 to interact with ALG-2 by overexpressing GFP-fused full-length PATL1 (PATL1-f) and compared with GFP-Sec31A-f (positive control), GFP-RBM22-f and unfused GFP (negative control). As shown in Fig. I-1E, regardless of similar intensities in WB signals of GFP (ctrl) and GFP-PATL1-f (lower panel), the FW signal for PATL1-f showed signal intensity similar to that of GFP-Sec31A-f (upper panel). The strongest FW signal was observed for RBM22 (RNA-binding motif 22, regulating splicing process) (Fig. I-1, A and E), which was previously found to be an ALG-2-interacting factor by the yeast two-hybrid method and was shown to induce translocation of ALG-2 to the nucleus by exogenous overexpression in NIH 3T3 cells (Montaville *et al.*, 2006).

Identification of ALG-2-binding region in PATL1

I selected PATL1 for further analyses. It has a long PRR (residue No. 155-338; Pro, 24.5%) in the first half of the primary structure and contains a sequence (307-QMLPPAPGFRAFFSA-321; ABM-2, underlined) similar to those of the second ALG-2-binding sites in PLSCR3 and Sec31A (Fig. I-2A). To determine whether this 15-residue ABM-2-containing sequence is sufficient for direct binding of PATL1 to ALG-2, I constructed expression vectors encoding this region as well as the full-length and truncated mutants of PATL1 that were fused with GFP and performed FW using bio-ALG-2. While signals of bio-ALG-2 binding were readily detected for the constructs encoding 1-770 (full-length) and 122-363 containing a PRR, the signals for the construct encoding 307-321 were detected only after a longer exposure regardless of similar or stronger WB signals (Fig. I-2B). No signals were detected for unfused GFP (ctrl) and for a degraded fragment of GFP-PATL1 363-770 (~32 kDa) under the condition used.

GST-pulldown assays

There exists an alternatively spliced minor isoform of human ALG-2 lacking Gly¹²¹Phe¹²² (designated ALG-2^{ΔGF122}; the longer major isoform being designated wild-type, WT, for convenience) (Maki *et al.*, 2011). Since Sec31A and PLSCR3 (ABM-2-containing proteins) bind both ALG-2^{WT} and ALG-2^{ΔGF122}, I investigated whether PATL1 and RBM22 also bind ALG-2^{ΔGF122} by GST-pulldown assays using GFP-PATL1 and GFP-RBM22 in the presence of 10 μM CaCl₂ (Fig. I-3). GST (negative control), GST-ALG-2^{WT} and ALG-2^{ΔGF122} were immobilized to glutathione Sepharose beads in molar excess of GST over the amount of GST-ALG-2 (CBB staining, lower panel). Proteins pulled down from the lysates (pulldown products) were analyzed

by WB with anti-GFP mAb. There were no detectable signals in the pulldown products of GST. As expected, signals of GFP-PATL1 were detected in the pulldown products of both GST-ALG-2^{WT} and GST-ALG-2^{ΔGF122}. Unexpectedly, however, signals were barely detectable for GFP-RBM22 even in the pulldown products of GST-ALG-2^{WT} as in the case of unfused GFP (negative control, ctrl).

Co-immunoprecipitation of endogenous PATL1 and ALG-2

Since anti-PATL1 antibody was not commercially available, I raised rabbit anti-PATL1 antisera and affinity-purified polyclonal antibody (pAb), which could be used for WB, immunoprecipitation and immunofluorescence microscopic analyses. I first investigated whether interaction between endogenous proteins of PATL1 and ALG-2 can be observed in the lysates of HEK293T cells by a co-immunoprecipitation assay, in which immunoprecipitates obtained in the presence of 5 mM EGTA or 100 μM CaCl₂ were analyzed by WB using respective antibodies for PATL1 and ALG-2. As shown in the upper panel of Fig. I-4, a band of approximately 100 kDa was detected by immunoprecipitation with anti-PATL1 pAb but not with control (ctrl) IgG. Specific doublet bands were detected by WB with anti-ALG-2 pAb in the case of immunoprecipitation with anti-PATL1 pAb in the presence of 100 μM CaCl₂ but not in the presence of 5 mM EGTA. No ALG-2 bands were detected in the case of IgG in either condition.

Immunofluorescence microscopic analyses

PATL1 is a scaffolding protein of P-bodies that are distributed as non-membranous cytoplasmic foci associated with translation repression and processing of mRNA for degradation (Scheller *et al.*, 2007; Ozgur *et al.*, 2010). Overexpression of GFP-PATL1 in HeLa cells showed punctate distribution by fluorescence microscopic analyses, and fluorescence signals of GFP-PATL1 were merged with those for endogenous ALG-2 as revealed by immunostaining with goat anti-ALG-2 pAb (Fig. I-5). I performed triple-immunostaining of HeLa cells with rabbit anti-PATL1 pAb and goat anti-ALG-2 pAb together with mouse mAb against either mRNA-decapping enzyme 1A (DCP1A) or Sec31A, a coat component of COPII, which is involved in endoplasmic reticulum (ER)-Golgi vesicular transport. Signals representing ALG-2 were shown as many puncta in the cytoplasm and also as a diffused image in the entire cell including the nucleus (Fig. I-6A, panels a and e). On the other hand, observed fluorescent puncta for PATL1 (panels b and f) were merged well with those for DCP1A (panels c and g), but the number of puncta was significantly smaller than the number of puncta representing

ALG-2. The punctate signals for PATL1 and DCP1A were merged with those for ALG-2 as shown by arrowheads in the merged images (panels d and h), but fluorescence intensities of ALG-2 in these puncta were weaker than those in other puncta. As shown in Fig. I-6B, most of the punctate fluorescence signals of ALG-2 were merged with those of Sec31A (panels i, k and l, open arrowheads), and only a few puncta contained signals of PATL1 (panels i, j and l, closed arrowheads). When fluorescence intensities along the line segment crossing two closely located puncta of PATL1 and Sec31A were quantitatively measured for relative fluorescence intensity with ImageJ (Fig. I-6B, panel m, from p_1 to p_2), the value of ALG-2 in PATL1 puncta was approximately 60% of that in Sec31A puncta (Fig. I-6B, panel n).

Discussion

Many non-enzymatic cellular proteins interact with other proteins to regulate their functions, bridge them to other targets as adaptors and form networks to induce various physiological phenomena. ALIX (also previously called AIP1) is the first protein identified as an ALG-2-interacting protein (Missotten *et al.*, 1999; Vito *et al.*, 1999). Okumura *et al.*, previously reported that a dimer of ALG-2 functions as a Ca²⁺-dependent adaptor that bridges ALIX and TSG101 (Okumura *et al.*, 2009). In addition to other previously published ALG-2-interacting proteins including Scotin (Draeby *et al.*, 2007), annexin A11 (Satoh *et al.*, 2002a), Sec31A (Yamasaki *et al.*, 2006; Shibata *et al.*, 2007) and PLSCR3 (Shibata *et al.*, 2007), several proteins have been registered as novel ALG-2-interacting partners in online-accessible public interactome databases (e.g., BioGRID, <http://thebiogrid.org/>), which document results of high-throughput yeast two-hybrid or mass spectrometric analyses of affinity-purified proteins with suitable tags that were expressed transiently in cultured cells, but their individual interactions have not been validated by other biochemical methods. To obtain more information on protein-protein interaction networks involving ALG-2, I carried out a semi-largescale screening of novel ALG-2-interacting proteins by different approaches in this study: first by *in silico* screening of a human amino acid sequence database by finding two types of ALG-2-binding motifs (ABM-1 and ABM-2) in Pro-rich regions (PRRs) and then by Far-Western (FW) screening of GFP-fused proteins expressed in HEK293T cells using biotinylated ALG-2 as a probe in protein interaction assays. Ten proteins with various potential physiological functions showed positive interactions with different degrees in FW signals (Fig. I-1, Table I-2). Among these potential targets of ALG-2, I focused on PATL1, which was identified as a human homolog of yeast mRNA decapping activator Pat1 (Scheller *et al.*, 2007) and was reported to promote mRNA degradation by connecting deadenylation with decapping (Ozgur *et al.*, 2010).

To confirm the authenticity of the interaction between ALG-2 and PATL1, I performed interaction analyses employing different methods: (i) GST-ALG-2 pulldown assays (Fig. I-3), (ii) co-immunoprecipitation assays using a specific antibody for

endogenous PATL1 (Fig. I-4), and (iii) immunofluorescence microscopic analyses of subcellular co-localization (Fig. I-6). Results of these experiments further support that PATL1 is a genuine ALG-2-interacting protein. On the other hand, physiological interaction between RBM22 and ALG-2 is open to question. Montaville *et al.* isolated RBM22 as an ALG-2-interacting protein by yeast two-hybrid screening and demonstrated that overexpression of RBM22-EGFP (enhanced GFP) caused translocation of co-expressed ALG-2 fused with monomeric red fluorescent protein (mRFP) in NIH3T3 cells, but interaction between the two proteins was not evaluated by biochemical analyses (Montaville *et al.*, 2006). Although the strongest FW signals were observed for both PRR and full-length of GFP-RBM22 (Fig. I-1, A and E), GFP-RBM22 was not detected in the pulldown products of GST-ALG-2 (Fig. I-3). No signals were detected for endogenous ALG-2 in the immunoprecipitates of GFP-RBM22 (data not shown). Failure in detection of their interaction in cell lysates may be explained as follows: the binding site for ALG-2 is masked by other RBM22-interacting proteins or by itself *in vivo*, but the concealed region is exposed upon SDS- and heat-denaturation during sample treatment for SDS-PAGE preceding FW. I cannot exclude the possibility, however, that exposure of the binding site may occur *in vivo* and RBM22 interacts with ALG-2 under unknown physiological conditions.

Mammalian ALG-2 has a shorter minor isoform, lacking Gly¹²¹Phe¹²² (Maki *et al.*, 2011; Tarabykina *et al.*, 2000) and generated by alternative splicing at the splicing donor site of exon 4 (Maki *et al.*, 2011). PATL1 has the ability for binding to both wild type and the isoform designated ALG-2^{ΔGF122} (Fig. I-3). Shibata *et al.* previously classified ALG-2-binding proteins into ALIX-type and non-ALIX-type based on the ability to bind to ALG-2^{ΔGF122} and similarity in the amino acid sequences of the ALG-2 binding sites (Shibata *et al.*, 2008). X-ray crystal structural analyses of the complex between ALG-2 and an ALIX peptide containing ABM-1 (PxPYP_{x3-5}YP) revealed that the peptide binds to two hydrophobic pockets (Pocket 1 and Pocket 2) that accept PPPYP and YP, respectively, where Pocket 1 is more important for interaction (Suzuki *et al.*, 2008). Pocket 1 is closed in the Ca²⁺-free form of ALG-2 but opened in the Ca²⁺-bound form, whereas it is kept closed in the Ca²⁺-bound form of ALG-2^{ΔGF122}

(Inuzuka *et al.*, 2010). Our research group recently found that a Sec31A peptide, containing ABM-2 (PxPGF), binds to a hydrophobic pocket different from Pocket 1 and Pocket 2 (unpublished observation), partly explaining the capability of ALG-2^{ΔGF122} for binding to ABM-2-containing proteins including PATL1 (Fig. I-3). Since FW analysis of GFP fused with a short segment containing ABM-2 of PATL1 showed weak ability to interact with ALG-2 compared with the entire PRR, regions other than ABM-2 in PRR may also contribute to interaction with ALG-2 (Fig. I-2B).

Immunofluorescence confocal microscopic analyses have revealed that endogenous ALG-2 is present both in the nucleus and in the cytoplasm (Shibata *et al.*, 2007; Shibata *et al.*, 2004), where it is distributed in a punctate pattern and mainly localizes to Sec31A-positive endoplasmic reticulum (ER) exit sites (Yamasaki *et al.*, 2006; Shibata *et al.*, 2007). Since PATL1 is localized to discrete cytoplasmic foci designated P-bodies (Scheller *et al.*, 2007; Ozgur *et al.*, 2010), I predicted at first that punctate signals of ALG-2 co-localized to PATL1 were as strong as those co-localized to Sec31A. However, in fact, I observed only a modest accumulation of ALG-2 at larger foci of PATL1, and the relative intensity of ALG-2 signal in a PATL1 focus was approximately 60% of that in Sec31A (Fig. I-6B). It is possible that anti-ALG-2 antibody may easily gain access to Sec31A in the ER exit sites but not to PATL1 in P-bodies. Franks and Lykke-Andersen suggested that the mRNA decay machinery is limited in a larger P-body that is visible under a microscope, whereas it is unlimited and active under the condition that the P-body remains submicroscopic before aggregation of mRNAs with various RNA-binding and -processing proteins (Franks *et al.*, 2007). ALG-2 may interact with PATL1 in a state invisible to the microscope during the process of P-body formation or function in other cellular pathways involving PATL1.

PATL1 and its ortholog in yeast are thought to regulate P-body formation (Pilkington *et al.*, 2008; Franks *et al.*, 2008). The N region in PATL1, corresponding to the PRR, strongly promotes the formation of P-bodies, and PATL1 self-interacts via this region (Ozgur *et al.*, 2010). Since ALG-2 interacts with PATL1 PRR Ca²⁺-dependently, I hypothesized that ALG-2 is involved in P-body formation by binding to the PRR in PATL1. To test this hypothesis, I carried out co-immunoprecipitation assays with anti-GFP serum using lysates of HEK293T cells transfected with expression vectors of

GFP-fused PATL1 and FLAG-tagged PATL1. FLAG-PATL1 was co-immunoprecipitated with GFP-PATL1 even in the presence of 5 mM EGTA, suggesting that Ca²⁺-dependent binding of ALG-2 to PATL1 does not influence oligomerization of PATL1 (Fig. I-7). PATL1 and its orthologs associate with other P-body components such as the decapping enzymes DCP2 and DCP1A and a component of the deadenylation complex, Caf1a, and they are involved in the 5' to 3' mRNA decay pathway (Ozgur *et al.*, 2010; Braun *et al.*, 2010; Haas *et al.*, 2010 and see Marnef *et al.*, 2010 for review). Future studies are necessary to determine whether ALG-2 is involved in post-transcriptional control in association with PATL1.

PATL1 and other P-body factors including DDX6/Rck/p54 and LSM1 are required for effective translation and replication of hepatitis C virus (HCV) RNA (Scheller *et al.*, 2009). HCV-JFH1 infection disrupts P-body formation of DDX6, LSM1, Xrn1, PATL1 and Ago2 and redistributes these factors to the HCV production factory around lipid droplets in HuH-7-derived RSc cells (Ariumi *et al.*, 2011). To investigate the possibility of involvement of ALG-2 in HCV RNA replication and infection, I performed immunofluorescence microscopic analysis of HCV-infected RSc cells and observed partial co-localization of ALG-2 and the HCV core that were both recruited around lipid droplets (data not shown). However, knockdown of ALG-2 in RSc cells by ALG-2 siRNA transfection did not show significant effects on HCV RNA replication and infectivity by real-time RT-PCR analysis and a focus-forming assay to measure virus titers, respectively (data not shown).

Marnef *et al.* recently reported that PATL1 is a nucleocytoplasmic shuttling protein and accumulates in nuclear speckles, foci close to or overlapping with PML bodies and nucleolar caps, suggesting that PATL1 may participate in several RNA-related nuclear processes such as transcription and splicing, in addition to cytoplasmic gene regulation (Marnef *et al.*, 2012). Although ALG-2 is present in the nucleus to some extent (Shibata *et al.*, 2007; Shibata *et al.*, 2004 and Fig. I-6A), the mechanism of nuclear translocation remains unclear. ALG-2, 22 kDa as a monomer, may move to the nucleus merely by passive diffusion or may be actively transported to this organelle by association with RNA-related proteins including PATL1 or other unknown proteins. Although the present study did not show involvement of ALG-2 in the cytoplasmic regulation of gene expression by PATL1 such as translation repression, mRNA degradation and P-body formation, there remains the possibility that ALG-2 and PATL1 play roles in RNA

processing or other subnuclear functions within the nucleus. Since ALG-2 functions as a Ca^{2+} -dependent adaptor protein (Maki *et al.*, 2011; Okumura *et al.*, 2009), PATL1 might also have a binding partner that associates in the presence of Ca^{2+} -loaded ALG-2. Studies are in progress to search for such partners among the potential ALG-2-interacting proteins that were newly identified in this study.

Table 1-1. Oligo nucleotide primers used for subcloning a cDNA fragment encoding a Pro-rich region (PRR) or full-length (FL) by PCR. For in-fusion PCR, the forward and reverse primers contain common sequences identical with the sequences of pEGFP-C3 (underlined); forward, ctaagcttgaattc; reverse, ccggctaccgtcgac. In-fusion PCR was performed by using (*) cDNA previously subcloned in the laboratory, (**) purchased cDNA from OpenBiosystems or (***) a cDNA library directly or (**) after the 1st PCR using primers located upstream and downstream of the forward and reverse primers for in-fusion PCR, respectively, (sandwich PCR). (From Osugi *et al.*, *Journal of Biochemistry*, 151:657-666, 2012)

Protein/Gene Names (subcloned region, aa)	NCBI Accession No.	Specific primers		Templates	Types of PCR
		Forward	Reverse		
ABIB PRR (111-310 aa)	NM_016428.2	5'- <u>ctcaacttccaa</u> ttcccttggccactgctccag-3'	5'- <u>cccccctaccctccca</u> caagc atgagcaaggc-3'	*2) MHSA771-99610790	In-fusion
AUX PRR (717-868 aa)	NM_013374.4	5'- <u>ctcaacttccaa</u> ttcccttggccactgctccag-3'	5'- <u>cccccctaccctccca</u> caagc atgagcaaggc-3'	*1) pEGFP-C3-hAlix	In-fusion
ANKA7 PRR (1-150 aa)	NM_001156.3	5'- <u>ctcaacttccaa</u> ttcccttggccactgctccag-3'	5'- <u>cccccctaccctccca</u> caagc atgagcaaggc-3'	*1) pmGFP-C2/annexin VII	In-fusion
BC19 PRR (870-1029 aa)	NM_004326.2	5'- <u>ctcaacttccaa</u> ttcccttggccactgctccag-3'	5'- <u>cccccctaccctccca</u> caagc atgagcaaggc-3'	*3) aHEK293 cell cDNA library	In-fusion
CHERP PRR (343-690 aa)	NM_006387.5	5'- <u>gtacttccaa</u> ttcccttggccactgctccag-3'	5'- <u>cccccctaccctccca</u> caagc atgagcaaggc-3'	*3) aHEK293 cell cDNA library	sandwich
GRINA PRR (1-165 aa)	NM_000837.1	5'- <u>ctcaacttccaa</u> ttcccttggccactgctccag-3'	5'- <u>cccccctaccctccca</u> caagc atgagcaaggc-3'	*4) 1st sandwich PCR product	In-fusion
LITFL FL (1-208 aa)	NM_00119054.1	5'- <u>ctcaacttccaa</u> ttcccttggccactgctccag-3'	5'- <u>cccccctaccctccca</u> caagc atgagcaaggc-3'	*2) MHS1011-98054368	In-fusion
MISS FL (1-245 aa)	NM_144578.3	5'- <u>ctcaacttccaa</u> ttcccttggccactgctccag-3'	5'- <u>cccccctaccctccca</u> caagc atgagcaaggc-3'	*3) aHEK293 cell cDNA library	In-fusion
PATL1 PRR (141-345 aa)	NM_152716.2	5'- <u>ctcaacttccaa</u> ttcccttggccactgctccag-3'	5'- <u>cccccctaccctccca</u> caagc atgagcaaggc-3'	*2) MHS1011-76472	In-fusion
RBBP6 PRR (332-829 aa)	NM_006910.4	5'- <u>ctcaacttccaa</u> ttcccttggccactgctccag-3'	5'- <u>cccccctaccctccca</u> caagc atgagcaaggc-3'	*3) aHEK293 cell cDNA library	In-fusion
RBML6 PRR (616-1081 aa)	NM_014892.3	5'- <u>ctcaacttccaa</u> ttcccttggccactgctccag-3'	5'- <u>cccccctaccctccca</u> caagc atgagcaaggc-3'	*3) aHEK293 cell cDNA library	sandwich
RBW22 PRR (306-420 aa)	NM_001031685.2	5'- <u>ctcaacttccaa</u> ttcccttggccactgctccag-3'	5'- <u>cccccctaccctccca</u> caagc atgagcaaggc-3'	*4) 1st sandwich PCR product	In-fusion
Scotin PRR (156-240 aa)	NM_016479.3	5'- <u>ctcaacttccaa</u> ttcccttggccactgctccag-3'	5'- <u>cccccctaccctccca</u> caagc atgagcaaggc-3'	*2) MHS1010-57567	In-fusion
SHSAA PRR (122-197 aa)	NM_198149.2	5'- <u>ctcaacttccaa</u> ttcccttggccactgctccag-3'	5'- <u>cccccctaccctccca</u> caagc atgagcaaggc-3'	*1) pMIE18 SFL3/Hs Scotin	In-fusion
SMARCC1 PRR (967-1105 aa)	NM_003074.3	5'- <u>ctcaacttccaa</u> ttcccttggccactgctccag-3'	5'- <u>cccccctaccctccca</u> caagc atgagcaaggc-3'	*3) aHEK293 cell cDNA library	In-fusion
SVNL1 PRR (327-488 aa)	NM_172230.2	5'- <u>ctcaacttccaa</u> ttcccttggccactgctccag-3'	5'- <u>cccccctaccctccca</u> caagc atgagcaaggc-3'	*3) aHEK293 cell cDNA library	sandwich
TFG PRR (156-400 aa)	NM_001007565.2	5'- <u>ctcaacttccaa</u> ttcccttggccactgctccag-3'	5'- <u>cccccctaccctccca</u> caagc atgagcaaggc-3'	*4) 1st sandwich PCR product	In-fusion
TP53BP2 PRR (810-903 aa)	NM_001031685.2	5'- <u>ctcaacttccaa</u> ttcccttggccactgctccag-3'	5'- <u>cccccctaccctccca</u> caagc atgagcaaggc-3'	*3) aHEK293 cell cDNA library	In-fusion
WBP2 PRR (141-261 aa)	NM_001031685.2	5'- <u>ctcaacttccaa</u> ttcccttggccactgctccag-3'	5'- <u>cccccctaccctccca</u> caagc atgagcaaggc-3'	*3) aHEK293 cell cDNA library	sandwich
ZNF598 PRR (562-768 aa)	NM_178167.2	5'- <u>ctcaacttccaa</u> ttcccttggccactgctccag-3'	5'- <u>cccccctaccctccca</u> caagc atgagcaaggc-3'	*4) 1st sandwich PCR product	In-fusion
ZNF28 FL (1-1055 aa)	NM_033113.2	5'- <u>ctcaacttccaa</u> ttcccttggccactgctccag-3'	5'- <u>cccccctaccctccca</u> caagc atgagcaaggc-3'	*3) aHEK293 cell cDNA library	sandwich
		5'- <u>ctcaacttccaa</u> ttcccttggccactgctccag-3'	5'- <u>cccccctaccctccca</u> caagc atgagcaaggc-3'	*4) 1st sandwich PCR product	In-fusion
		5'- <u>ctcaacttccaa</u> ttcccttggccactgctccag-3'	5'- <u>cccccctaccctccca</u> caagc atgagcaaggc-3'	*2) BHS1001-9409051	In-fusion

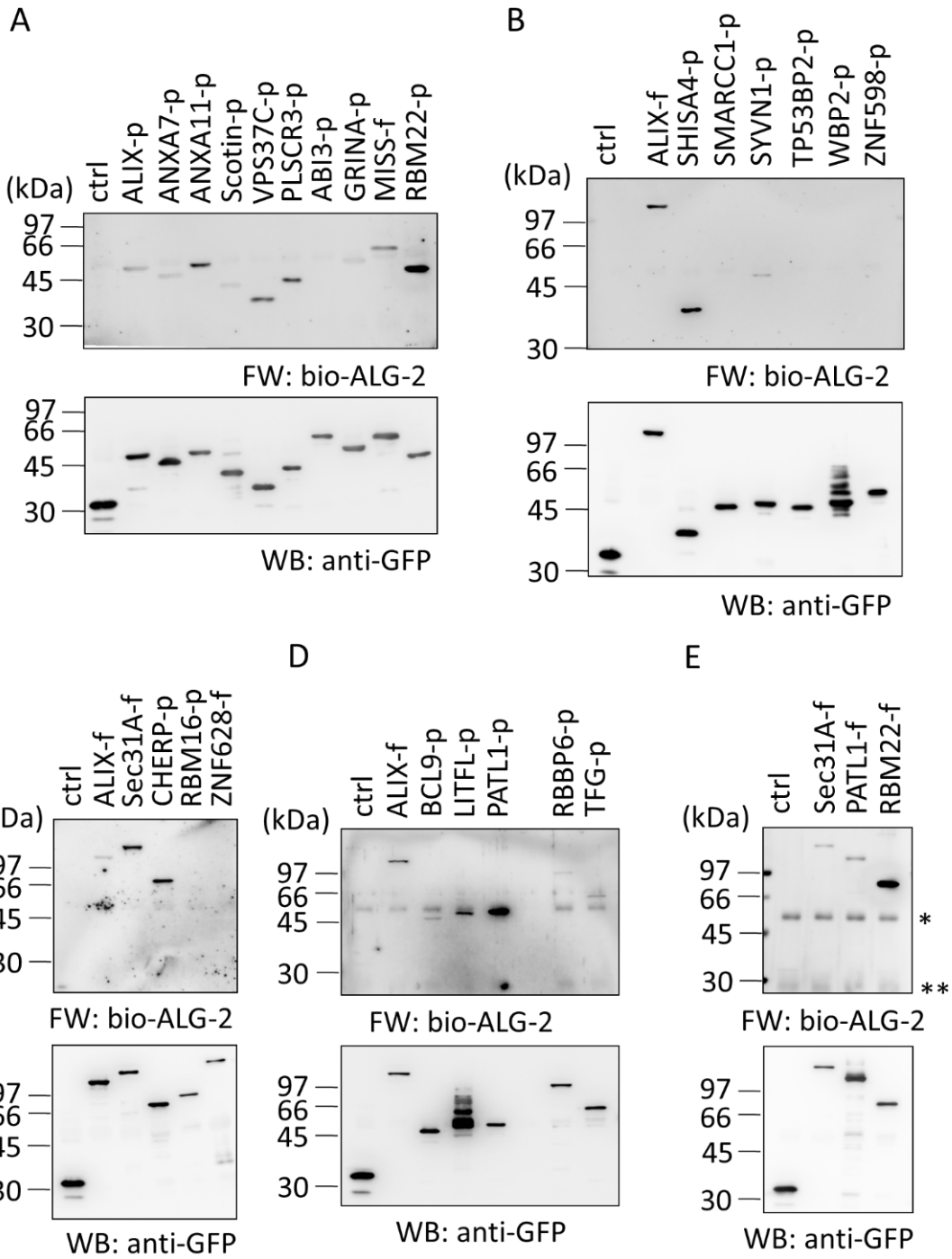


Fig. I-1 Far Western blot analyses of ALG-2-interacting proteins with biotinylated ALG-2. HEK293T cells were transfected with expression vectors for GFP (used as a negative control, ctrl) or each candidate of GFP-fused ALG-2-interacting proteins. At 24 h after transfection, cells were lysed with buffer T (see Materials and Methods) by gentle mixing (A-D) or by sonication (E), and the supernatants (cleared lysates) obtained after centrifugation at 10,000g for 15 min were immunoprecipitated with a rabbit anti-GFP serum. The immunoprecipitates were resolved by SDS-PAGE and subjected to Far Western blot analyses (FW) using biotinylated ALG-2 (bio-ALG-2) (upper panels) and Western blot analyses (WB) using anti-GFP mAb (lower panels). GFP-fusion proteins containing only proline-rich regions and full-length sequences of the analyzed human proteins are designated -p and -f after the protein names, respectively (A-D). GFP-fused full-length proteins of Sec31A, PATL1 and RMB22 were similarly analyzed (E). Single and double asterisks indicate non-specific binding of bio-ALG-2 to immunoglobulin G (IgG) heavy and light chains, respectively. UniProt accession codes, features and evaluation of abilities to interact with ALG-2 are listed in Table I-2. (From Osugi *et al.*, *Journal of Biochemistry*, 151: 657-666, 2012)

Table 1-2. List of proteins analyzed by Far-Western blotting (FW) in this study. *By in silico* screening, sequences of proteins with Pro-rich regions (PRR) containing ALG-2-binding motifs (ABM-1 type, 246 ; ABM-2 type, 36) were retrieved from 20332 entries of human protein database at UniProt/SwissProt, and 17 proteins were further selected for FW. Previously known ALG-2-interacting proteins were also analyzed. Accession No. and features are cited from UniProt/SwissProt (<http://www.uniprot.org/>). Semi-quantitative evaluation of FW shown in Fig. 1 are scored and indicated by +++ (very strong), ++ (strong), + (moderate), + (weak) and - (negative). (From Osugi et al., Journal of Biochemistry, 151: 657-666, 2012)

Protein/gene names	UniProt Accession No.	Length (aa)	Alternative names & Features	Far-Western evaluation
ABM-1				
<i>Previously known for interaction with ALG-2</i>				
ALIX	Q8WUM4	868	PDCD6IP, apoptosis, cell cycle, cell division, host-virus interaction, protein-transport	++
Annexin A7	P20073	488	ANXA7, Synexin, calcium/phospholipid-binding protein, membrane fusion, exocytosis	++
Annexin A11	P50995	505	ANXA11, Annexin XI, calcium/phospholipid-binding protein, cell cycle, cell division	+++
Scotin	Q8N114	240	SHISA5, p53 dependent-apoptosis	+
<i>Candidates selected for FW</i>				
CHERP	Q8IWX8	916	ERPROT213-21, ER protein, calcium homeostasis, cell growth, proliferation	+++
GRINA	Q7Z429	371	NMDARA1, glutamate [NMDA] receptor-associated protein	+
MISS	Q8NDC0	245	MAPK1IP1L, MAPK-interacting and spindle-stabilizing protein-like	++
SMARCC1	Q92922	1105	SW/SNF complex 155 kDa subunit, chromatin remodeling	-
TP53BP2	Q13625	1128	Apoptosis-stimulating of p53 protein 2, involved in apoptosis and cell cycle	-
VPS37C	A5D8V6	355	A component of the ESCRT- I complex, a regulator of vesicular trafficking process	+++
WBP2	Q969T9	261	WW domain-binding protein 2; interacts with NEDD4	-
ABM-2				
<i>Previously known for interaction with ALG-2</i>				
RBM22	Q9NW64	420	RNA-binding motif protein 22, pre-mRNA splicing factor	+++
Sec31A	O94979	1220	COP II component, ER-Golgi transport vesicles	+++
<i>Candidates selected for FW</i>				
ABI3	Q9P2A4	366	Nesh, regulation of cell migration, SH3	-
BCL9	O00512	1426	B-cell CLL/lymphoma 9 protein, involved in signal transduction through the Wnt pathway	+
LITFL	Q9H305	208	LITAF-like protein, p53 dependent-apoptosis	++
PATL1	Q86TB9	770	PAT1-like protein 1, P-body formation, mRNA decay	+++
RBBP6	Q7Z6E9	1792	Retinoblastoma-binding protein 6, E3 ubiquitin-protein ligase	+
RBM16	Q9UPN6	1271	RNA-binding motif protein 16, SCAF8, mRNA processing	-
SYVN1	Q86TM6	617	Synovial apoptosis inhibitor 1, like an E3 ubiquitin-protein ligase, ER-associated degradation	+
TFG	Q92734	400	TRK-fused gene protein, positive regulation of I-kappaB kinase/NF-kappaB cascade	+
ZNF598	Q86UK7	904	C2H2 and RING-type zinc finger protein	-
ZNF628	Q5EBL2	1055	transcription activator, C2H2 zinc finger protein	-
ABM-1 & ABM-2				
<i>Previously known for interaction with ALG-2</i>				
PLSCR3	Q9NRY6	295	Named after phospholipid scramblase, but the activity seems unphysiological	+++
<i>A candidate selected for FW</i>				
SHISA4	Q96DD7	197	SHISA family protein, single-transmembrane protein	++

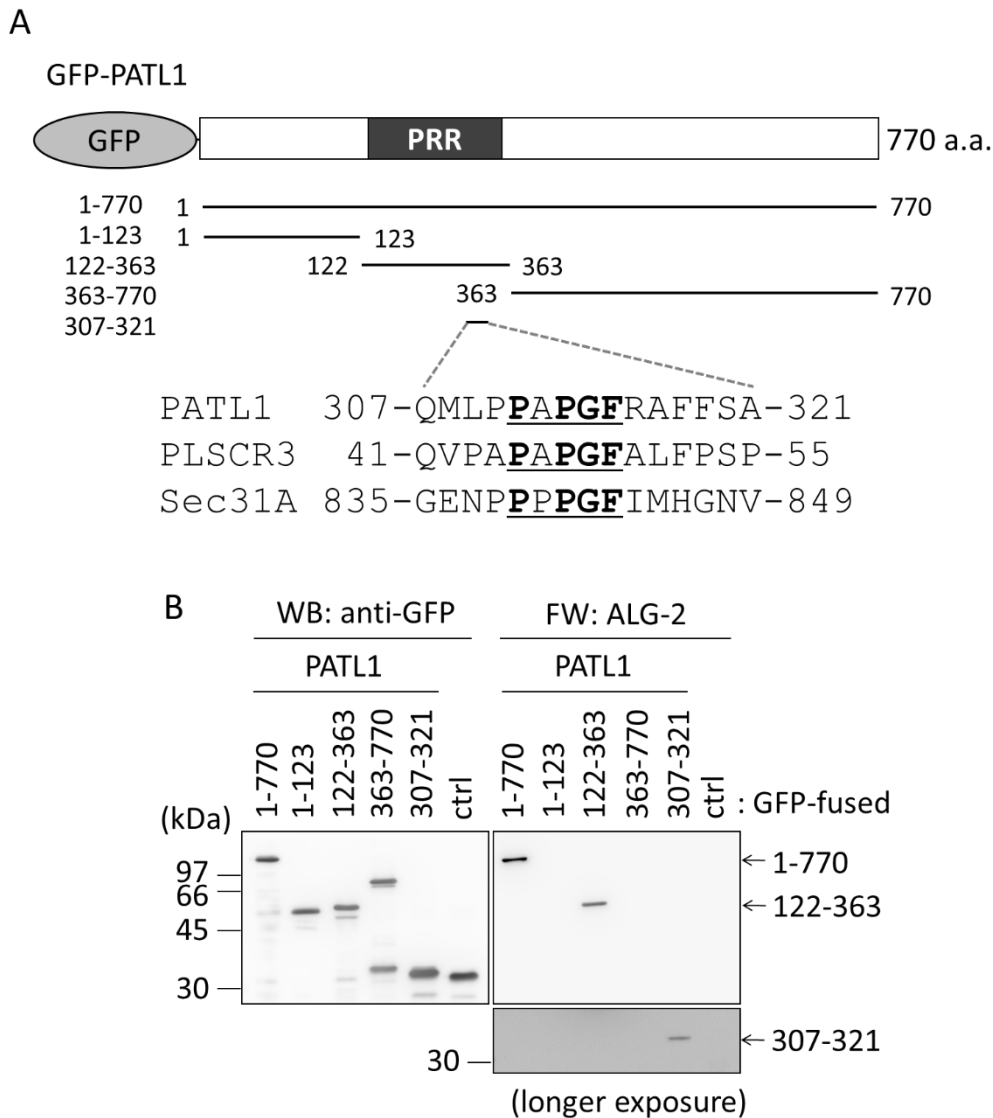


Fig. I-2 Identification of the ALG-2-binding site in PATL1. (A) A schematic diagram of GFP-fused PATL1 and its deletion mutants expressed transiently in HEK293T cells. The proline-rich region (PRR) is indicated by a closed box. Numbers indicate fragments of PATL1 fused with GFP. A segment containing an ALG-2 binding motif 2 (ABM-2) has a consensus sequence of P α PGF (marked with asterisks above the sequence) that is found in the minimal binding regions of PLSCR3 and Sec31A. Identical residues found in these regions of PATL1, PLSCR3 and Sec31A are represented in bold face. (B) Far Western blot analysis was performed as described in the legend to Fig. I-1. Exposure time in chemiluminescence detection, 30 s. An image of longer exposure time (300 s) is shown in the right lower panel for the area surrounded by broken line in the upper panel. (From Osugi *et al.*, *Journal of Biochemistry*, 151: 657-666, 2012)

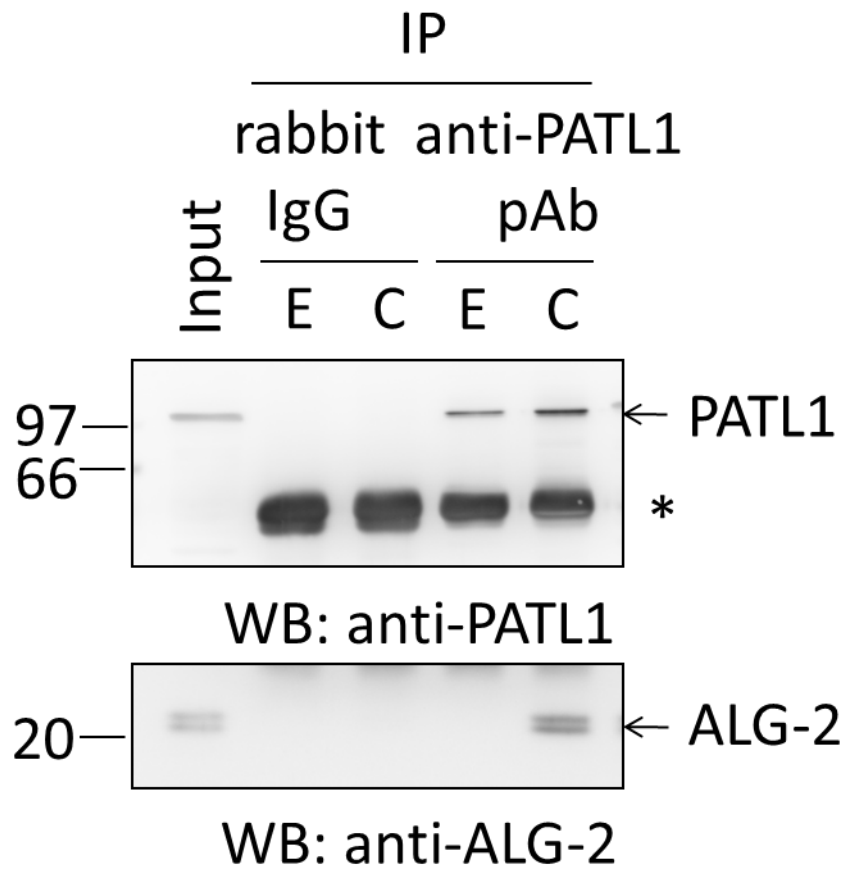


Fig. I-4 Co-immunoprecipitation of endogenous PATL1 and ALG-2. HEK293T cells were lysed with lysis buffer T (see Materials and Methods). After addition of EGTA to 5 mM (E) or CaCl₂ to 100 μM (C), the cleared cell lysate (Input) was subjected to immunoprecipitation by incubating first with either rabbit IgG (used as a negative control, ctrl) or rabbit anti-PATL1 polyclonal antibody (pAb) for 2 h at 4 °C and then with magnetic beads carrying Protein G. After the beads had been collected and washed, immunoprecipitated proteins (IP) were resolved by SDS-PAGE and subjected to WB using anti-PATL1 pAb (upper panel) and anti-ALG-2 (lower panel). Asterisk, IgG heavy chain. The relative amount of cleared cell lysate proteins (Input) used for analysis of IP products was 1.5%. (From Osugi *et al.*, *Journal of Biochemistry*, 151: 657-666, 2012)

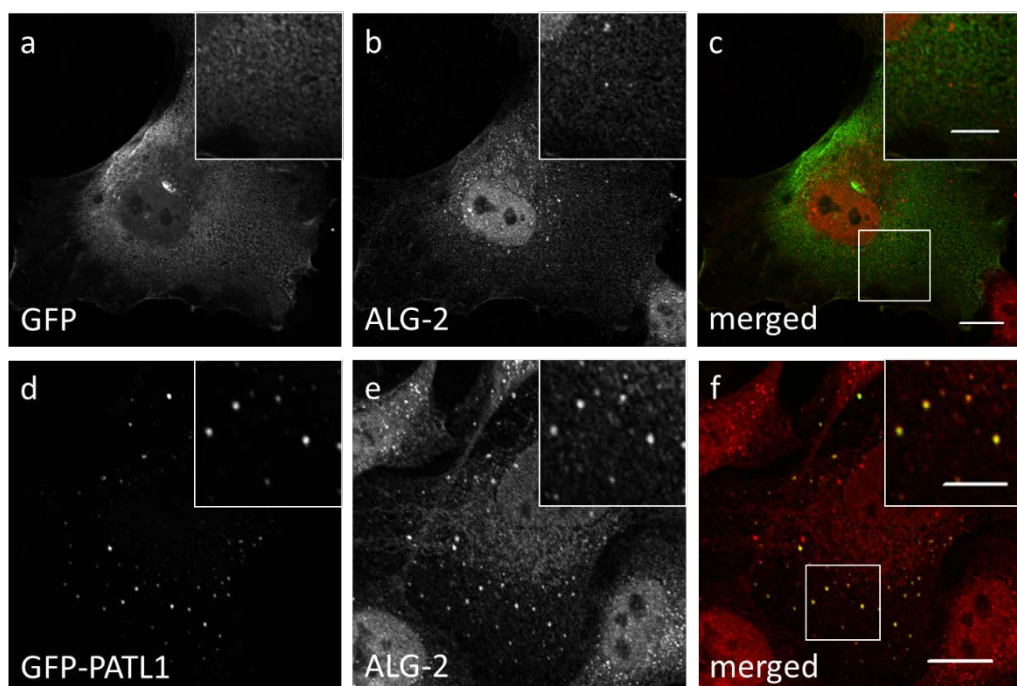


Fig. I-5 Colocalization of ALG-2 with GFP-PATL1 at cytoplasmic puncta. HeLa cells were seeded on coverslips and transfected with an expression vector for GFP (a-c) or GFP-PATL1 (d-f). After 24 h, the cells were fixed and permeabilized with 0.1% Triton X-100 and then immunostained with a goat anti-ALG-2 polyclonal antibody. Alexa 555-labeled donkey anti-goat IgG was used as a secondary antibody. The fluorescence signals of GFP (a, d, green) and Alexa 555 (b, e, red) were analyzed with a confocal laser-scanning microscope and are represented in black and white. Merged images are shown in (c) and (f), respectively, in color. The small boxed areas are magnified in the respective large boxed areas. Bars, 10 μ m. (From Osugi *et al.*, *Journal of Biochemistry*, 151: 657-666, 2012)

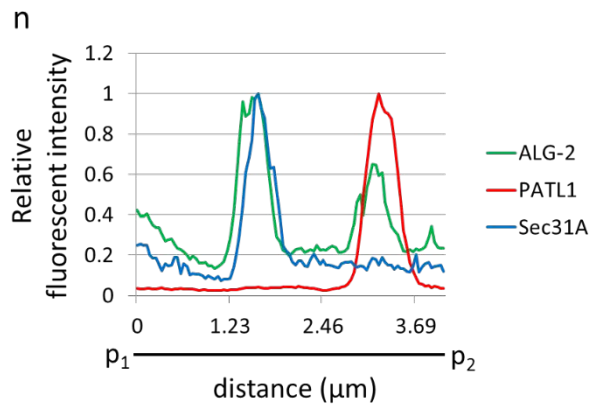
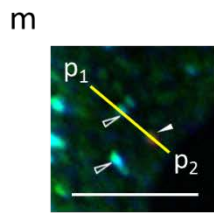
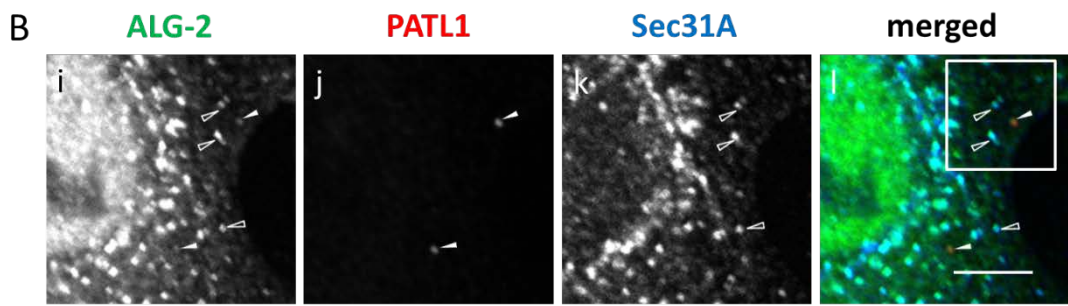
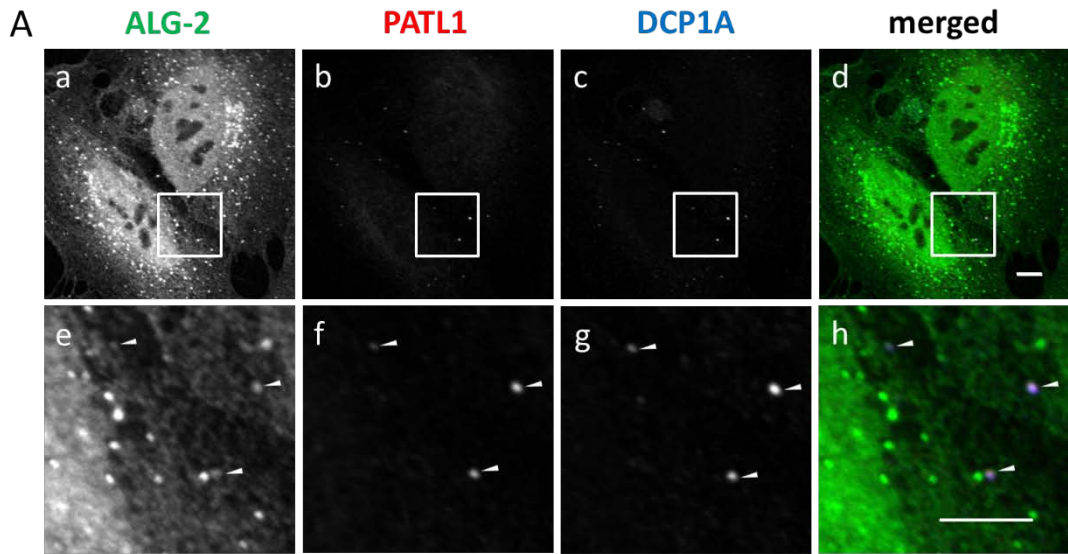


Fig. I-6 Punctate subcellular distribution of PATL1 and partial colocalization with ALG-2. HeLa cells were cultured on coverslips, fixed, and permeabilized with 0.1% Triton X-100. Then the cells were triple-stained with a goat anti-ALG-2 pAb (green), a rabbit anti-PATL1 pAb (red) and either (A) a mouse anti-DCP1A mAb (blue) or (B) a mouse anti-Sec31A. The fluorescence signals were analyzed with a confocal laser-scanning microscope and are represented in black and white. Merged images are shown in (d), (h), (l) and (m). Panels (e)-(h) and (m) are magnified images of panels (a)-(d) in (A) and (l) in B, respectively. Bars, 5 μ m. Fluorescence intensities along the line segment (from p_1 to p_2) crossing two puncta indicated by open and closed arrowheads shown in (m) were measured by ImageJ, and relative fluorescence intensities derived from Alexa Fluor 488 (ALG-2), Alexa Fluor 555 (PATL1) and Alexa Fluor 647 (Sec31A) are represented by green, red and blue curves in a graph (n), where the maximum value is 1.0. (From Osugi *et al.*, *Journal of Biochemistry*, 151: 657-666, 2012)

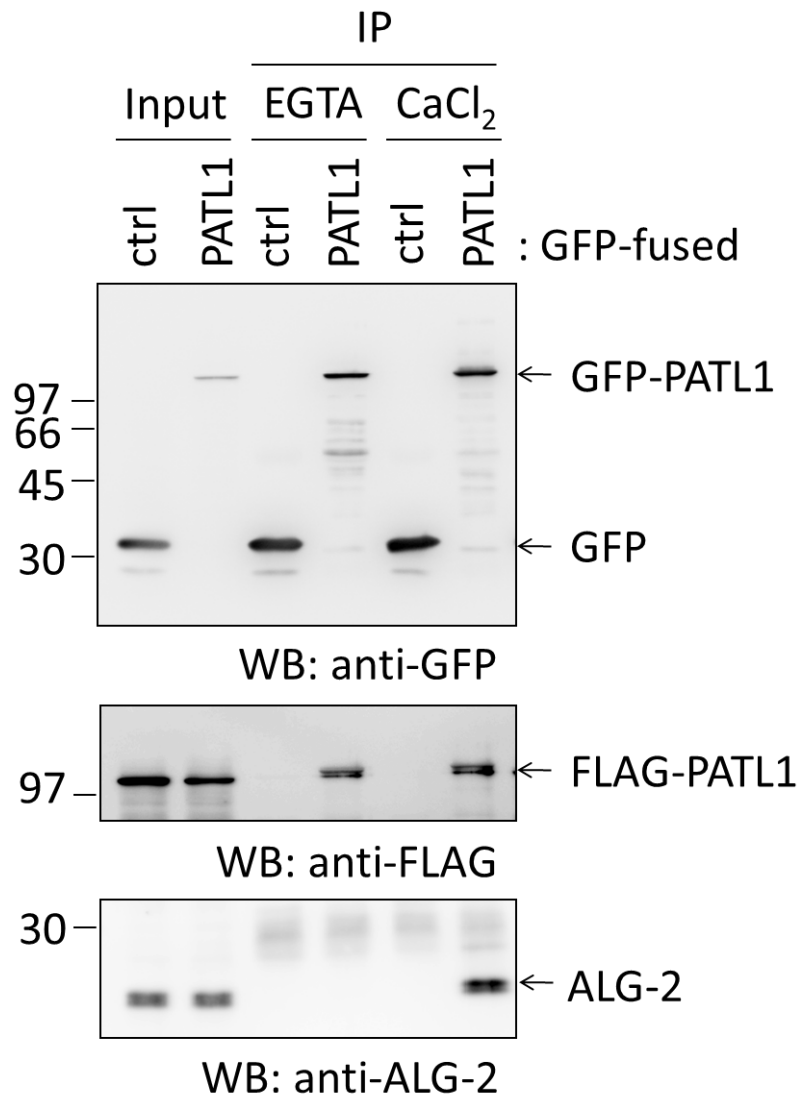


Fig. I-7 Co-immunoprecipitation of GFP-PATL1 with FLAG-PATL1. HEK293T cells expressing GFP-fused and FLAG-tagged PATL1 were lysed with buffer T (see Materials and Methods) and the cleared cell lysate (Input) was treated with RNase A (final concentration: 125 μ g/ml) and, after addition of EGTA to 5 mM or CaCl₂ to 100 μ M, was subjected to immunoprecipitation by incubating first with rabbit anti-GFP serum for 1 h at 4 °C and then with magnetic beads carrying Protein G overnight. After the beads had been collected and washed, immunoprecipitated proteins (IP) were resolved by SDS-PAGE and subjected to WB using anti-GFP mAb (top panel), anti-FLAG mAb (middle panel) and anti-ALG-2 pAb (bottom panel). The relative amount of cleared cell lysate proteins (Input) used for analysis of IP products was 1.5%. (From Osugi *et al.*, *Journal of Biochemistry*, 151: 657-666, 2012)

Chapter II

Nuclear ALG-2 Interacts with CHERP Ca²⁺-Dependently and
Participates in Regulation of Alternative Splicing of Inositol
Trisphosphate Receptor Type 1 (IP₃R1) Pre-mRNA

Abstract

The intracellular Ca^{2+} signaling pathway is important for the control of broad cellular processes from fertilization to cell death. ALG-2 is a Ca^{2+} -binding protein that contains five serially repeated EF-hand motifs and interacts with various proteins in a Ca^{2+} -dependent manner. Although ALG-2 is present both in the cytoplasm and in the nucleus, little is known about its nuclear function. CHERP (Ca^{2+} homeostasis endoplasmic reticulum protein) was first identified as an endoplasmic reticulum (ER) protein that regulates intracellular Ca^{2+} mobilization in human cells, but recent proteomics data suggest an association between CHERP and spliceosomes. Here I report that CHERP, containing a Pro-rich region and a phosphorylated Ser/Arg-rich RS-like domain, is a novel Ca^{2+} -dependent ALG-2-interactive target in the nucleus. Immunofluorescence microscopic analysis revealed localization of CHERP to the nucleoplasm with prominent accumulation at nuclear speckles, which are the sites of storage and modification for pre-mRNA splicing factors. Live-cell time-lapse imaging showed that nuclear ALG-2 was recruited to the CHERP-localizing speckles upon Ca^{2+} -mobilization. Results of co-immunoprecipitation assays revealed binding of CHERP to a phosphorylated form of RNA polymerase II. Knockdown of CHERP or ALG-2 in HT1080 cells resulted in generation of alternatively spliced isoforms of the $\text{IP}_3\text{R1}$ pre-mRNA that included exons 41 and 42 in addition to the major isoform lacking exons 40-42. Furthermore, binding between CHERP and $\text{IP}_3\text{R1}$ RNA was detected by an RNA immunoprecipitation assay using a polyclonal antibody against CHERP. These results indicate that CHERP and ALG-2 participate in regulation of alternative splicing of $\text{IP}_3\text{R1}$ pre-mRNA and provide new insights into post-transcriptional regulation of splicing variants in Ca^{2+} signaling pathways.

Intoroduction

ALG-2 (apoptosis-linked gene 2, also named programmed cell death 6; gene name, *PDCD6*), a 22-kDa Ca^{2+} -binding protein, was identified by a method to select genes involved in apoptosis of murine cells (Vito *et al.*, 1996). Although accumulating data indicate involvement of ALG-2 in apoptosis and cancer in mammals (Rao *et al.*, 2004; Draeby *et al.*, 2007; Mahul-Mellier *et al.*, 2008; Yamada *et al.*, 2008; Aviel-Ronen *et al.*, 2008), details of its physiological functions at the molecular level have remained unclear. ALG-2 has five serially repeated EF-hand motifs (penta-EF-hand, a PEF domain) (Maki *et al.*, 1997; Maki *et al.*, 2002) and interacts with various proteins, including ALIX (Missotten *et al.*, 1999; Vito *et al.*, 1999), Sec31A (Yamasaki *et al.*, 2006; Shibata *et al.*, 2007), and PLSCR3 (see Shibata *et al.*, 2008 and Maki *et al.*, 2011, and references therein). Most ALG-2-binding proteins contain a proline-rich region (PRR), through which they interact with a Ca^{2+} -bound form of ALG-2. Identification of ALG-2-binding sites (ABS) in ALIX (Shibata *et al.*, 2004; Suzuki *et al.*, 2008), Sec31A (Shibata *et al.*, 2010), and PLSCR3 (Shibata *et al.*, 2008) allowed me to determine two different types of ALG-2-binding motifs: type 1, PPYP(x)_nYP (x, variable; n=4 in ALIX and PLSCR3-ABS1); type 2, PxPGF (x, variable; Sec31A and PLSCR3-ABS2). I recently developed a method to screen novel ALG-2-interacting proteins using these motifs in PRRs for an *in silico* search, followed by Far-Western blot analysis of GFP-fused PRR proteins (Osugi *et al.*, 2012). In this study, I selected one of the previously obtained positive candidates, named CHERP (Ca^{2+} homeostasis endoplasmic reticulum protein), for further characterization as an ALG-2-interacting protein and investigated its biological functions.

CHERP was first identified as a target of a monoclonal antibody that blocked 1,4,5-trisphosphate (IP_3)-induced Ca^{2+} -release from the isolated endoplasmic reticulum (ER) (O'Rourke *et al.*, 1994), and its cDNA was immunoscreened from a cDNA expression library of human erythroleukemia (HEL) cells (LaPlante *et al.*, 2000). CHERP was shown to co-localize with IP_3 receptors throughout the cytoplasmic and perinuclear regions in HEL cells and in Jurkat cells (LaPlante *et al.*, 2000; O'Rourke *et al.*, 2003). Antisense-mediated knockdown of CHERP impaired intracellular Ca^{2+} -mobilization and cell growth and proliferation. A recent study has indicated that CHERP interacts with ryanodine receptor 1 (RyR1) and that knockdown of CHERP affects Ca^{2+} -release from the ER (Ryan *et al.*, 2011).

On the other hand, proteomics analyses showed that CHERP was present in the

fractions of 17S U2 snRNP (Will *et al.*, 2002) and nuclear speckles (Saitoh *et al.*, 2004), which are storage and assembly sites for splicing factors. Lin-Moshier *et al.* (2013) re-investigated subcellular localization of CHERP by immunostaining with a specific antibody and by fluorescence microscopic analysis of GFP-fused CHERP, and they identified nuclear localization signals and concluded that CHERP exclusively localizes to the nucleus including nuclear speckles. Nuclear function of CHERP, however, has not been demonstrated yet. There is a segment of Arg-Ser dipeptide repeats near the C-terminus of CHERP. Ser/Arg-rich SR proteins containing a region of Arg-Ser dipeptide repeats (an RS domain) and RNA recognition motifs (RRMs) constitute a family of splicing regulatory factors (Fu *et al.*, 1992; Zahler *et al.*, 1992; Manley *et al.*, 2010). RS domains of SR proteins are phosphorylated at numerous serine residues, and the phosphorylation is thought to play important roles in broad phenomena of RNA processing including alternative splicing (Ghosh *et al.*, 2011). Phosphorylation of the RS-like domain of CHERP, however, has not been reported yet.

In this chapter, I show that ALG-2 interacts with CHERP in a Ca^{2+} -dependent manner through at least two sites containing ALG-2-binding motif-like sequences in the PRR. ALG-2 was shown to be recruited to CHERP-positive nuclear speckles upon Ca^{2+} -mobilization in living cells by time-lapse imaging of fluorescent-protein-fused proteins. Depletion of CHERP or ALG-2 by the RNA interference method affected alternative splicing of the pre-mRNA of inositol 1,4,5-trisphosphate receptor 1 (IP₃R1). Association of CHERP with IP₃R1 RNA was demonstrated. These findings suggest that CHERP has a new role as an SR superfamily protein and regulates alternative splicing of IP₃R1 pre-mRNA. ALG-2 may also participate in the post-transcriptional regulation of IP₃R1 pre-mRNA at least in part by interacting with CHERP.

Materials and Methods

Antibodies and Reagents—The following antibodies were purchased: mouse anti-GFP monoclonal antibody (mAb) clone B-2 (sc-9996), rabbit anti-FBP21 (WBP4) polyclonal antibody (pAb) (N-16; sc-84249), mouse anti-GAPDH mAb (clone 6C5, sc-32233), and rabbit anti-pol II pAb (N-20, sc-899) from Santa Cruz Biotechnology (Santa Cruz, CA); mouse anti-calnexin mAb (clone 37) from BD Biosciences (Franklin Lakes, NJ); rabbit anti-AIF pAb (ab1998) and mouse anti-SF3A2 mAb (ab77800) from Abcam (Cambridge, UK); mouse anti-CHERP mAb (clone 2H5) from Abnova (Taipei, Taiwan); mouse anti-SC35 mAb (clone S4045) from Sigma-Aldrich (St. Louis, MO); and mouse mAb against pan-SR proteins (clone 1H4) from Invitrogen/Molecular Probes (Carlsbad, CA). Affinity-purification of rabbit anti-human ALG-2 pAb using the recombinant ALG-2 protein immobilized on an N-Hydroxysuccinimide (NHS) column (GE Healthcare Japan, Tokyo) was described previously (Shibata *et al.*, 2007). Anti-human ALG-2 antiserum was also raised in a goat using glutathione-*S*-transferase (GST)-fused ALG-2 as an antigen, and the antibody was similarly affinity-purified (Osugi *et al.*, 2012). Anti-human CHERP antisera were raised in rabbits using a CHERP C-terminal region (820-916 a.a.) protein (CHERPcT) that was fused with GST, and specific antibodies were affinity-purified using CHERPcT that was fused with maltose-binding protein (MBP). Protease inhibitors 4-(2-aminoethyl)-benzenesulfonyl fluoride hydrochloride (AEBSF, pefabloc) and *L-trans*-epoxysuccinyl-leucylamido(4-guanidino)butane (E-64) were from Merck (Darmstadt, Germany) and the Peptide Institute (Osaka, Japan), respectively. Thapsigargin, an inhibitor of sarcoplasmic/endoplasmic reticulum Ca²⁺-ATPase (SERCA), was from Wako (Osaka, Japan).

Plasmid Construction—Human CHERP cDNA (clone MHS1011-76655) was purchased from Open Biosystems (Lafayette, CO), and the cDNA of full-length (FL) was inserted between the *Xho*I site and the *Sal*I site of pEGFP-C1 (Clontech/Takara Bio, Otsu, Japan) or pSGFP2-C1 (kindly provided by Dr. Wada, Fukushima Medical University School of Medicine, who constructed the vector according to Ref 30) using an In-Fusion Advantage PCR Cloning Kit (Clontech). To construct plasmids for expression of GFP-fused CHERP deletion mutants designated GFP-CHERP ΔCID and GFP-CHERP ΔRS, cDNA fragments lacking CID (149-293 a.a.) or RS (725-822 a.a.) were amplified by the overlap PCR method using pEGFP-C1/CHERP FL as a template

DNA and with two different pairs of specific primers, and each fragment was inserted into the *XhoI/SalI* site of pEGFP-C1. To construct pEGFP-C1/CHERP Δ PRR, a cDNA fragment encoding the PRR of CHERP (352-705 a.a.) was removed from pEGFP-C1/CHERP FL by cleavage at two *EcoRV* sites generated by site-directed mutagenesis, followed by self-ligation. Construction of pSGFP2-C1/ALG-2 and pEGFP-C3/CHERP PRR was described previously (Shibata *et al.*, 2010; Osugi *et al.*, 2012). Other constructs were obtained by the PCR-based subcloning method with specific primers. pmCherry-C1/ALG-2 was constructed by insertion of an *EcoRI/XhoI* fragment of pFLAG-ALG-2^{WT}/RNAi^R (Okumura *et al.*, 2009) into the *EcoRI/SalI* site of pmCherry-C1 (Clontech). The nuclear Ca²⁺-sensor vector CMV-NLS-R-GECO (Zhao *et al.*, 2011) was obtained from the non-profit plasmid repository Addgene (plasmid 32462; <http://www.addgene.org/>).

Cell Culture and DNA Transfection—HEK293T, HeLa SS4 (subcloned HeLa cells, see Shibata *et al.*, 2007), and HT1080 cells were cultured in DMEM (Nissui, Tokyo, Japan) supplemented with 4 mM glutamine, 10% fetal bovine serum (FBS), 100 units/ml penicillin, and 100 μ g/ml streptomycin at 37 °C under humidified air containing 5% CO₂. Cells were seeded and cultured for one day, and then they were transfected with the expression plasmid DNAs by the conventional calcium phosphate precipitation method for HEK293T cells or by using FuGENE 6 (Promega, Madison, WI) for HeLa and HT1080 cells.

Far-Western Blot Analysis—Far-Western (FW) blot analysis with biotin-labeled ALG-2 was performed as described previously (Osugi *et al.*, 2012; Osugi *et al.*, 2013). Briefly, HEK293T cells that had been transfected with pEGFP-C1/CHERP FL or its deletion mutants were lysed with lysis buffer T (50 mM Tris-HCl, pH 7.5, 150 mM NaCl, 1.5 mM MgCl₂, and 0.2% Triton X-100 containing protease inhibitors). The cleared lysate was subjected to immunoprecipitation with GFP-TrapA (ChromoTek, Martinsried, Germany), followed by Western blot (WB) and FW analyses.

Subcellular Fractionation and Immunoprecipitation—HEK293T cells were suspended in a hypotonic buffer (10 mM HEPES-KOH, pH 7.6, 10 mM KCl, 1.5 mM MgCl₂, 5 mM 2-mercaptoethanol) containing protease inhibitors (0.1 mM pefabloc, 3 μ g/ml leupeptin, 1 μ M E-64, 1 μ M pepstatin and 0.1 mM phenylmethylsulfonyl fluoride) and homogenized by passing 25 times through a 26-gauge needle. After adding a solution of NaCl to 0.15 M, the homogenate was fractionated by differential successive

centrifugations at 4 °C. Pellets of 600 × g (P_{0.6}), 10,000 × g (P₁₀), 100,000 × g (P₁₀₀), and the final supernatant of 100,000 × g (S₁₀₀) were subjected to WB analysis. For co-immunoprecipitation assays, P_{0.6} fraction was obtained without supplemental NaCl and CHERP was extracted with lysis buffer T by brief sonication. After centrifugation at 10,000 × g for 10 min at 4 °C, the supernatant treated with RNase A (final 10 µg/ml) was subjected to immunoprecipitation with anti-CHERP or control IgG in the presence of various concentrations of CaCl₂ or in the presence of 5 mM EGTA.

Size-exclusion Chromatography—HEK293T cells transiently transfected with plasmids expressing GFP-fused CHERP deletion mutants were lysed with buffer C (50 mM Tris-HCl, pH7.5, 150 mM NaCl, 1.5 mM MgCl₂, 0.2% CHAPS) containing 3 µg/ml leupeptin, 1 µM pepstatin, and 0.1 mM pefabloc. After centrifugation at 8,400 × g for 10 min at 4 °C, the supernatant were treated with RNase A at a final concentration of 10 µg/ml for 60 min. About 25 µg proteins were loaded onto a Shodex KW403-4F column (Showa Denko, Tokyo, Japan) pre-equilibrated with buffer C, and were eluted at 0.3 ml/min. The GFP signals derived from each GFP-CHERP variant were monitored with a fluorescence detector (RF-20A, Shimadzu, Kyoto, Japan). The apparent molecular weights were estimated using the calibration curve obtained from molecular mass standards and the retention times.

Immunofluorescence Microscopic Analysis and Live-cell Imaging—Immunostaining and live-cell time-lapse imaging were performed essentially as described previously (Shibata *et al.*, 2010; Osugi *et al.*, 2012). Briefly, HeLa cells were seeded in a glass-bottom dish for time-lapse imaging (Asahi Glass, Tokyo, Japan), and the medium was replaced with Leibovitz's L15 medium (Invitrogen, Grand Island, NY) containing 1% fetal bovine serum. Time-lapse images were acquired under an FV1000-D confocal laser-scanning microscope equipped with a 100x, 1.4 numerical aperture (NA) oil-immersion objective (UPLSAPO100XO, Olympus, Tokyo, Japan) before and after treatment with thapsigargin (final concentration of 2 µM) at 37 °C.

RNA Interference and RNA Sample Preparation—All siRNAs (siCHERP#1, 5'-gcuagacaugaacgaguugacaac-3'; siCHERP#2, 5'-gguuuaggucuagaaagaagauac-3'; siALG-2#1, 5'-agcaauaaagggaauguuagacgtg-3'; siALG-2#4, 5'-aaagacaggaguggagugauaucag-3'; Negative Control, 5'-cguaaauacgcguauauacgcguat-3'; sequences of sense strand shown) were purchased from Integrated DNA Technologies (Coralville, IA). HT1080 cells were transfected with

10 nM siRNA duplexes targeting CHERP, ALG-2 or negative control siRNA using RNAiMAX (Invitrogen) according to the reverse transfection method described in the manufacturer's instructions. Cells were harvested 72 h after siRNA transfection. Total RNA was prepared with Sepasol super G (Nacalai Tesque, Kyoto, Japan), and genome DNA was digested with 20 units/ml DNase (Nippon Gene, Tokyo, Japan).

Quantitative RT-PCR—RT-PCR and quantitative PCR (qPCR) were performed using a PrimeScript™ RT Reagent Kit (Perfect Real Time, RR037A, Takara Bio) and FastStart Essential DNA Green Master (Roche), respectively. Reverse transcription products were analyzed by LightCycler® Nano (Roche) using specific primers for IP₃R1 isoforms (Table II-1). GAPDH mRNA was used as an internal control for all qPCR reactions except for RNA immunoprecipitation assay. Ratios among transcript levels of individual IP₃R1 isoforms were obtained by dividing each expression level by the sum of all isoforms.

RNA Immunoprecipitation Assay—RNA immunoprecipitation (RIP) was performed using a RIP-assay kit (MBL, Nagoya, Japan) according to the manufacturer's instructions. Briefly, HEK293T cells were lysed in the provided lysis buffer supplemented with 1.5 mM dithiothreitol, 80 U/ml RNase inhibitor (RNaseOUT™, Invitrogen), and protease inhibitors. An aliquot (2%) of the supernatant obtained by centrifugation at 12,000 × g was used for total RNA isolation. The remainder was incubated at 4 °C for 3 h with Protein G Sepharose beads (GE Healthcare) that were pre-incubated with rabbit anti-CHERP pAb or control rabbit IgG. After washing with the buffer 4 times, RNA in the immunoprecipitates was purified and subjected to RT-PCR and qPCR analyses using primers for IP₃R1, GAPDH and histone H3 (HIST2H3) (Table II-1). All RNA levels were normalized to 18S rRNA.

Results

ALG-2 interacts with CHERP in a Ca²⁺-dependent manner— I previously reported that the GFP-fused PRR of CHERP showed a positive signal in Far-Western (FW) blot analysis with biotin-labeled ALG-2 (Osugi *et al.*, 2012), but interaction between endogenous CHERP and ALG-2 has remained to be established. Since there have been conflicting reports about the subcellular localization of CHERP (ER or nucleus), the subcellular distribution of CHERP first investigated. As shown in Fig. II-1A, biochemical cell fractionation of HEK293T cells by the differential centrifugation method revealed that Western blot (WB) signals of CHERP were mostly present in the 600 × g pellets (P_{0.6} fraction) in a manner similar to that of the nuclear marker WW domain-binding protein 4 (WBP4). Detection of GAPDH (cytosolic protein) only in the 100,000 × g supernatant (S₁₀₀ fraction) indicated that cells were sufficiently lysed by the homogenization procedure used in this study. Since calnexin (ER-transmembrane protein) and apoptosis-inducing factor (AIF, mitochondrial inter-membrane space protein) were detected in both the P_{0.6} and P₁₀ fractions, separation of nuclei from the ER and mitochondria was not complete. Signal intensities of ALG-2 were similar in the two fractions of P_{0.6} and S₁₀₀, and a faint signal was also detected in the P₁₀ fraction. Next, CHERP was extracted from the P_{0.6} fraction with sonication in the buffer containing a non-ionic detergent (0.2% Triton X-100), and then the supernatant was subjected to co-immunoprecipitation assay. As shown in Fig. II-1B, an ALG-2-specific band was detected in the immunoprecipitation (IP) product with an antibody against CHERP (anti-CHERP) in the presence of 10 μM CaCl₂ (C) but not in the presence of 5 mM EGTA (E). No ALG-2 bands were observed in the case of control (ctrl) IgG in either condition, IgG bands of light and heavy chains (IgG_L and IgG_H) being detected with similar intensities in the two conditions. Faster migrating bands detected with anti-CHERP (upper panel) probably correspond to degradation products of CHERP.

As shown in Fig. II-1C, the amount of ALG-2 that was co-immunoprecipitated with CHERP was increased by increasing the concentration of supplemented CaCl₂ from none (lane 3) to 100 μM (lane 6). Under the conditions used, while more than 80% of input CHERP was immunoprecipitated with the antibody (data not shown), approximately 1-3% of input ALG-2 was co-immunoprecipitated (lane 1, input, 1.5%). Although the increase of ALG-2 binding at higher concentrations of CaCl₂ (lanes 5 and 6) is reproducible, the degree was variable from experiment to experiment, and the detected signal of ALG-2 at the lowest supplementation of CaCl₂ (lane 4, 1 μM) was

comparable to that without supplementation (lane 3). The apparent Ca^{2+} -independency at the lower Ca^{2+} concentration range might have been partly due to a trace of Ca^{2+} derived from cells or from the lysis buffer and partly due to the complex that had been already formed Ca^{2+} -dependently within the nucleus, since addition of 5 mM EGTA (lane 2) caused disappearance of the ALG-2 band.

Multiple ALG-2-binding sites in the PRR of CHERP—In addition to the PRR, CHERP has four distinct regions with sequences similar to those designated SURP (also named SWAP), CID (RNA polymerase II C-terminal domain-interacting domain), RS (Arg-Ser dipeptide repeats), and G-patch. The PRR of CHERP has a sequence, 565-PPYPHRFDYP-574, that is in accordance with the type 1 ALG-2-binding motif (conserved residues underlined). To obtain evidence that this sequence is essential for CHERP to interact with ALG-2, I first constructed GFP-fusion expression vectors encoding the full-length (FL) CHERP protein and a deletion mutant of this region ($\Delta 557$ -585) as well as various other mutants (Fig. II-2A), and then I carried out FW with biotin-labeled (bio-) ALG-2 and WB with anti-GFP to check the relative amounts of proteins resolved by SDS-PAGE (Fig. II-2B). Unexpectedly, FW signals were detected for $\Delta 557$ -585 (Fig. II-2B, left lower panel, lane 6) with intensity only slightly weaker than that of the FL protein (lane 1), indicating that other regions also contribute to the ALG-2 binding. Since mutants with deletion of CID (Δ CID, lane 2) and deletion of the RS domain (Δ RS, lane 4) retained binding abilities, but the PRR-deletion mutant (Δ PRR, lane 3) did not, I focused on the PRR for further search for ALG-2-binding sites. The N-terminal end of the PRR has a unique Pro-Ala repeat sequence (354-TPPPPAPPPAPAPAPAIPP-372), but deletion of this sequence had little effect on the binding ($\Delta 354$ -372, lane 5). Although it is not in accordance with the previously proposed type 2 motif (PxPGF), the PRR has a similar sequence of 614-PPPHGF-619. To determine the importance of this type 2 motif-like sequence for ALG-2 binding, I further deleted this region ($\Delta 557$ -585/ $\Delta 613$ -623) or replaced Phe⁶¹⁹ with Ser ($\Delta 557$ -585/F619S) in addition to the deletion of type 1 motif-like sequence ($\Delta 557$ -585). These mutations caused a significant decrease in signal intensity in FW, but faint bands still remained (lanes 7 and 8). As shown in the right panels in Fig. II-2B, compared with GFP-PRR, intensity of FW signals of GFP-PRR decreased by truncation of the C-terminal region containing the type 2 motif-like sequence (GFP 343-599) or FW signals disappeared in GFP 343-462. Since signal intensity of GFP 550-636 was weaker than that of GFP PRR (lane 10 vs lane 13), there may exist at least one more important site in either side of 550-636 for ALG-2-binding.

CHERP is present in the nucleus and concentrated at nuclear speckles—I performed fluorescence microscopic analysis of GFP-CHERP mutant proteins expressed in HeLa cells. While the full-length (FL) and the mutants deleted in CID or PRR showed exclusively nuclear localization, a deletion mutant of RS (GFP-CHERP Δ RS) showed cytoplasmic as well as nuclear localization (Fig. II-2C). All cytoplasmic punctate signals of GFP-CHERP Δ RS merged with those of ALG-2 and partially overlapped with those of Sec31A, a component of COPII (Fig. II-2D). To investigate the subnuclear distribution of endogenous CHERP, I carried out triple-immunostaining of HeLa cells with rabbit anti-CHERP pAb, goat anti-ALG-2 pAb and mouse mAb against SC35 (alternatively called SRSF2), which is a splicing factor that mediates specific interactions between U1 and U2 small nuclear ribonucleoprotein particles (snRNP) at the 3' splice site (Fu *et al.*, 1992) and which is a well-known marker of nuclear speckles (Spector *et al.* 2011). Effects of pre-permeabilization with digitonin before fixation were also investigated. Immunofluorescence signals of CHERP were observed in the nucleus (Fig. II-3), and the pre-permeabilization had little effects (panels b and f). Dense signals of CHERP in the nucleus partially overlapped with those for SC35 (panels c and g), indicating partial localization of CHERP at nuclear speckles. Nuclear ALG-2 signals were rather uniformly diffused in the nucleoplasm compared to those of CHERP without pre-permeabilization (panel a) but became punctate by pre-permeabilization with digitonin (panel e).

ALG-2 transiently accumulates at nuclear speckles in response to Ca^{2+} -mobilization—By live-cell imaging, ALG-2 has been shown to translocate to the Sec31A-positive ER exit sites transiently in response to Ca^{2+} -mobilization (Shibata *et al.*, 2010; la Cour *et al.*, 2007). I previously noticed the appearance of ALG-2 puncta in the nucleus but left them uncharacterized (Shibata *et al.*, 2010). Now I know that ALG-2 binds to CHERP Ca^{2+} -dependently, I have decided to re-investigate whether fluorescent protein-fused ALG-2 in living cells responds to thapsigargin (a SERCA pump inhibitor and Ca^{2+} -elevating agonist) and accumulates at nuclear speckles by co-localizing with CHERP. First, I expressed SGFP2-ALG-2 and NLS-R-GECO, which is a nuclear Ca^{2+} -indicator protein (Zhao *et al.*, 2011). Thapsigargin (TG) administration resulted in redistribution of cytoplasmic and nuclear ALG-2 concomitantly with an increase in NLS-R-GECO signals (Fig. II-4A, panels a-d, II-4B). Fluorescent signals of SGFP2-ALG-2 at nucleoplasmic puncta were increased transiently (ROI-1 and ROI-2), whereas the signals remained constant in the nucleoplasm (ROI-3) and were decreased in the nucleolus (ROI-4). Next, cells expressing SGFP2-CHERP and mCherry-ALG-2

at low to middle levels were used for time-lapse analysis. Like SGFP2-ALG-2, mCherry-ALG-2 localized throughout the cytoplasm and nucleus, uniformly in the nucleoplasm outside of nucleoli before stimulation with thapsigargin (Fig. II-4C, panel f). On the other hand, SGFP2-CHERP localized within the nucleoplasm and accumulated at nuclear speckles (panels e and g) in a manner similar to that for immunostaining of fixed cells with anti-CHERP pAb (Fig. II-3, panel b). Thapsigargin treatment induced enhancement of nuclear mCherry-ALG-2 signals in a speckled pattern, and these speckled signals of mCherry-ALG-2 partially merged with those of SGFP2-CHERP (Fig. 4C, panels g and h). No significant alteration of SGFP2-CHERP was observed after stimulation with thapsigargin (Fig. II-4D).

Arg/Ser-rich region in CHERP is constitutively phosphorylated—An RS domain is defined as a region of at least 50 amino acids with >40% Arg/Ser content characterized by consecutive Arg-Ser or Ser-Arg dipeptide repeats (Manley *et al.*, 2010). CHERP has a similar Arg/Ser-rich region (718-817) and the dipeptides span 737-817 a.a. with 25 repeats (62% RS content). The RS domains of SR proteins, which are defined as RNA-binding proteins with RS domains and RRM, are known to be constitutively phosphorylated (Ghosh *et al.*, 2011). To investigate whether the Arg/Ser-rich region of CHERP is similarly phosphorylated, CHERP was immunoprecipitated with rabbit anti-CHERP pAb from HEK293T cells, and then the immunoprecipitates were subjected to WB analysis with rabbit anti-CHERP pAb and with commercially available mouse mAb against pan-SR proteins (clone 1H4), which recognizes a broad range of phosphorylated RS domains (Neugebauer *et al.*, 1997; Mathew *et al.*, 2008). As shown in Fig. II-5, upper panel, CHERP-specific bands detected with anti-CHERP shifted downward after treatment with calf intestine alkaline phosphatase (CIAP) for 4 h in the absence of phosphatase inhibitors, but the presence of inhibitors partially blocked the downward shift. Anti-SR mAb recognized endogenous CHERP proteins that were not treated with CIAP, treated with phosphatase inhibitors alone, and treated with CIAP in the presence of phosphatase inhibitors (Fig. II-5, lower panel). As expected, this antibody did not detect the downward-shifted band of CHERP after CIAP treatment, strongly suggesting that the RS domain of CHERP is phosphorylated at Ser residues in a manner similar to the RS domains of SR proteins.

CHERP interacts with phosphorylated RNA polymerase II—According to annotation in the protein database of Uniprot/Swiss-Prot, CHERP contains a CTD (C-terminal domain of RNA polymerase II)-interacting domain (CID) based on the primary sequence

similarity. To experimentally investigate whether CHERP interacts with RNA polymerase II (pol II), I performed a co-immunoprecipitation assay with anti-pol II pAb or with anti-CHERP pAb in the presence or absence of Ca^{2+} using the nuclear extract (NE) from HEK293T cells. As shown in the upper panel of Fig. II-6A, CHERP-specific bands were detected in the immunoprecipitates (IP) with anti-CHERP but not with control (ctrl) IgG. Two specific bands were detected by WB with anti-pol II in the total and NE fractions. The upper bands (pol IIO), absent in the post-nuclear supernatant (PNS), correspond to the phosphorylated transcriptionally engaged forms of pol II, and the lower bands (pol IIA) correspond to the unphosphorylated and transcriptionally unengaged forms (Muñoz *et al.*, 2010). Only pol IIO bands were detected in the immunoprecipitates with anti-CHERP both in the presence of 10 μM CaCl_2 and in the presence of 5 mM EGTA, indicating that CHERP and pol IIO interact Ca^{2+} -independently. On the other hand, ALG-2 bands were observed in the immunoprecipitates with anti-CHERP in the presence of 10 μM CaCl_2 but not in the presence of 5 mM EGTA. I performed a complementary co-immunoprecipitation assay with anti-pol II for immunoprecipitation and detected CHERP in the immunoprecipitates (Fig. II-6B). ALG-2 was also co-immunoprecipitated with anti-pol II pAb but only in the presence of CaCl_2 .

The PRR of CHERP associates with RNA polymerase II—Next, I examined whether the database-annotated CID of CHERP is essential for interaction between CHERP and RNA pol II by expressing various deletion mutants of GFP-CHERP and carrying out immunoprecipitation with anti-pol II pAb, followed by WB with anti-GFP mAb. As shown in Fig. II-7, unexpectedly, GFP-CHERP ΔCID was co-immunoprecipitated equally well in comparison with GFP-CHERP FL. The remaining PRR within GFP-CHERP ΔCID is likely responsible for the binding, because the PRR of CHERP alone was sufficient for the association with RNA pol II, whereas the deletion of the PRR (GFP-CHERP ΔPRR) failed to bind to RNA pol II.

As shown in Fig. II-8, panel A, the results of size exclusion chromatography revealed that a majority of the GFP-fusion protein of the full-length was eluted at approximately 163 kDa, slightly greater than the molecular mass of monomeric protein calculated from the amino acid sequence (132.7 kDa, Table II-2). A second peak appeared faster (>669 kDa), suggesting that some portion of CHERP population exists in an aggregate, oligomeric form or in a complex with other proteins, probably including RNA pol II and RNA processing factors. Although GFP-CHERP ΔCID exhibited a single band of expected size by Western blotting (panel B), multiple peaks of smaller molecular mass

than that of the monomeric form (116 kDa) were observed, suggesting a higher susceptibility of the deletion mutant to proteolysis during the analytical size exclusion chromatography that was performed at room temperature. GFP-CHERP Δ PRR (93 kDa) was eluted at >669kDa, 395 kDa and 204 kDa in an approximate peak height ratio of 3:11:8, suggesting occurrence as an aggregate, oligomeric form or in a complex with other proteins. GFP-CHERP Δ RS was eluted at ~172 kDa, slightly greater than a monomeric form (121.5 kDa). GFP-CHERP-PRR (68 kDa) was eluted at ~81 kDa. Effects of deletions in CHERP displayed a different pattern in the size exclusion chromatography, suggesting that each region has a different structural role in protein-protein interactions. Although the PRR itself is likely to be sufficient for interaction with pol II, potential misfolding of the GFP-CHERP proteins caused by deletion should be also considered, and I cannot exclude the possibility that other regions including CID also have a capacity to interact with pol II independently of the PRR.

CHERP knockdown increases inclusion of exons 41 and 42 in IP₃R1 pre-mRNA—CHERP was first identified as a modulator of IP₃ receptor and was shown to regulate Ca²⁺ homeostasis (O'Rourke *et al.*, 1994; LaPlante *et al.*, 2000). Since CHERP localizes partly at nuclear speckles, contains the phosphorylated RS domain and interacts with RNA pol II, I speculated that abnormality in Ca²⁺ homeostasis caused by CHERP depletion in the previous reports might have been due to indirect effects of nuclear events. Hence, in this study, I analyzed roles of CHERP and ALG-2 on alternative splicing of pre-mRNAs of Ca²⁺-related proteins. IP₃ receptor 1 (IP₃R1) has three segments (S1, S2 and S3) that are reported to be variable in the splicing variants (Danoff *et al.*, 1991; Nakagawa *et al.*, 1991; Nucifora *et al.*, 1995). S2 corresponds to exons 40, 41 and 42. To investigate whether knockdown of CHERP causes changes in a splicing pattern of variable segments of S2 in IP₃R1 pre-mRNA, I performed RT-PCR using total RNA obtained from HT1080 cells that were transfected with siRNAs targeting CHERP (siCHERP#1 and #2) or negative control siRNA (NC) and with the use of S2-specific primers 1F and 1R (see Fig. II-9A). Amplicons that skip exons 40, 41 and 42 were exclusively produced from cells of mock transfection (data not shown) and NC siRNA, and amplicons that lack only exon 40 (Δ E40) or both exons 40 and 41 (Δ E40/41) were increased by transfection with siCHERP#1 and #2 compared with NC (Fig. II-9B). No significant alteration of splicing patterns was observed in S1 and S3 segments (data not shown). To further quantitatively analyze the effects of knockdown of CHERP or ALG-2 on alternative splicing in S2, I performed real-time qPCR using

each isoform-specific primer, which corresponds to the splice junction sequence (Fig. II-9A). Transfection of HT1080 cells with siCHERP#1 or siCHERP #2 reduced the level of CHERP mRNA to approximately 25% as shown in the lower panel of Fig. II-9C. I observed statistically significant increases in percentage of isoforms $\Delta E40$ and $\Delta E40/41$ in CHERP knockdown cells compared with the control (percentage of $\Delta E40$: NC, 0.0410 ± 0.0063 ; siCHERP#1, 0.659 ± 0.149 ; siCHERP#2, 0.506 ± 0.0625 ; percentage of $\Delta E40/41$: NC, 1.16 ± 0.0820 ; siCHERP#1, 4.60 ± 0.597 ; siCHERP#2, 4.64 ± 0.579) (Fig. II-9C, upper panel). Likewise, increases in $\Delta E40$ and $\Delta E40/41$ were observed (percentage of $\Delta E40$: NC, 0.0434 ± 0.00440 ; siALG-2#1, 0.186 ± 0.0242 ; siALG-2#4, 0.288 ± 0.0367 ; percentage of $\Delta E40/41$: NC, 1.11 ± 0.114 ; siALG-2#1, 2.16 ± 0.199 ; siALG-2#4, 2.65 ± 0.227) (Fig. II-9D, upper panel) in ALG-2 knockdown cells, in which ALG-2 mRNA was reduced to less than 20% of the negative control (Fig. II-9D, lower panel).

CHERP physically associates with IP₃R1 RNA—To investigate more direct contribution of CHERP to alternative splicing of IP₃R1 pre-mRNA, an RNA immunoprecipitation assay with anti-CHERP pAb was performed, and associated RNAs were analyzed by RT-PCR. A CHERP-specific WB band was detected in the IP product of anti-CHERP pAb but not in that of rabbit control IgG (Fig. II-10A). The cDNA fragment, amplicon of 118 bp, corresponding to segment S2 in IP₃R1 was detected by 5% polyacrylamide gel electrophoresis (PAGE) followed by ethidium bromide staining in the total fraction and in the IP product of anti-CHERP pAb after reverse transcription (+RT) but not without reverse transcription (-RT) (Fig. II-10B). Furthermore, RT-qPCR was carried out to measure the relative abundance of IP₃R1 mRNA contained in the IP product of anti-CHERP pAb. As shown in Fig. II-10C, the degree of enrichment of IP₃R1 mRNA from total RNA by immunoprecipitation with anti-CHERP pAb (2.38 ± 0.245) was approximately 8-fold greater than that by immunoprecipitation with control IgG (0.311 ± 0.176), whereas mRNAs of histone H3 and GAPDH were not enriched.

DISCUSSION

CHERP (Ca²⁺ homeostasis endoplasmic reticulum protein) was first identified as an ER-localizing protein that modulates the IP₃ receptor (O'Rourke *et al.*, 1994; LaPlante *et al.*, 2000). Lin-Moshier *et al.* (2013) recently re-investigated the subcellular localization of CHERP and concluded that CHERP is a nuclear protein, and they identified four nuclear localization signals (NLSs): one in the boundary of the RS domain, two within the RS domain and one near the C-terminus. I also observed predominant nuclear localization of endogenous CHERP in several types of cells including HeLa, HEK293, HT1080 and Jurkat cells by immunostaining with a specific antibody (Fig. II-3, data not shown). GFP-fused CHERP, fused at the N-terminus or C-terminus, also showed nuclear localization by fluorescence microscopic analysis (Fig. II-2 and data not shown). Although immunostaining with a commercially available monoclonal antibody against CHERP also showed predominant nuclear localization of CHERP, it displayed weak signals of CHERP throughout the cytoplasm (data not shown). Expression of GFP-CHERP Δ RS resulted in partial distribution of the mutant in the cytoplasm (Fig. II-2C). Interestingly, a fraction of cytoplasmic GFP-CHERP Δ RS co-localized with Sec31A (Fig. II-2D), a COPII component, which is found co-localized with ALG-2 at ER exit sites (Yamasaki *et al.*, 2006; Shibata *et al.*, 2007). It was found that CHERP is phosphorylated and is recognized by a monoclonal antibody against pan-SR proteins with phosphorylated RS domains (Fig. II-5). A recent study has indicated that CHERP is likely to be a substrate of SRPK1 and SRPK2 (Varjosalo *et al.*, 2013), which are SR-specific protein kinases and control nuclear entry and speckle formation of SR proteins (Ghosh *et al.*, 2011). CHERP may shuttle between the nucleus and the cytoplasm under regulation by SRPKs. Since an ALG-2 dimer has the capacity to bridge two different interacting proteins as a Ca²⁺-dependent adaptor (Okumura *et al.*, 2009), CHERP may have an intrinsic property of association with the ER membrane through the ALG-2/Sec31A complex under certain physiological or non-physiological conditions including *in vitro* biochemical experiments.

In the protein database of UniProt, CHERP is also designated SR-related RNA polymerase II C-terminal domain (CTD)-associated factor 6 (SCAF6) as an alternative name, and it has been assigned to contain a CID (a CTD-interacting domain). The CID of RBM16/SCAF8 was previously shown to bind to the phosphorylated form of the CTD of pol II (Becker *et al.*, 2008). The CID of CHERP exhibits a lower degree of similarity with SCAF4 (31% identity) and with SCAF8 (26% identity) than the

similarity (81% identity) between SCAF8 and SCAF4 at the primary structural level, and it remains to be clarified whether CHERP binds to the CTD of pol II directly. Some SR proteins interact with pol II directly or *via* nascent pre-mRNAs and function in coupling transcription to splicing (Das *et al.*, 2007). Since CHERP does not have an RRM common to SR proteins, CHERP might associate with RNA via interacting with other proteins that possess RNA binding motifs such as SR140, a potential interacting protein of CHERP (Lin-Moshier *et al.*, 2013). Results of our preliminary experiments showed that another RRM-containing protein, SCAF4, was also co-immunoprecipitated with an antibody against CHERP (data not shown). However, I cannot completely rule out the possibility of direct interaction between CHERP and RNA. Since the PRR of CHERP is well conserved in vertebrates (data not shown), it might have a functional role in protein-protein or protein-RNA interactions in addition to the presence of the direct binding sites for ALG-2 and direct or indirect binding sites for RNA pol II.

In contrast to the punctate distribution of CHERP and SC35 at the nuclear speckles, nuclear ALG-2 showed a diffuse pattern by immunofluorescence microscopic analysis (Fig. II-3). Pre-permeabilization of cells with digitonin before fixation, however, enhanced the relative signal intensity of ALG-2 at nuclear speckles, probably due to washing out of nucleoplasmic free ALG-2 through nuclear pores but anchoring of ALG-2 to speckles *via* association with speckle components (Fig. II-3). I demonstrated thapsigargin-induced Ca^{2+} -dependent transient accumulation of ALG-2 at the nuclear speckles by time-lapse live-cell imaging (Fig. II-4). SGFP2-ALG-2 co-localized with mCherry-fused splicing factor 3A subunit 2 (SF3A2), which is a component of U2 snRNP (Fig. II-11A). Increase in nuclear Ca^{2+} caused no obvious change in nuclear speckle accumulation of CHERP and SF3A2, indicating that Ca^{2+} /ALG-2 is not essential for subnuclear localization of these proteins. Knockdown of CHERP by siRNA did not abolish the Ca^{2+} -dependent accumulation of ALG-2 (data not shown). It remains unknown whether depletion of CHERP by the siRNA method was merely insufficient or whether ALG-2 associates with other nuclear speckle-localizing proteins in addition to CHERP. Studies are in progress to search for additional nuclear proteins that associate with ALG-2 in a Ca^{2+} -dependent manner.

RBM22, a spliceosome associated RNA-binding protein, was previously shown to induce translocation of ALG-2 from the cytoplasm to the nucleus by overexpression experiments, and interaction with ALG-2 was proposed (Montaville *et al.*, 2006). RBM22 contains the sequence 433-PPPPGF-439, which matches with an ALG-2-binding motif type 2. I previously reported that GFP-RBM22 showed a strong signal by Far Western blot analysis with biotin-labeled ALG-2 but that GFP-RBM22

was not pulled down with GST-ALG-2 in the presence of Ca^{2+} , suggesting that RBM22 exists in a form inaccessible to ALG-2, for instance tightly bound with RNA, in the cell (Osugi *et al.*, 2012). In the present study I also performed live-cell imaging of GFP-RBM22 (Fig. II-11B), but this protein showed relatively diffuse cytoplasmic localization in accordance with the previous report (Montaville *et al.*, 2006). Co-localization at the nuclear speckles with ALG-2 after Ca^{2+} stimulation was not evident for RBM22. RBM22 is evolutionarily conserved, and human RBM22 as well as the yeast ortholog Cwc2 have recently been shown to function in a catalytic center of the spliceosome by making contact with catalytically important RNA elements, including the U6 internal stem-loop and regions of U6 and the pre-mRNA intron near the 5' splice site (Rasche *et al.*, 2012). On the other hand, CHERP is not found in fungi, and PRRs are lacking in the CHERP proteins from *C. elegans* and *Drosophila*, suggesting that Ca^{2+} -dependent interaction between CHERP and ALG-2 is a unique phenomenon in vertebrates.

Variants of $\text{IP}_3\text{R1}$ contain or lack three alternatively spliced exons (S1, S2 and S3), and expression of variants is regulated in a tissue-specific and temporally specific manner (Danoff *et al.*, 1991; Nakagawa *et al.*, 1991; Choi *et al.*, 2004). The S2-containing form is predominant in neurons and absent from peripheral tissues (Schell *et al.*, 1993). S2 is located between the two PKA phosphorylation sites, and alternative splicing of S2 is thought to contribute to the susceptibility of $\text{IP}_3\text{R1}$ to phosphorylation by PKA (Danoff *et al.*, 1991; Wagner *et al.*, 2003), but the major effect of alternative splicing of $\text{IP}_3\text{R1}$ pre-mRNA on its physiological functions is still unknown. The levels of the alternatively spliced transcripts of $\text{IP}_3\text{R1}$ mRNA generated by the knockdown of CHERP or ALG-2 were very low compared to the major $\Delta\text{E40/41/42}$ transcript (Fig. II-9B, C and D). Alternatively spliced isoforms might have differences in sensitivities against post-translational modifications or have much longer half-lives, and they contribute to the altered $\text{IP}_3\text{R1}$ functions more than the apparent mRNA levels. It would be interesting to know whether the degree of knockdown effects of CHERP or ALG-2 on alternative splicing is different in cell lines and cells at different developmental stages. I investigated the effects of CHERP knockdown on alternative splicing of other pre-mRNAs that encode proteins involved in Ca^{2+} -homeostasis regulation including sarcoplasmic reticulum Ca^{2+} -ATPase 1 (SERCA1) and CRACR2A, but no significant changes were observed in these pre-mRNAs (data not shown). Decrease in the CHERP mRNA by the anti-sense method induced growth arrest in HEL cells (LaPlante *et al.*, 2000). In addition to $\text{IP}_3\text{R1}$ pre-mRNA, CHERP and ALG-2 may have proper targets of pre-mRNAs for proteins

that regulate cell growth, proliferation, and Ca²⁺-mobilization.

Ca²⁺-dependent alternative splicing has been shown for pre-mRNAs of several proteins, including BK channel *slo*, IP₃R1, plasma membrane Ca²⁺-ATPase, neurexin II α , and NMDA receptor 1 (Xie *et al.*, 2001; Rozic-Kotliroff *et al.*, 2007; Li *et al.*, 2007; Xie *et al.*, 2008; Krebs *et al.*, 2011). CaMK IV, a calmodulin-dependent kinase, is involved in alternative splicing influenced by Ca²⁺ elevation that is triggered by depolarization in neuronal cells (Choi *et al.*, 2004; Xie *et al.*, 2001). Identification of CHERP as an ALG-2-interacting protein and as a splicing modulator in the present study has added new players in the Ca²⁺-dependent alternative splicing system and should contribute to an understanding of the sophisticated post-transcriptional regulation in mammalian cells.

Table II-1. Oligonucleotide primers used for detection of RNA by RT-PCR and quantification of RNA by real-time PCR (RT-qPCR).

Gene names	Isoforms	Primer sequences	
		Forward	Reverse
ALG-2		5'-tcgataaagacaggagtggagtg-3'	5'-caaacatggatatgatcgacctg-3'
CHERP		5'-ccaatgtgcctacttcgat-3'	5'-tgtactcgtgatcttccagctt-3'
GAPDH		5'-atgttcgcatgggtgtgaa-3'	5'-ggtgctaagcagttgggtg-3'
18S rRNA		5'-ttgactcaacacgggaaacc-3'	5'-tcgctccaccaactaagaacg-3'
Histone H3 (HIST2H3)		5'-cgcaggactttaagacgga-3'	5'-atgtcctgggcataatggt-3'
	Δ E40	5'-tggagaaaagcttctccag-3'	5'-gttgaccagaactgcctgag-3'
IP ₃ R1	Δ E40/41	5'-tggagaaaaggagcttgaacc-3'	5'-ccaaagctggttaaggctctctc-3'
	Δ E40/41/42	5'-atggagaaaagggtgagc-3'	5'-ccaaagctggttaaggctctctc-3'
	All	5'-agctctgcattaaggtctctac-3'	5'-ctgacgttccatagtaacgg-3'

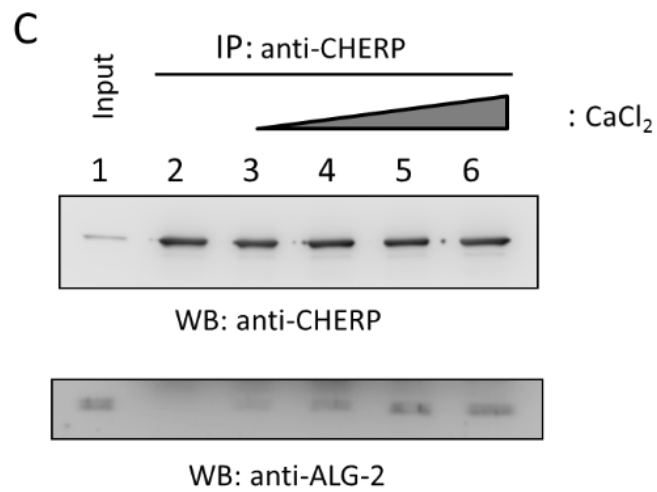
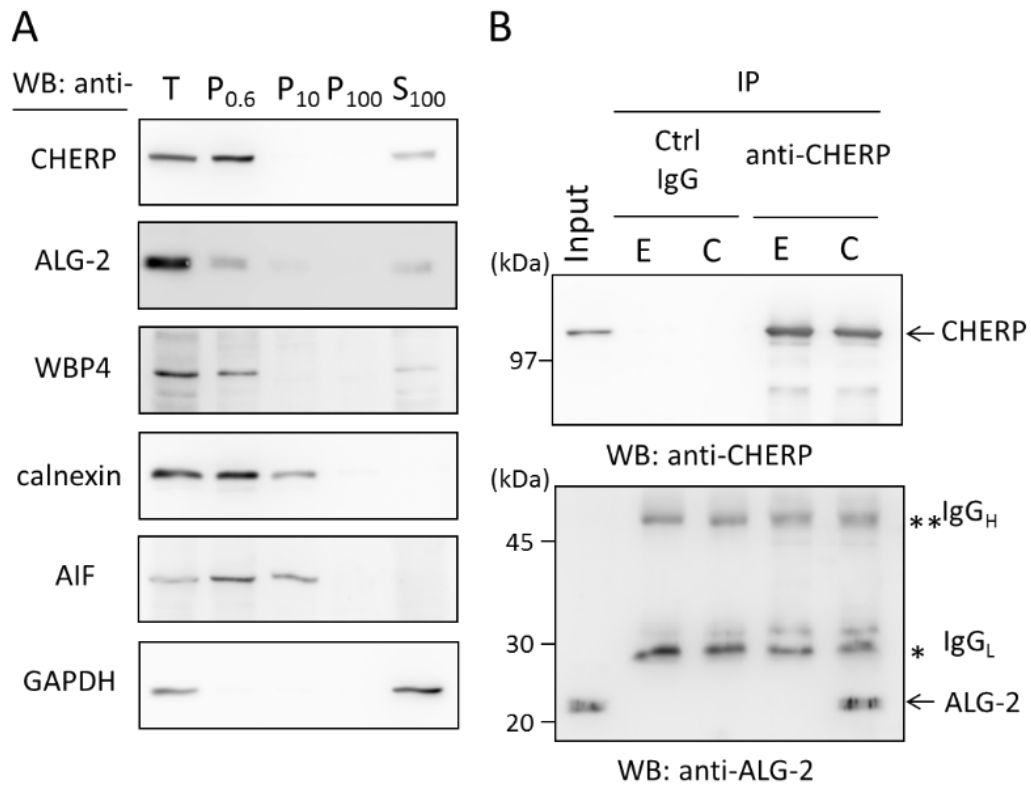


FIGURE II-1. Ca²⁺-dependent interaction between ALG-2 and CHERP. *A*, Subcellular fractionation of endogenous CHERP. HEK293T cells were homogenized and fractionated by differential successive centrifugations at 4 °C. Pellets of 600 × g (P_{0.6}), 10,000 × g (P₁₀), 100,000 × g (P₁₀₀), and the final supernatant of 100,000 × g (S₁₀₀) were subjected to Western blotting (WB) with antibodies against CHERP, ALG-2, WW domain-binding protein 4 (WBP4), calnexin, apoptosis-inducing factor (AIF), and glyceraldehyde-3-phosphate dehydrogenase (GAPDH). *B*, Co-immunoprecipitation of endogenous CHERP and ALG-2. CHERP was extracted from the P_{0.6} fraction by brief sonication with lysis buffer T (50 mM Tris-HCl, pH 7.5, 150 mM NaCl, 1.5 mM MgCl₂, and 0.2% Triton X-100 containing protease inhibitors). After centrifugation at 10,000 × g for 10 min at 4 °C, the supernatant (Input) was treated with RNase A (10 µg/ml) and supplemented with 5 mM EGTA (*E*) or 10 µM CaCl₂ (*C*). Each sample was subjected to immunoprecipitation by incubating first with mouse IgG (negative control, ctrl) or anti-CHERP mAb for 1 h at 4 °C and then with magnetic beads carrying Protein G overnight. After the beads had been collected and washed, immunoprecipitated proteins (IP products) were subjected to SDS-PAGE using 12.5% gel, transferred to a sheet of PVDF membrane, which was cut into halves (high and low molecular weight) and subjected to WB with anti-CHERP mAb (upper panel) and with anti-ALG-2 pAb (lower panel). Single and double asterisks indicate light and heavy chains of IgG, respectively. The relative amount of cleared cell lysate proteins (Input) used for analysis of IP products was 1.5%. *C*, Analysis of Ca²⁺-dependency of binding between ALG-2 and CHERP. Nuclear extracts were supplemented with 5 mM EGTA (lane 2) or with different concentrations of CaCl₂ (lane 3, none; lane 4, 1 µM; lane 5, 10 µM; lane 6, 100 µM) and subjected to co-immunoprecipitation with anti-CHERP mAb. The relative amount of cleared cell lysate proteins (Input) used for analysis of IP products was 1.5%. Representative data obtained from three (*A*), two (*B*), and four (*C*) independent experiments are shown. (From Sasaki-Osugi *et al.*, *Journal of Biological Chemistry*, 288: 33361-33375, 2013)

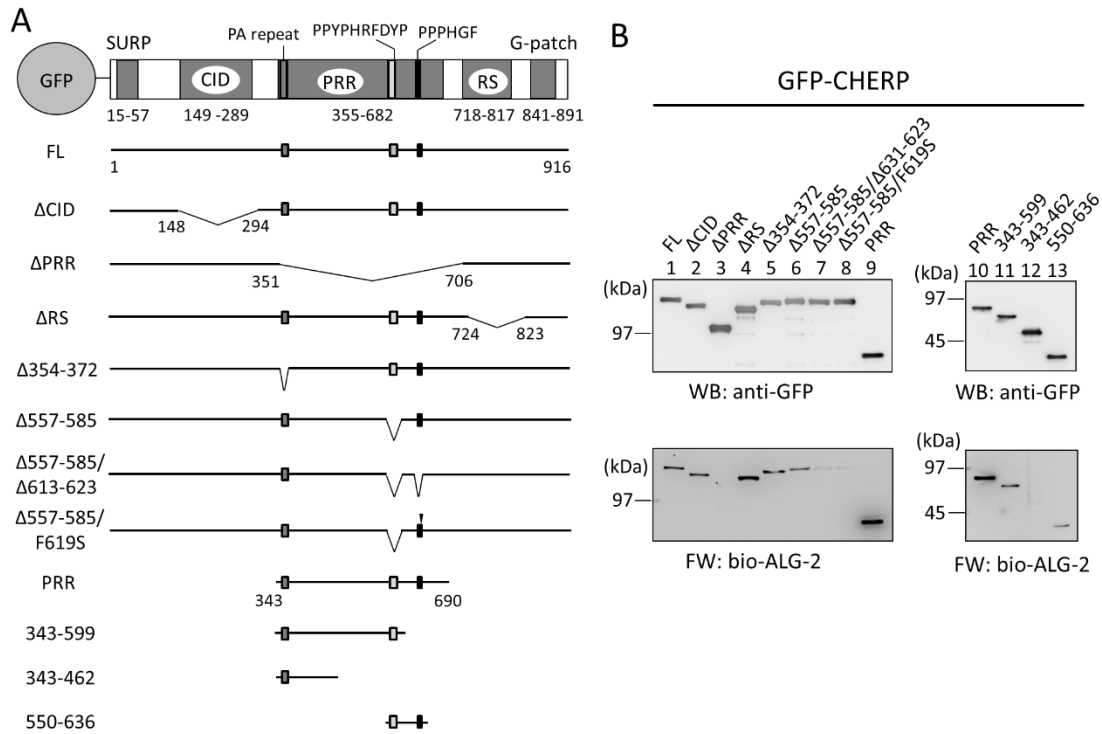
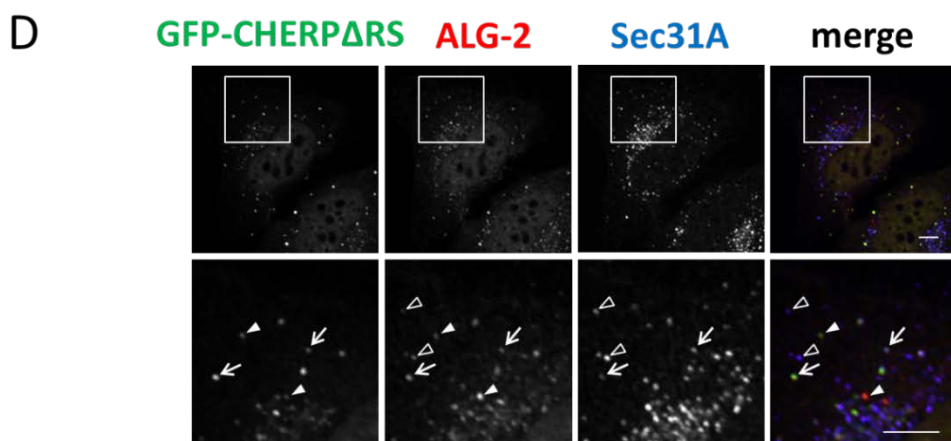
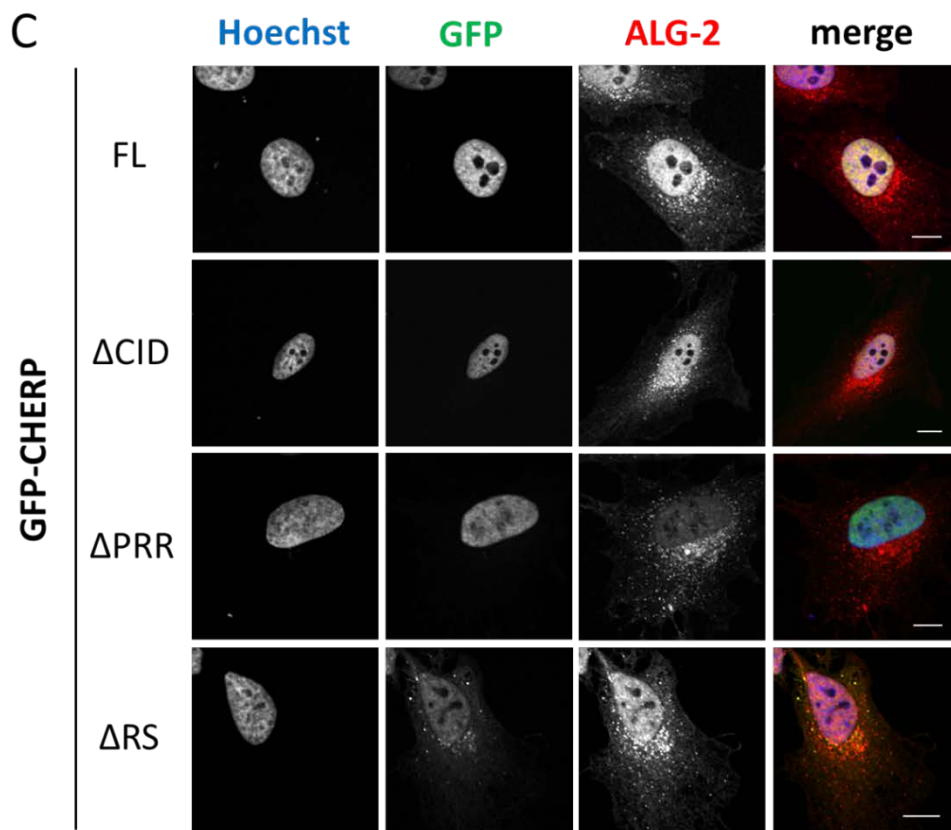


FIGURE II-2. Identification of ALG-2-binding sites and subcellular localization of GFP-CHERP mutants. *A*, Schematic diagrams of GFP-fused CHERP and its deletion mutants. CHERP has five distinct regions containing sequences similar to those designated SURP, CID (RNA polymerase II C-terminal domain-interacting domain), PRR (Pro-rich region), RS (Arg/Ser-rich region), and G-patch. Approximate positions of three motifs (PA repeat, PPYPHRFDYP and PPPHGF) are indicated at the top bar and marked with small filled boxes in black and gray in each expression construct. Filled arrowhead indicates replacement of Phe⁶¹⁹ with Ser (F619S mutation). *B*, FW blot analysis of GFP-fused CHERP and its deletion mutants with biotin-labeled ALG-2. HEK293T cells expressing GFP-fused CHERP FL and mutant proteins were lysed and centrifuged at $10,000 \times g$ for 10 min. GFP-fusion proteins were immunoprecipitated with GFP-TrapA from the cleared cell lysates and subjected to FW blot analysis with biotin-labeled ALG-2 (bio-ALG-2) and WB analysis using anti-GFP mAb. *C*, HeLa cells expressing GFP-fused CHERP full length (FL) and deletion mutants were fixed in 4% paraformaldehyde in PBS and permeabilized with 0.1% Triton X-100. Then the cells were immunostained with anti-ALG-2 pAb. Nuclear DNA was stained with Hoechst 33342. Fluorescence signals in the merged images are represented in pseudocolors: Hoechst, blue; GFP, green; ALG-2, red. Bars, 10 μ m. *D*, HeLa cells expressing GFP-CHERP Δ RS were fixed in 4% paraformaldehyde in PBS and

permeabilized with 0.1% Triton X-100. Then the cells were double-immunostained with anti-ALG-2 pAb (red) and anti-Sec31A mAb (blue). Bars, 5 μ m. Lower panels are magnified images of upper panels. Arrows: Puncta of GFP-CHERP Δ RS are co-localized with those of ALG-2 and Sec31A. Solid arrowheads: Puncta of GFP-CHERP Δ RS are co-localized only with those of ALG-2. Unfilled arrowheads: Puncta of ALG-2 are co-localized only with those of Sec31A. Representative data obtained from at least two independent experiments are shown for B, C, and D. (From Sasaki-Osugi *et al.*, *Journal of Biological Chemistry*, 288: 33361-33375, 2013)



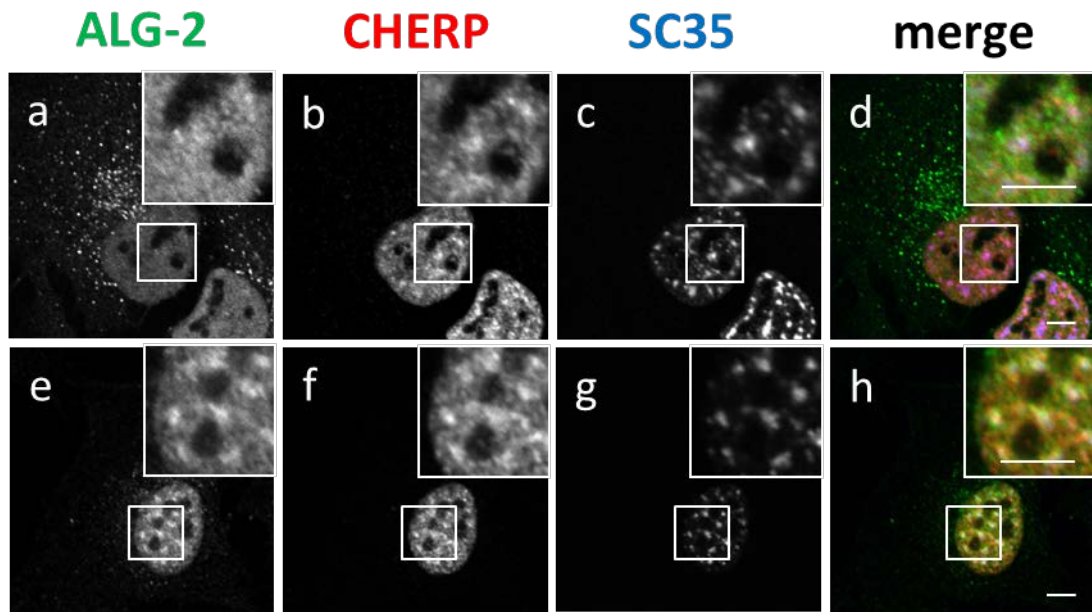


FIGURE II-3. Localization of endogenous CHERP at nuclear speckles by immunofluorescence microscopic analysis. HeLa cells were cultured on coverslips, fixed, and processed for pre-permeabilization with 50 $\mu\text{g/ml}$ digitonin in buffer D (20 mM HEPES-KOH, pH7.6, 50 mM NaCl, 2 mM MgCl_2 , 250 mM sucrose, 1 mM DTT) (e-h) on ice for 10 min and washed with buffer D or unprocessed for pre-permeabilization (a-d), fixed in 4% paraformaldehyde in PBS and permeabilized with 0.1% Triton X-100. Then, the cells were triple-immunostained with goat anti-ALG-2 pAb (green), rabbit anti-CHERP pAb (red) and mouse anti-SC35 mAb (blue). The fluorescence signals were analyzed with a confocal laser-scanning microscope and are represented in black and white. Merged images are shown in (d) and (h) in color. The small boxed areas are magnified in the respective large boxed areas. Bars, 5 μm . Representative data obtained from three independent experiments are shown. (From Sasaki-Osugi *et al.*, *Journal of Biological Chemistry*, 288: 33361-33375, 2013)

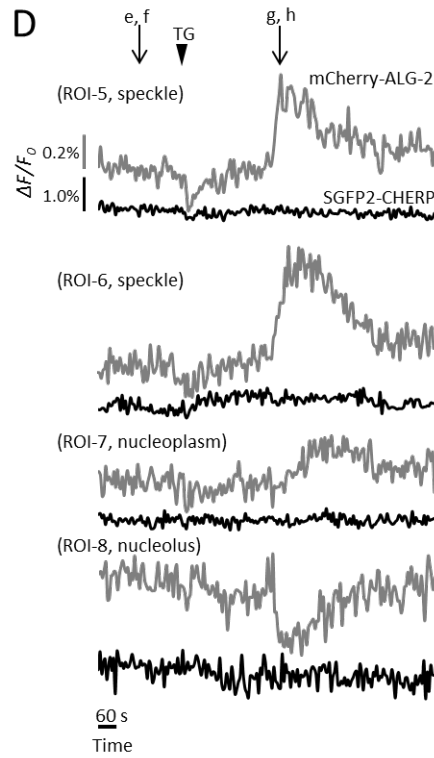
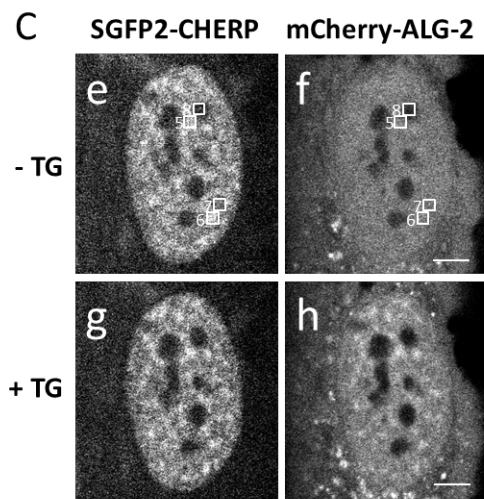
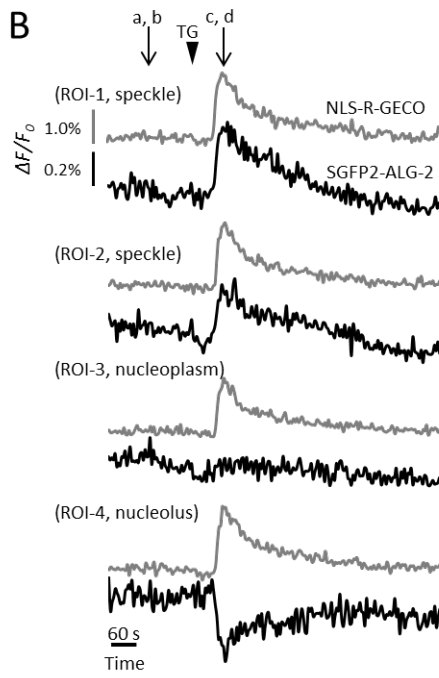
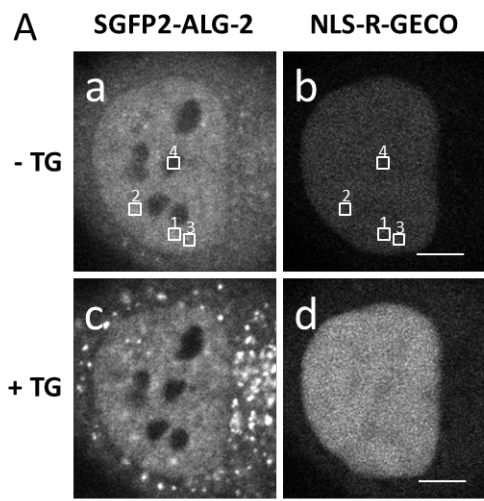


FIGURE II-4. Transient translocation of GFP-ALG-2 to nuclear speckles by treatment with thapsigargin. *A* and *C*, HeLa cells co-expressing (*A*) SGFP2-ALG-2 and NLS-R-GECO or (*C*) SGFP2-CHERP and mCherry-ALG-2 were incubated for 15 min in Leibovitz L15 medium containing 1% fetal bovine serum. Time-lapse images were acquired using a confocal microscope. Panels (*a*)-(*b*) and (*c*)-(*d*) correspond to images before (at 160 s) and after (at 276 s) addition of thapsigargin (TG, final concentration of 2 μ M at 196 s) in (*A*), respectively (time after starting acquisition of images indicated in parentheses). Panels (*e*)-(*f*) and (*g*)-(*h*) correspond to images before (at 231 s) and after (at 603 s) addition of TG (at 276 s) in (*C*), respectively. Bars, 5 μ m. *B* and *D*, Temporal changes in fluorescence intensities of four areas (regions of interest, ROI) indicated by white boxes shown in panel (*a*) and (*b*) in (*A*) and those in panel (*e*) and (*f*) in (*C*) were measured by Olympus FV10-ASW software (*B*, ROI-1, speckle; ROI-2, speckle; ROI-3, nucleoplasm; ROI-4, nucleolus; *D*, ROI-5, speckle; ROI-6, speckle; ROI-7, nucleoplasm; ROI-8, nucleolus). Changes in relative fluorescence intensity ($\Delta F/F_0$) derived from (*B*) SGFP2-ALG-2 and NLS-R-GECO and in that derived from (*D*) SGFP2-CHERP and mCherry-ALG-2 are represented with black and gray curves for each ROI as indicated. The time of addition of TG and the time points at which images are shown in *A* and *C* are indicated by arrowheads and arrows, respectively. Representative data obtained from three independent experiments are shown. (From Sasaki-Osugi *et al.*, *Journal of Biological Chemistry*, 288: 33361-33375, 2013)

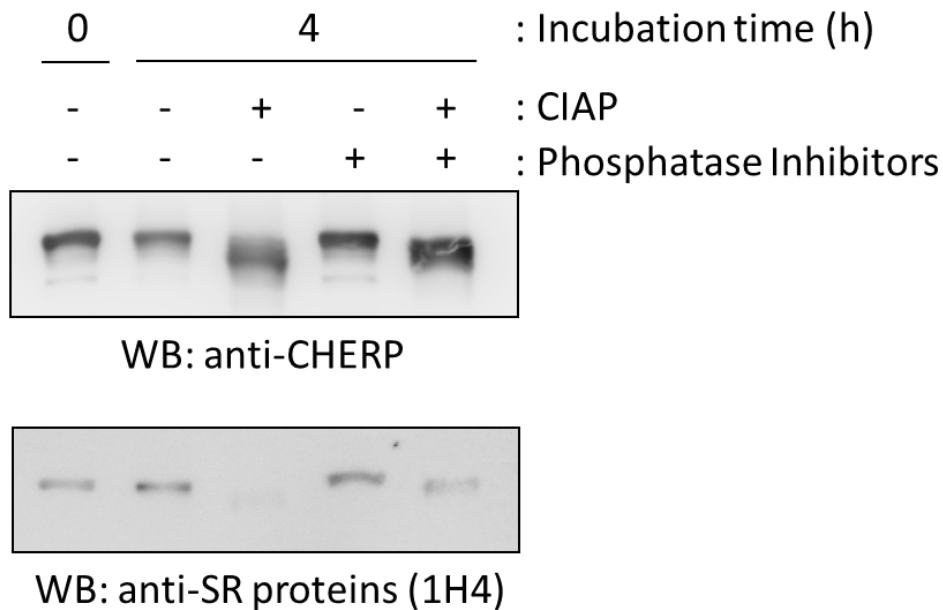


FIGURE II-5. Detection of CHERP with anti-phosphorylated RS domains by WB. HEK293T cells were lysed with buffer T and the cleared cell lysate was subjected to immunoprecipitation with rabbit anti-CHERP pAb. The IP products were treated with or without 0.5 units/ μ l CIAP in a reaction buffer {50 mM Tris-HCl, pH 8.0, 0.1 mM Zn(OAc)₂, 1 mM MgCl₂} in the presence or absence of phosphatase inhibitors (10 mM NaF, 1 mM NaVO₄, 5 mM sodium pyrophosphate, and 10 mM β -glycerophosphate) at 37 °C for 4 h and then subjected to WB with rabbit anti-CHERP pAb (upper panel) and mouse mAb against pan-SR proteins (1H4) (lower panel). Representative data obtained from two independent experiments are shown. (From Sasaki-Osugi *et al.*, *Journal of Biological Chemistry*, 288: 33361-33375, 2013)

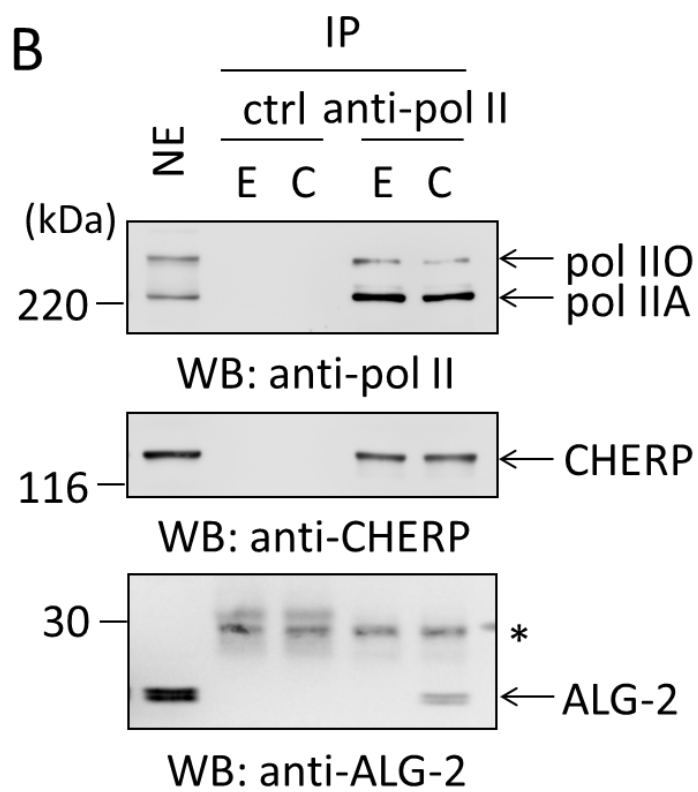
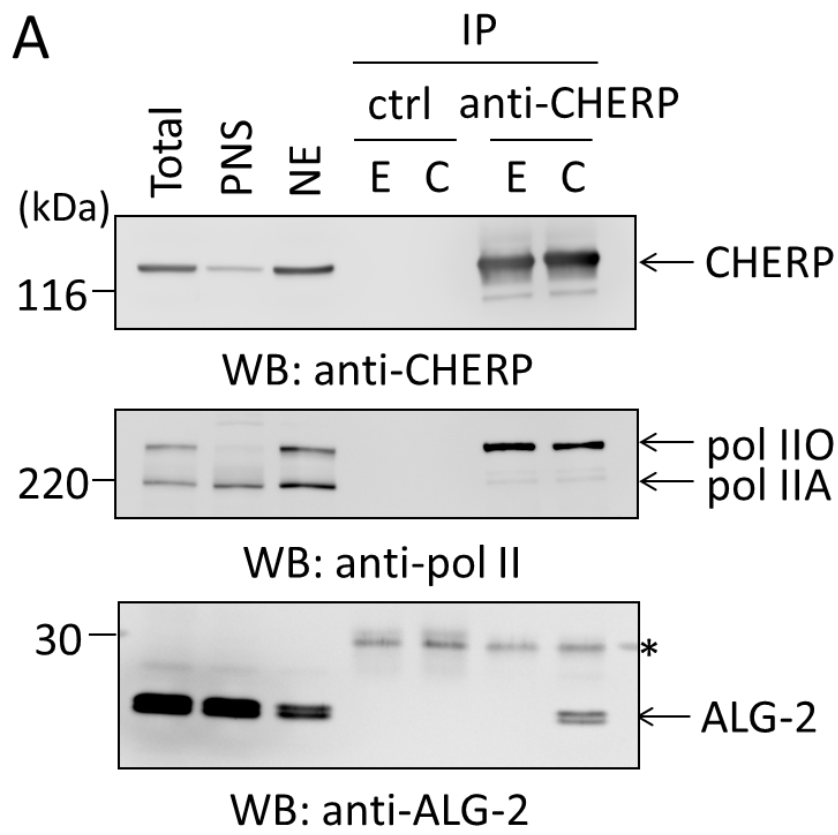


FIGURE II-6. Binding between CHERP and RNA polymerase II. The crude nuclear fraction (P_{0.6} fraction) was prepared from HEK293T cells and the nuclear extract (NE) was treated with 10 µg/ml RNase A. After addition of 5 mM EGTA or 10 µM CaCl₂, and the NE was subjected to immunoprecipitation with (A) rabbit anti-CHERP pAb or (B) rabbit anti-pol II pAb as well as with rabbit IgG as a negative control. The immunoprecipitated proteins (IP) were subjected to WB with rabbit anti-CHERP pAb, anti-pol II pAb, or rabbit anti-ALG-2 pAb. The relative amounts of cleared cell lysate proteins (NE) used for analysis of IP products were 5% except for ALG-2 (2.5%) in B. PNS, post nuclear supernatant; pol IIO, phosphorylated form of RNA polymerase II; pol IIA, unphosphorylated form of RNA polymerase II. Asterisk, IgG light chain. Representative data obtained from two (A) and three (B) independent experiments are shown. (From Sasaki-Osugi *et al.*, *Journal of Biological Chemistry*, 288: 33361-33375, 2013)

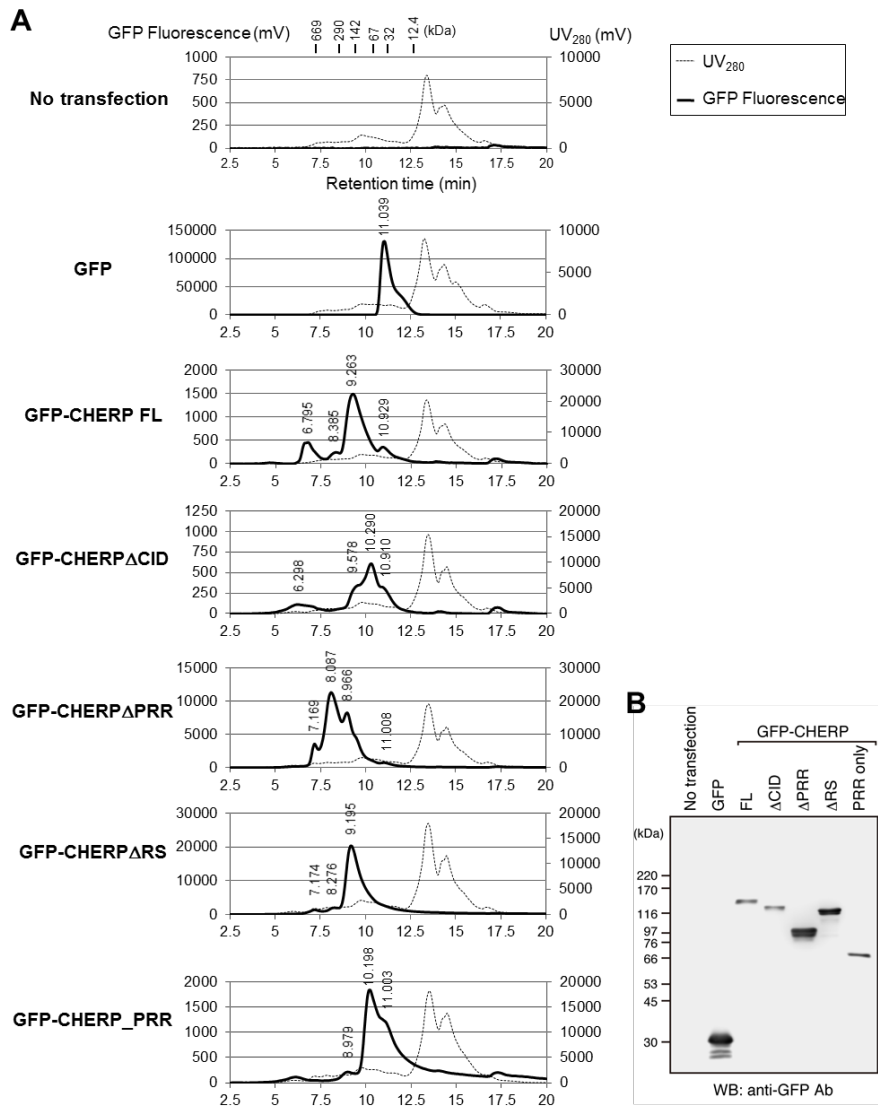


FIGURE II-8. Size-exclusion chromatography profiles of GFP-fused CHERP deletion mutants. (A) HEK293T cells transiently expressing indicated GFP-fused CHERP deletion mutants were lysed, and cell extracts treated with RNase A were resolved by size-exclusion chromatography. The GFP signals derived from each GFP-CHERP deletion mutants were monitored with a fluorescence detector. A number indicated on the top of each GFP signal peak stands for the retention time. The positions of molecular mass standards (in kilodaltons, kDa) are indicated in the panel for control (No transfection).

(B) Cell extracts used for (A) were analyzed by WB with anti-GFP mAb. (From Sasaki-Osugi *et al.*, *Journal of Biological Chemistry*, 288: 33361-33375, 2013)

Table II-2. Size-exclusion chromatography analyses of GFP-fused CHERP deletion mutants.

Sample	MW ($\times 10^3$)	Peak retention time (min)	Peak height (>100)	Calculated MW ($\times 10^3$)
GFP	29	11.039	131836	42.9
GFP-CHERP FL	132.7	6.795	463	>669
		8.385	247	315.9
		9.263	1497	163.3
		10.929	357	46.6
GFP-CHERP Δ CID	116	6.298	118	>669
		9.578	345	128.8
		10.29	615	75.4
		10.91	330	47.3
GFP-CHERP Δ PRR	93	7.169	3376	>669
		8.087	11116	395.3
		8.966	8086	204.1
		11.008	145	44.0
GFP-CHERP Δ RS	121.5	7.174	1168	>669
		8.276	1708	342.9
		9.195	20076	171.8
GFP-CHERP-PRR	68	8.979	201	202.1
		10.198	1832	80.8
		11.003	1223	44.1

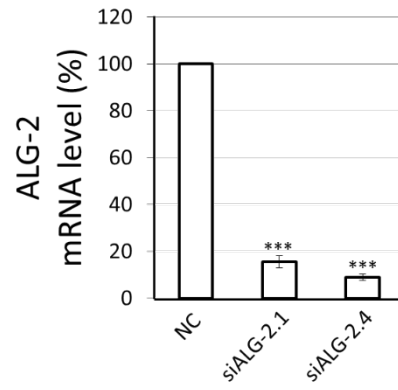
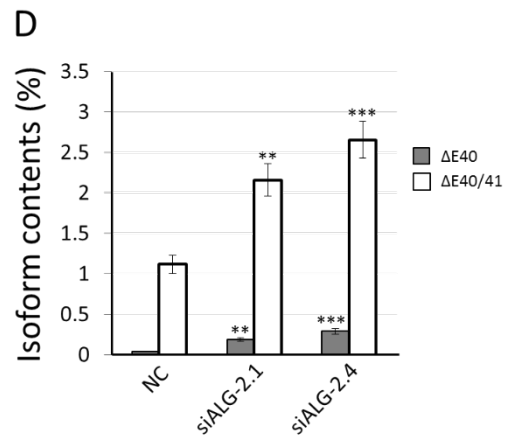
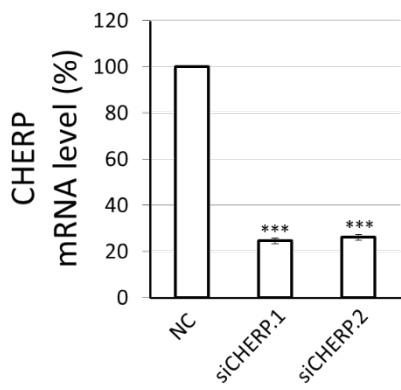
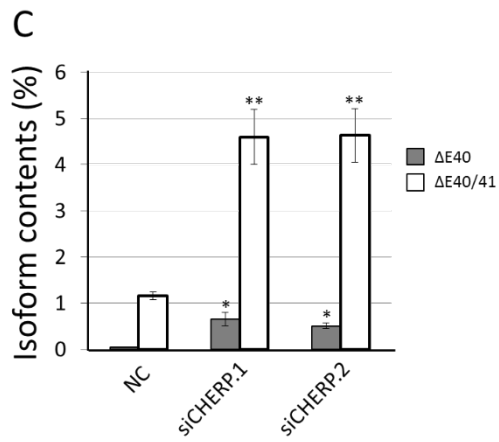
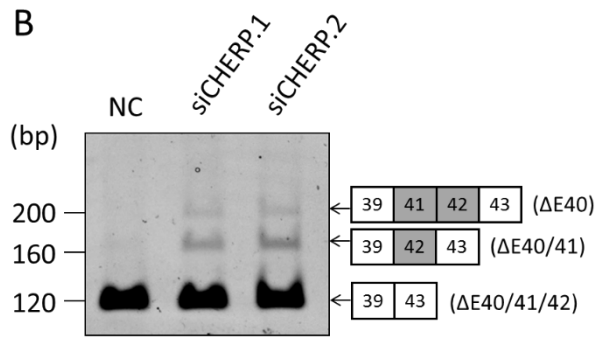
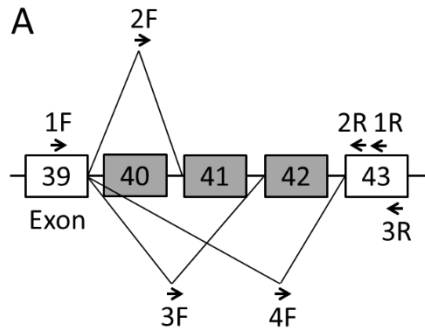


FIGURE II-9. Effects of CHERP or ALG-2 knockdown on alternative splicing of IP₃R1 pre-mRNA. *A*, A schematic diagram of the alternative spliced region (S2 splice site: exons 40 to 42) of IP₃R1 pre-mRNA. Arrows indicate PCR primers used in the present study. *B*, Total RNA was extracted from HT1080 cells transfected with siRNAs specific for CHERP (siCHERP#1 and siCHERP#2) or negative control siRNA (NC) and analyzed by RT-PCR with forward (1F) and reverse (1R) primers to detect all isoforms. Representative data obtained from three independent experiments are shown. *C* and *D*, Total RNA was extracted from HT1080 cells that were transfected with siRNAs specific for CHERP, ALG-2 (siALG-2#1 and siALG-2#4) or negative control (NC). After reverse transcription, real-time quantitative PCR (RT-qPCR) was performed with primers for the detection of each splicing isoform of IP₃R1 pre-mRNA (Δ E40: 2F and 2R; Δ E40/41: 3F and 3R; Δ E40/41/42: 4F and 3R) as well as the mRNA levels of CHERP and ALG-2. * p <0.05, ** p <0.01, *** p <0.001 vs each control (ANOVA followed by Dunnett's test; mean \pm SE; n =4). All RNA levels were normalized to GAPDH mRNA that was used as a reference RNA. (From Sasaki-Osugi *et al.*, *Journal of Biological Chemistry*, 288: 33361-33375, 2013)

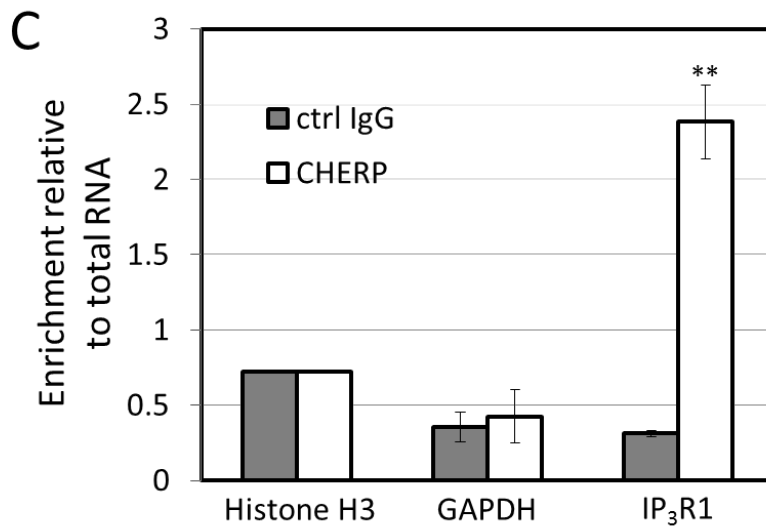
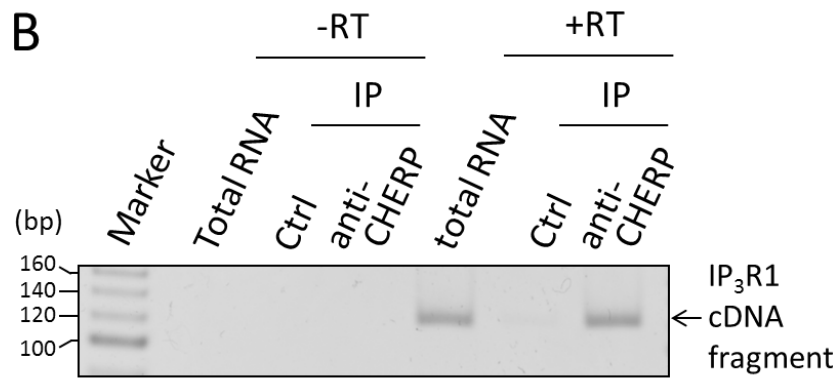
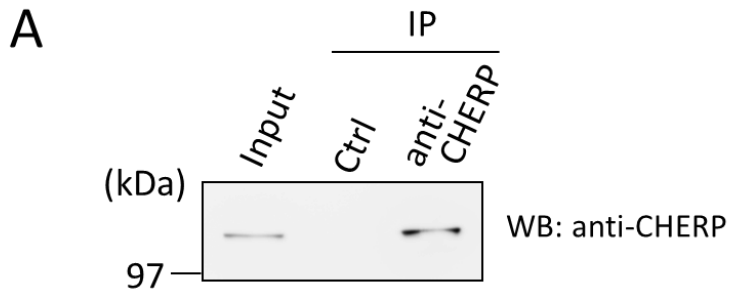


FIGURE II-10. Physical association of CHERP with IP₃R1 RNA. *A*, RNA immunoprecipitation (RIP) was performed with rabbit IgG (control, ctrl) or rabbit anti-CHERP pAb. Immunoprecipitated (IP) proteins were subjected to WB using rabbit anti-CHERP pAb. The relative amount of cleared cell lysate proteins (Input) used for analysis of IP products was 1.5%. *B*, RNAs were isolated from whole cells (total RNA) or immunoprecipitates (IP) and subjected to RT-PCR after reverse transcription (+RT) or without reverse transcription (-RT) for the detection of IP₃R1 segment S2 with the primers of 1F and 1R as indicated in Fig. II-8A. RT-PCR products were analyzed by 5% PAGE and stained with ethidium bromide. *C*, Relative amounts of RNA in the immunoprecipitates were measured by RT-qPCR for histone H3, GAPDH, and IP₃R1 RNAs using 18S rRNA as a reference RNA. Relative degree of enrichment of analyzed RNA in the immunoprecipitates compared with total RNA is expressed in the ordinate. ** $p < 0.01$ vs each control IgG (Student's t-test; mean \pm SE; $n=3$). Representative data obtained from three independent experiments are shown. (From Sasaki-Osugi *et al.*, *Journal of Biological Chemistry*, 288: 33361-33375, 2013)

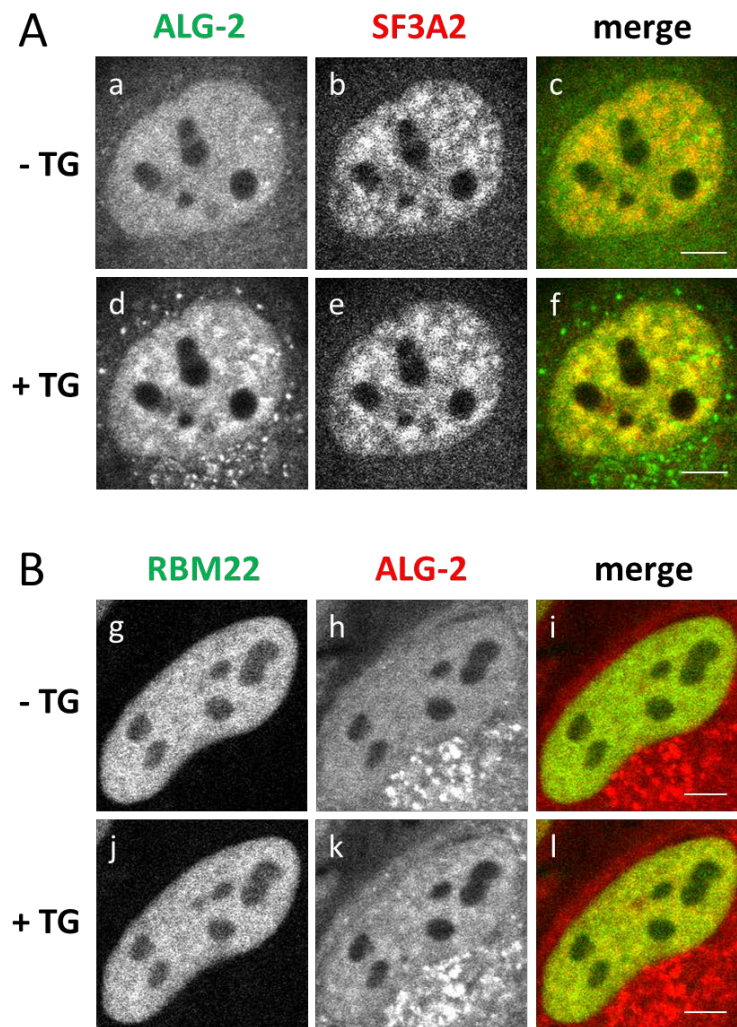


FIGURE II-11. Transient translocation of ALG-2 to nuclear speckles by treatment with thapsigargin. HeLa cells co-expressing (A) SGFP2-ALG-2 (ALG-2 N-terminally fused with SGFP2) and mCherry-SF3A2 (SF3A2 N-terminally fused with mCherry), or (B) EGFP-RBM22 (RBM22 N-terminally fused with EGFP) and mCherry-ALG-2 (ALG-2 N-terminally fused with mCherry) were incubated for 15 min in Leibovitz L15 medium containing 1% fetal bovine serum. Before and after treatment with 2 μ M thapsigargin (TG), time-lapse images were acquired every (A) 5.25 s and (B) 4.57 s using a confocal microscope. Panels (a)-(c) and (d)-(f) correspond to images before (2 min 6.00 s) and after (9 min 48.02 s) addition of TG (4 min 17.25 s) in (A), respectively (time after starting acquisition of images indicated in the parentheses). Panels (g)-(i) and (j)-(l) correspond to images before (1 min 49.64 s) and after (6 min 5.41 s) addition of TG (3 min 43.81 s) in (B), respectively. Bars, 5 μ m. (From Sasaki-Osugi *et al.*, *Journal of Biological Chemistry*, 288: 33361-33375, 2013)

References

Ariumi, Y., Kuroki, M., Kushima, Y., Osugi, K., Hijikata, M., Maki, M., Ikeda, M., and Kato, N. (2011) Hepatitis C virus hijacks P-body and stress granule components around lipid droplets. *J. Virol.* **85**, 6882-6892

Aviel-Ronen, S., Coe, B.P., Lau, S.K., da Cunha Santos, G., Zhu, C.Q., Strumpf, D., Jurisica, I., Lam, W.L., and Tsao, M.S. (2008) Genomic markers for malignant progression in pulmonary adenocarcinoma with bronchioloalveolar features. *Proc. Natl. Acad. Sci. USA.* **105**, 10155-10160

Braun, J.E., Tritschler, F., Haas, G., Igreja, C., Truffault, V., Weichenrieder, O., and Izaurralde, E. (2010) The C-terminal alpha-alpha superhelix of Pat is required for mRNA decapping in metazoa. *EMBO J.* **29**, 2368-2380

Becker, R., Loll, B., and Meinhart, A. (2008) Snapshots of the RNA processing factor SCAF8 bound to different phosphorylated forms of the carboxyl-terminal domain of RNA polymerase II. *J. Biol. Chem.* **283**, 22659-22669

Chen, C., and Sytkowski, A.J. (2005) Apoptosis-linked gene-2 connects the Raf-1 and ASK1 signalings. *Biochem. Biophys. Res. Commun.* **333**, 51-57

Choi, J. Y., Beaman-Hall, C. M., and Vallano, M. L. (2004) Granule neurons in cerebellum express distinct splice variants of the inositol trisphosphate receptor that are modulated by calcium. *Am. J. Physiol. Cell Physiol.* **287**, C971-980

Danoff, S. K., Ferris, C. D., Donath, C., Fischer, G. A., Munemitsu, S., Ullrich, A., Snyder, S. H., and Ross, C. A. (1991) Inositol 1,4,5-trisphosphate receptors: distinct neuronal and nonneuronal forms derived by alternative splicing differ in phosphorylation. *Proc. Natl. Acad. Sci. USA.* **88**, 2951-2955

Das, R., Yu, J., Zhang, Z., Gygi, M. P., Krainer, A. R., Gygi, S. P., and Reed, R. (2007) SR proteins function in coupling RNAP II transcription to pre-mRNA splicing. *Mol. Cell* **26**, 867-881

Draeby, I., Woods, Y.L., la Cour, J.M., Mollerup, J., Bourdon, J.C., and Berchtold, M.W. (2007) The calcium binding protein ALG-2 binds and stabilizes Scotin, a p53-inducible gene product localized at the endoplasmic reticulum membrane. *Arch. Biochem. Biophys.* **467**, 87-94

Franks, T.M., and Lykke-Andersen, J. (2007) TTP and BRF proteins nucleate processing body formation to silence mRNAs with AU-rich elements. *Genes Dev.* **15**, 719-735.

Franks, T.M., and Lykke-Andersen, J. (2008) The control of mRNA decapping and P-body formation. *Mol. Cell* **32**, 605-615

Fu, X. D., and Maniatis, T. (1992) The 35-kDa mammalian splicing factor SC35 mediates specific interactions between U1 and U2 small nuclear ribonucleoprotein particles at the 3' splice site. *Proc. Natl. Acad. Sci. USA.* **89**, 1725-1729

Ghosh, G., and Adams, J. A. (2011) Phosphorylation mechanism and structure of serine-arginine protein kinases. *FEBS J.* **278**, 587-597

Gifford, J.L., Walsh, M.P., and Vogel, H.J. (2007) Structures and metal-ion-binding properties of the Ca²⁺-binding helix-loop-helix EF-hand motifs. *Biochem. J.* **405**, 199-221

Haas, G., Braun, J.E., Igreja, C., Tritschler, F., Nishihara, T., and Izaurralde, E. (2010) HPat provides a link between deadenylation and decapping in metazoa. *J. Cell Biol.* **189**, 289-302

Hoj, B.R., la Cour, J.M., Mollerup, J., and Berchtold, M.W. (2009) ALG-2 knockdown in HeLa cells results in G2/M cell cycle phase accumulation and cell death. *Biochem. Biophys. Res. Commun.* **378**, 145-148

Hwang, I.S., Jung, Y.S., and Kim, E. (2002) Interaction of ALG-2 with ASK1 influences ASK1 localization and subsequent JNK activation. *FEBS. Lett.* **529**, 183-187

Ichioka, F., Kobayashi, R., Katoh, K., Shibata, H., and Maki, M. (2008) Brox, a novel farnesylated Bro1 domain-containing protein that associates with charged

multivesicular body protein 4 (CHMP4). *FEBS J.* **275**, 682-692

Inuzuka, T., Suzuki, H., Kawasaki, M., Shibata, H., Wakatsuki, S., and Maki, M. (2010) Molecular basis for defect in Alix-binding by alternatively spliced isoform of ALG-2 (ALG-2^{ΔGF122}) and structural roles of F122 in target recognition. *BMC Struct. Biol.* **10**:25

Jang, I.K., Hu, R., Lacana, E., D'Adamio, L., and Gu, H. (2002) Apoptosis-linked gene 2-deficient mice exhibit normal T-cell development and function. *Mol. Cell. Biol.* **22**, 4094-4100

Jia, J., Tarabykina, S., Hansen, C., Berchtold, M., Cygler, M. (2001) Structure of apoptosis-linked protein ALG-2: Insights into Ca²⁺-induced changes in penta-EF-hand proteins. *Structure* **9**, 267-275

Katoh, K., Shibata, H., Suzuki, H., Nara, A., Ishidoh, K., Kominami, E., Yoshimori, T., and Maki, M. (2003) The ALG-2-interacting protein Alix associates with CHMP4b, a human homologue of yeast Snf7 that is involved in multivesicular body sorting. *J. Biol. Chem.* **278**, 39104-39113

Katoh, K., Suzuki, H., Terasawa, Y., Mizuno, T., Yasuda, J., Shibata, H., and Maki, M. (2005) The penta-EF-hand protein ALG-2 interacts directly with the ESCRT-I component TSG101, and Ca²⁺-dependently co-localizes to aberrant endosomes with dominant-negative AAA ATPase SKD1/Vps4B. *Biochem. J.* **391**, 677-685

Kay, B.K., Williamson, M.P., and Sudol, M. (2000) The importance of being proline: the interaction of proline-rich motifs in signaling proteins with their cognate domains. *FASEB J.* **14**, 231-241

Kitaura, Y., Matsumoto, S., Satoh, H., Hitomi, K., and Maki, M. (2001) Peflin and ALG-2, members of the penta-EF-hand protein family, form a heterodimer that dissociates in a Ca²⁺-dependent manner. *J. Biol. Chem.* **276**, 14053-14058

Krebs, J., Groenendyk, J., and Michalak, M. (2011) Ca²⁺-signaling, alternative splicing and endoplasmic reticulum stress responses. *Neurochem. Res.* **36**, 1198-1211

Kremers, G. J., Goedhart, J., van den Heuvel, D. J., Gerritsen, H. C., and Gadella, T. W., Jr. (2007) Improved green and blue fluorescent proteins for expression in bacteria and mammalian cells. *Biochemistry* **46**, 3775-3783

la Cour, J. M., Mollerup, J., and Berchtold, M. W. (2007) ALG-2 oscillates in subcellular localization, untemporally with calcium oscillations. *Biochem. Biophys. Res. Commun.* **353**, 1063-1067

LaPlante, J. M., O'Rourke, F., Lu, X., Fein, A., Olsen, A., and Feinstein, M. B. (2000) Cloning of human Ca²⁺ homeostasis endoplasmic reticulum protein (CHERP): regulated expression of antisense cDNA depletes CHERP, inhibits intracellular Ca²⁺ mobilization and decreases cell proliferation. *Biochem. J.* **348**, 189-199

Li, Q., Lee, J. A., and Black, D. L. (2007) Neuronal regulation of alternative pre-mRNA splicing. *Nat. Rev. Neurosci.* **8**, 819-831

Lin-Moshier, Y., Sebastian, P. J., Higgins, L., Sampson, N. D., Hewitt, J. E., and Marchant, J. S. (2013) Re-evaluation of the role of calcium homeostasis endoplasmic reticulum protein (CHERP) in cellular calcium signaling. *J. Biol. Chem.* **288**, 355-367

Mahul-Mellier, A.L., Strappazzon, F., Petiot, A., Chatellard-Causse, C., Torch, S., Blot, B., Freeman, K., Kuhn, L., Garin, J., Verna, J.M., Fraboulet, S., and Sadoul, R. (2008) Alix and ALG-2 are involved in tumor necrosis factor receptor 1-induced cell death. *J. Biol. Chem.* **283**, 34954-34965

Maki, M., Narayana, S.V., and Hitomi, K. (1997) A growing family of the Ca²⁺-binding proteins with five EF-hand motifs. *Biochem. J.* **328** (Pt 2), 718-720

Maki, M., Yamaguchi, K., Kitaura, Y., Satoh, H., and Hitomi, K. (1998) Calcium-induced exposure of a hydrophobic surface of mouse ALG-2, which is a member of the penta-EF-hand protein family. *J. Biochem.* **124**, 1170-1177

Maki, M., Kitaura, Y., Satoh, H., Ohkouchi, S., and Shibata, H. (2002) Structures, functions and molecular evolution of the penta-EF-hand Ca²⁺-binding proteins. *Biochim. Biophys. Acta* **1600**, 51-60

- Maki, M., Suzuki, H., and Shibata, H. (2011) Structure and function of ALG-2, a penta-EF-hand calcium-dependent adaptor protein. *Sci. China Life Sci.* **54**, 770-779
- Manley, J. L., and Krainer, A. R. (2010) A rational nomenclature for serine/arginine-rich protein splicing factors (SR proteins). *Genes Dev.* **24**, 1073-1074
- Marnef, A., and Standart, N. (2010) Pat1 proteins: a life in translation, translation repression and mRNA decay. *Biochem. Soc. Trans.* **38**, 1602-1607
- Marnef, A., Weil, D., and Standart, N. (2012) RNA-related nuclear functions of human Pat1b, the P-body mRNA decay factor. *Mol. Biol. Cell* **23**, 213-224
- Mathew, R., Hartmuth, K., Möhlmann, S., Urlaub, H., Ficner, R., and Lührmann, R. (2008) Phosphorylation of human PRP28 by SRPK2 is required for integration of the U4/U6-U5 tri-snRNP into the spliceosome. *Nat. Struct. Mol. Biol.* **15**, 435-443
- Missotten, M., Nichols, A., Rieger, K., and Sadoul, R. (1999) Alix, a novel mouse protein undergoing calcium-dependent interaction with the apoptosis-linked-gene 2 (ALG-2) protein. *Cell Death Differ.* **6**, 124-129
- Montaville, P., Dai, Y., Cheung, C.Y., Giller, K., Becker, S., Michalak, M., Webb, S.E., Miller, A.L., and Krebs, J. (2006) Nuclear translocation of the calcium-binding protein ALG-2 induced by the RNA-binding protein RBM22. *Biochim. Biophys. Acta* **1763**, 1335-1343
- Muñoz, M. J., de la Mata, M., and Kornblihtt, A. R. (2010) The carboxy terminal domain of RNA polymerase II and alternative splicing. *Trends Biochem. Sci.* **35**, 497-504
- Nakagawa, T., Shiota, C., Okano, H., and Mikoshiba, K. (1991) Differential localization of alternative spliced transcripts encoding inositol 1,4,5-trisphosphate receptors in mouse cerebellum and hippocampus: *in situ* hybridization study. *J. Neurochem.* **57**, 1807-1810
- Neugebauer, K. M., and Roth, M. B. (1997) Distribution of pre-mRNA splicing factors at sites of RNA polymerase II transcription. *Genes Dev.* **11**, 1148-1159

Nucifora, F. C., Jr., Li, S. H., Danoff, S., Ullrich, A., and Ross, C. A. (1995) Molecular cloning of a cDNA for the human inositol 1,4,5-trisphosphate receptor type 1, and the identification of a third alternatively spliced variant. *Brain. Res. Mol. Brain Res.* **32**, 291-296

Okumura, M., Ichioka, F., Kobayashi, R., Suzuki, H., Yoshida, H., Shibata, H., and Maki, M. (2009) Penta-EF-hand protein ALG-2 functions as a Ca²⁺-dependent adaptor that bridges Alix and TSG101. *Biochem. Biophys. Res. Commun.* **386**, 237-241

O'Rourke, F., Soons, K., Flaumenhaft, R., Watras, J., Baio-Larue, C., Matthews, E., and Feinstein, M. B. (1994) Ca²⁺ release by inositol 1,4,5-trisphosphate is blocked by the K⁺-channel blockers apamin and tetrapentylammonium ion, and a monoclonal antibody to a 63 kDa membrane protein: reversal of blockade by K⁺ ionophores nigericin and valinomycin and purification of the 63 kDa antibody-binding protein. *Biochem. J.* **300**, 673-683

O'Rourke, F. A., LaPlante, J. M., and Feinstein, M. B. (2003) Antisense-mediated loss of calcium homeostasis endoplasmic reticulum protein (CHERP; ERPROT213-21) impairs Ca²⁺ mobilization, nuclear factor of activated T-cells (NFAT) activation and cell proliferation in Jurkat T-lymphocytes. *Biochem. J.* **373**, 133-143

Osugi, K., Suzuki, H., Nomura, T., Ariumi, Y., Shibata, H., and Maki, M. (2012) Identification of the P-body component PATL1 as a novel ALG-2-interacting protein by *in silico* and far-Western screening of proline-rich proteins. *J. Biochem.* **151**, 657-666

Osugi, K., Shibata, H., and Maki, M. (2013) Biochemical and immunological detection of physical interactions between penta-EF-hand protein ALG-2 and its binding partners. *Methods Mol. Biol.* **963**, 187-200

Ozgur, S., Chekulaeva, M., and Stoecklin, G. (2010) Human Pat1b connects deadenylation with mRNA decapping and controls the assembly of processing bodies. *Mol. Cell Biol.* **30**, 4308-4323

Park, S.H., Lee, J.H., Lee, G.B., Byun, H.J., Kim, B.R., Park, C.Y., Kim, H.B., and Rho, S.B. (2012) PDCD6 additively cooperates with anti-cancer drugs through activation of

NF- κ B pathways. *Cell. Signal.* **24**, 726-733

Pilkington, G.R., and Parker, R. (2008) Pat1 contains distinct functional domains that promote P-body assembly and activation of decapping. *Mol. Cell Biol.* **28**, 1298-1312

Rao, R.V., Poksay, K.S., Castro-Obregon, S., Schilling, B., Row, R.H., del Rio, G., Gibson, B.W., Ellerby, H.M., and Bredesen, D.E. (2004) Molecular components of a cell death pathway activated by endoplasmic reticulum stress. *J. Biol. Chem.* **279**, 177-187

Rasche, N., Dybkov, O., Schmitzova, J., Akyildiz, B., Fabrizio, P., and Luhrmann, R. (2012) Cwc2 and its human homologue RBM22 promote an active conformation of the spliceosome catalytic centre. *EMBO J.* **31**, 1591-1604

Ren, X., and Hurley, J.H. (2011) Proline-rich regions and motifs in trafficking: from ESCRT interaction to viral exploitation. *Traffic* **12**, 1282-1290

Rho, S.B., Song, Y.J., Lim, M.C., Lee, S.H., Kim, B.R., and Park, S.Y. (2012) Programmed cell death 6 (PDCD6) inhibits angiogenesis through PI3K/mTOR/p70S6K pathway by interacting of VEGFR-2. *Cell Signal.* **24**, 131-139

Rozic-Kotliroff, G., and Zisapel, N. (2007) Ca²⁺-dependent splicing of neurexin II α . *Biochem. Biophys. Res. Commun.* **352**, 226-230

Ryan, T., Sharma, P., Ignatchenko, A., MacLennan, D. H., Kislinger, T., and Gramolini, A. O. (2011) Identification of novel ryanodine receptor 1 (RyR1) protein interaction with calcium homeostasis endoplasmic reticulum protein (CHERP). *J. Biol. Chem.* **286**, 17060-17068

Saitoh, N., Spahr, C. S., Patterson, S. D., Bubulya, P., Neuwald, A. F., and Spector, D. L. (2004) Proteomic analysis of interchromatin granule clusters. *Mol. Biol. Cell* **15**, 3876-3890

Satoh, H., Shibata, H., Nakano, Y., Kitaura, Y., and Maki, M. (2002a) ALG-2 interacts with the amino-terminal domain of annexin XI in a Ca²⁺-dependent manner. *Biochem.*

Biophys. Res. Commun. **291**, 1166-1172

Satoh, H., Nakano, Y., Shibata, H., and Maki, M. (2002b) The penta-EF-hand domain of ALG-2 interacts with amino-terminal domains of both annexin VII and annexin XI in a Ca^{2+} -dependent manner. *Biochim. Biophys. Acta* **1600**, 61-67

Schell, M. J., Danoff, S. K., and Ross, C. A. (1993) Inositol (1,4,5)-trisphosphate receptor: characterization of neuron-specific alternative splicing in rat brain and peripheral tissues. *Brain Res. Mol. Brain Res.* **17**, 212-216

Scheller, N., Resa-Infante, P., de la Luna, S., Galao, R.P., Albrecht, M., Kaestner, L., Lipp, P., Lengauer, T., Meyerhans, A., and Diez, J. (2007) Identification of PatL1, a human homolog to yeast P body component Pat1. *Biochim. Biophys. Acta* **1773**, 1786-1792

Scheller, N., Mina, L.B., Galao, R.P., Chari, A., Gimenez-Barcons, M., Noueiry, A., Fischer, U., Meyerhans, A., and Diez, J. (2009) Translation and replication of hepatitis C virus genomic RNA depends on ancient cellular proteins that control mRNA fates. *Proc. Natl. Acad. Sci. USA.* **106**, 13517-13522

Shibata, H., Yamada, K., Mizuno, T., Yorikawa, C., Takahashi, H., Satoh, H., Kitaura, Y., and Maki, M. (2004) The penta-EF-hand protein ALG-2 interacts with a region containing PxY repeats in Alix/AIP1, which is required for the subcellular punctate distribution of the amino-terminal truncation form of Alix/AIP1. *J. Biochem.* **135**, 117-128

Shibata, H., Suzuki, H., Yoshida, H., and Maki, M. (2007) ALG-2 directly binds Sec31A and localizes at endoplasmic reticulum exit sites in a Ca^{2+} -dependent manner. *Biochem. Biophys. Res. Commun.* **353**, 756-763

Shibata, H., Suzuki, H., Kakiuchi, T., Inuzuka, T., Yoshida, H., Mizuno, T., and Maki, M. (2008) Identification of Alix-type and Non-Alix-type ALG-2-binding sites in human phospholipid scramblase 3: differential binding to an alternatively spliced isoform and amino acid-substituted mutants. *J. Biol. Chem.* **283**, 9623-9632

Shibata, H., Inuzuka, T., Yoshida, H., Sugiura, H., Wada, I., and Maki, M. (2010) The

ALG-2 binding site in Sec31A influences the retention kinetics of Sec31A at the endoplasmic reticulum exit sites as revealed by live-cell time-lapse imaging. *Biosci. Biotechnol. Biochem.* **74**, 1819-1826

Spector, D. L., and Lamond, A. I. (2011) Nuclear speckles. *Cold Spring Harb Perspect Biol* **3** pii: a000646. doi: 10.1101/cshperspect.a000646.

Suzuki, H., Kawasaki, M., Inuzuka, T., Okumura, M., Kakiuchi, T., Shibata, H., Wakatsuki, S., and Maki, M. (2008) Structural basis for Ca²⁺-dependent formation of ALG-2/Alix peptide complex: Ca²⁺/EF3-driven arginine switch mechanism. *Structure* **16**, 1562-1573

Tarabykina, S., Moller, A.L., Durussel, I., Cox, J., and Berchtold, M.W. (2000) Two forms of the apoptosis-linked protein ALG-2 with different Ca²⁺ affinities and target recognition. *J. Biol. Chem.* **275**, 10514-10518

Varjosalo, M., Keskitalo, S., Van Drogen, A., Nurkkala, H., Vichalkovski, A., Aebersold, R., and Gstaiger, M. (2013) The protein interaction landscape of the human CMGC kinase group. *Cell Rep.* **3**, 1306-1320

Vito, P., Lacana, E., and D'Adamio, L. (1996) Interfering with apoptosis: Ca²⁺-binding protein ALG-2 and Alzheimer's disease gene ALG-3. *Science* **271**, 521-525

Vito, P., Pellegrini, L., Guiet, C., and D'Adamio, L. (1999) Cloning of AIP1, a novel protein that associates with the apoptosis-linked gene ALG-2 in a Ca²⁺-dependent reaction. *J. Biol. Chem.* **274**, 1533-1540

Wagner, L. E., 2nd, Li, W. H., and Yule, D. I. (2003) Phosphorylation of type-1 inositol 1,4,5-trisphosphate receptors by cyclic nucleotide-dependent protein kinases: a mutational analysis of the functionally important sites in the S2⁺ and S2⁻ splice variants. *J. Biol. Chem.* **278**, 45811-45817

Will, C. L., Urlaub, H., Achsel, T., Gentzel, M., Wilm, M., and Luhrmann, R. (2002) Characterization of novel SF3b and 17S U2 snRNP proteins, including a human Prp5p homologue and an SF3b DEAD-box protein. *EMBO J.* **21**, 4978-4988

Willamson, M.P. (1994) The structure and function of proline-rich regions in proteins. *Biochem. J.* **297**, 249-260

Xie, J., and Black, D. L. (2001) A CaMK IV responsive RNA element mediates depolarization-induced alternative splicing of ion channels. *Nature* **410**, 936-939

Xie, J. (2008) Control of alternative pre-mRNA splicing by Ca²⁺ signals. *Biochim. Biophys. Acta* **1779**, 438-452

Yamada, Y., Arao, T., Gotoda, T., Taniguchi, H., Oda, I., Shirao, K., Shimada, Y., Hamaguchi, T., Kato, K., Hamano, T., Koizumi, F., Tamura, T., Saito, D., Shimoda, T., Saka, M., Fukagawa, T., Katai, H., Sano, T., Sasako, M., and Nishio, K. (2008) Identification of prognostic biomarkers in gastric cancer using endoscopic biopsy samples. *Cancer Sci.* **99**, 2193-2199

Yamasaki, A., Tani, K., Yamamoto, A., Kitamura, N., and Komada, M. (2006) The Ca²⁺-binding protein ALG-2 is recruited to endoplasmic reticulum exit sites by Sec31A and stabilizes the localization of Sec31A. *Mol. Biol. Cell* **17**, 4876-4887

Zahler, A. M., Lane, W. S., Stolk, J. A., and Roth, M. B. (1992) SR proteins: a conserved family of pre-mRNA splicing factors. *Genes Dev.* **6**, 837-847

Zhao, Y., Araki, S., Wu, J., Teramoto, T., Chang, Y. F., Nakano, M., Abdelfattah, A. S., Fujiwara, M., Ishihara, T., Nagai, T., and Campbell, R. E. (2011) An expanded palette of genetically encoded Ca²⁺ indicators. *Science* **333**, 1888-1891

Acknowledgement

This study was done in the Laboratory of Molecular and Cellular Regulation, Department of Applied Molecular Biosciences, Graduate School of Bioagricultural Sciences, Nagoya University.

I would like to express the deepest appreciation to Dr. Masatoshi Maki (Professor of Graduate School of Bioagricultural Sciences, Nagoya University) for his direction, significant suggestions and discussions to achieve my work. I also would like to show my greatest appreciation to Dr. Hideki Shibata (Associate professor of Graduate School of Bioagricultural Sciences, Nagoya University) and Dr. Terunao Takahara (Assistant professor of Graduate School of Bioagricultural Sciences, Nagoya University) for their valuable suggestions and discussions.

I am deeply grateful to Dr. Kevin Wang (Chief Operations and Scientific Officer - Banyan Biomarkers Inc. Executive Director, Center of Innovative Research - Banyan Biomarkers Inc., Alachua, FL) and all members in his company for giving me a wonderful and exciting experience of the internship in the United States. I also greatly appreciate to Dr. Yasuo Ariumi (Associate professor of Center for AIDS Research, Kumamoto University) and his laboratory member, Dr. Misao Kuroki for their cooperation and supports. I also thank Dr. Kiyotaka Hitomi (Professor of Graduate School of Pharmaceutical Sciences, Nagoya University) and Dr. Seiji Masuda (Associate professor of Graduate School of Biostudies, Kyoto University) for their helpful advices and discussions.

Special thanks also go to my coworkers, Dr. Hironori Suzuki, Tomomi Nomura, Chiaki Imoto, Keiko Yamamoto, Mai Kawasaki and all other members of the laboratory of molecular and cellular regulation and the laboratory of cell signaling (Dr. Fumitaka Ichioka, Dr. Yoshiaki Sugimura, Takeshi Kakiuchi, Dr. Yohei Osako, Yuri Miyake, Haruna Yoshida, Miyako Kitamura, Kanako Tsunoda, Dr. Tatsutoshi Inuzuka, Dr. Mayumi Okumura, Ryohei Tanaka, Takao Shinkai, Hiroyuki Yamashita, Yuki Maemoto, Hirofumi Sugiura, Asaka Yamane, Kazuya Watanabe, Emi Gotoh, Takeru Yokoyama, Cen Chen, Takeshi Takahashi, Miho Itoh, Mina Fukui, Masaru Ito, Eri Nozawa, Masaki Nishikawa, Katsuma Kuramoto, Yoshitaka Shimizu, Ryo Inokawa, Satomi Kiso, Takashi Kanadome, Minami Yamamuro, Mai Saitoh, Iku Higuchi, Ken Ueda, Kuniko Inoue, Kyosuke Kojima, Satoshi Kamura, Akane Satoh, Zhang Wei and Eri Yoshikawa) for their cooperation and helpful discussions.

This study was partly supported by fellowships for young scientists from Japan Society for the Promotion of Sciences (JSPS) and by Program for Leading Graduate Schools"

Integrative Graduate Education and Research in Green Natural Sciences", MEXT, Japan.

Finally, I want to thank my parents and husband for their help and supports.

Kanae Sasaki-Osugi

January 21, 2014